Universidade de Lisboa

Faculdade de Ciências

Departamento de Física

Optical solitons in inhomogeneous quadratic media

Frederico Correia Moreira

Doutoramento em Física

2013

Universidade de Lisboa

Faculdade de Ciências

Departamento de Física

Optical solitons in inhomogeneous quadratic media

Frederico Correia Moreira

Tese orientada pelos Professores Doutores Vladimir V. Konotop e Solange B. Cavalcanti, especialmente elaborada para a obtenção do grau de doutor em Física

2013

I would like to dedicate this thesis to my wife and loving parents...

Acknowledgements

I would like to thank my thesis advisor, Prof. Vladimir Konotop, for everything the taught me during my doctorate. His vision of how scientific work should be done really helped me to be a better researcher. The rigor of his analyses and advices helped me to do my best every time. This was never easy, and was never supposed to be, overcoming difficulties has much more value than simply asking someone for answers. I thank him for the support in these years. I really think I carry with me not only scientific knowledge, but a way on seeing things that makes me believe that I can really contribute to science, specially in my country. He introduced me to very special people in the center, all of them helped me in one way or another.

I would like to thank my thesis advisor and personal friend, Prof. Solange Cavalcanti. She supported me since I was a undergraduate student, and all the way through here, offering help and advice whenever I needed. I also would like to thank Prof. Luiz Oliveira for the encouraging words and support.

I thank Prof. Fatkhulla Abdullaev for his help. He offered some kind words in difficult times and discussions with him offered great value in the development of this work. His physical insights and coffee breaks, many in the black board, helped the work in research to be more fun than work sometimes.

I say thanks to Prof. Boris Malomed. His observations, many times done in funny remarks, made the tiring work of calculating solutions again and checking some results fun because he always made clear the importance of doing such things. He was of great help in doing this work.

I would like to thank doctor Alexey Yulin. His patience to teach me with words some answers to difficult problems was very important. He many times let me use his powerful computer, affectionately called Bigbrain. I know that it was inconvenient some times, but he always showed that he had pleasure in helping me, and for that I say thanks.

I would like to thank doctors Valeriy Brazhnyy and Yuliy Bludov. They were the first people I met in this old continent (completely new for me). They helped me a lot in personal things as searching for an apartment and how to get around in the city. They offered an help that really started my doctorate going, teaching me many things, always with joy and good will. I also would like to thank doctor Chao Hang. He also shared his knowledge with me many times.

My colleagues at my room, Helena Cruz, Pamela Pacciani and Carlos Reis provided a very good ambient. It was good to pass the days working at the center.

I would like to thank all my friends, It would be impossible to cite then all, but I cite a few here: Marcelo, Graziella, Paula, Sabrina and Antonio.

I would like to thank my father-in-law, Guillermo Jorge Romero and mother-in-law, Zilma Romero for they support while we were away. I also would like to thank Zilma and her daughter Darla. Thanks!

My parents, Antonio Moreira and Lindoya Martins Correia, are the reason I never gave up. I owe them everything. I wish they were here.

Of all people my wife deserves the most gratitude. She went to a new country with me, gave all she had to support me in every way possible. Maritza Moreira, I will be forever grateful.

I could not do everything I done in the last year if were not for one person: My newborn son, Max Guillermo Moreira. His mere existence taught my that persistence and desire to win makes possible to overcome even the greatest difficulties.

I would like to thank the Projeto Estratégico PEst-OE/FIS/UI0618/2011 for the financial support and Alban for the three years of scholarship.

Abstract

In this thesis we investigate optical solitons in systems with spatial modulations of the Dielectric Permittivity (DP) and quadratic nonlinear susceptibility $\chi^{(2)}$ that are transverse to the propagation of light. We consider three physical arrangements. The first consists in a periodic modulation of the DP and $\chi^{(2)}$ in a lossless medium. The second system considers a medium with gain and loss terms in the DP which satisfy the $\mathcal{PT}$-symmetry, i.e., the real part of the dielectric permittivity is even in respect to the transverse spatial coordinate, while the imaginary part, responsible for the gain and loss, is odd. It is also assumed a constant $\chi^{(2)}$. In the third system we consider a localized DP with gain and loss DP which satisfy the $\mathcal{PT}$ -symmetry, with constant $\chi^{(2)}$.

The study of solitons is a very important topic of fundamental research which also has found practical applications, specially as a medium to carry digital information. Nonlinear systems such as the ones investigated in this thesis, with quadratic nonlinearity, were found to exhibit interesting applications such as conversion of infrared radiation into visible light and all-optical switching in multichannel optical communication systems.

The search for solitonic solutions in the present thesis is done using several numerical methods such as a shooting algorithm and Newton-Raphson, used to find solutions and a split-step method to study the dynamics of solitons. The implementation of the methods relies on the careful analysis of symmetry and asymptotic properties of the systems under investigation. The stability of solutions is, in addition to numerical evaluation of perturbed solitons, studied by linear sta-

bility analysis in all cases and links between the two approaches are discussed.

The phenomenon of bistability occurs in the periodic lossless system, as two stable solutions can exist with same power and different symmetries and corresponding symmetry axes. An effective equation with cubic nonlinearity that successfully predicts when bifurcations occurs is presented.

The $\mathcal{PT}$-symmetric system with periodic DP is found to support three different types of bifurcations, related to the edge of the gap where it occurs, it can be an edge of the Fundamental Field (FF), Second-Harmonic (SH) or both. Quadratic solitons in this system support stable embedded solitons in the case fundamental field edge bifurcations.

The system with $\mathcal{PT}$-symmetric localized potential supports soliton branches which are limited in maximal power. Three types of bifurcations are discussed in a way similar to the periodic system. We found that branches that bifurcate from a linear mode of the SH can have finite amplitude of the SH component even when the amplitude of the FF goes to zero. In the same previously refered bifurcation, solitons with propagation constant close to the propagation constant of the linear mode can be stable for strengths of gain and loss well above the $\mathcal{PT}$-symmetry breaking treshold.

Keywords: soliton, quadratic nonlinearity, periodic potential, localized potential, gap solitons, nonlinear dynamics, parity-time symmetry.

Resumo

Nesta tese investigamos solitões óticos em sistemas com modulações espaciais da Permitividade Dielétrica (DP) e da susceptibilidade não linear quadrática $\chi^{(2)}$ transversas à propagação da luz. Consideramos três sistemas físicos. O primeiro consiste numa modulação periódica da DP e $\chi^{(2)}$ num meio sem perdas. O segundo sistema considera um meio com ganhos e perdas presentes na DP que satisfazem a simetria $\mathcal{PT}$, i.e. a parte real da permitividade dielétrica é par em relação à coordenada espacial transversa, enquanto a parte imaginária, responsável pelos ganhos e perdas, é ímpar e $\chi^{(2)}$ considerado constante. No terceiro sistema consideramos uma DP localizada, com ganhos e perdas, que satisfaz a simetria $\mathcal{PT}$, com $\chi^{(2)}$ constante. O estudo de solitons.

O estudo de solitões é não somente um importante tópico de pesquisa fundamental, também foram encontradas aplicações práticas, especialmente como um meio de transporte de informação digital. Em sistemas não-lineares como os considerados nesta tese, com não linearidade quadrática, foram descobertas aplicações tais como a conversão de radiação infravermelha em luz visível e comutação feita totalmente óticamente em multicanais de comunicação óticos.

A busca por soluções solitônicas é feita nessa tese utilizando vários métodos numéricos tais como um algoritmo de *shooting* e outro de Newton-Raphson, usados na busca de soluções e um método de *split-step* utilizado no estudo da dinamica dos solitões. A implementação dos métodos basea-se na análise cuidadosa da simetria e do comportamento assintótico dos solitões nos sistemas investigados. A estabilidade das soluções é, em adição à integração numérica das equações de

evolução, estudada através da análise de estabilidade linear em todos os casos. Ligações entre as duas análises são estabelecidas.

O fenômeno da bi-estabilidade no sistema periódico sem perdas é encontrado, duas soluções estáveis podem ocorrer com a mesma potência com simetrias e centros de simetria diferentes. Uma equação efetiva com não-linearidade cúbica que prevê com sucesso quando uma bifurcação ocorre é desenvolvida.

No sistema periódico com simetria $\mathcal{PT}$ são encontradas três tipos de bifurcações, relacionadas com qual fronteira do hiato nas constantes de propagação elas ocorrem. Elas podem ser numa fronteira do campo fundamental (FF), do segundo harmônico (SH) ou de ambos. Solitões quadráticos esáveis nesse sistema podem ser encontrados dentro da região de hiato do SH no caso de bifurcações advindas de uma fronteira do FF.

No sistema com potencial localizado e simetria $\mathcal{PT}$ há ramos de soluções com um máximo nos valores da potência. Três tipos de bifurcações são discutidas numa maneira similar ao sistema periódico. Ramos que bifurcão de um modo linear do SH podem ter amplitudes finitas do componente SH mesmo quando a amplitude do FF aproxima-se de zero. Na mesma bifurcação é encontrado que solitons com constantes de propagação com valores próximos da constante de propagação do modo linear podem ser estáveis mesmo valores de amplitude da parte imaginária da DP muito acima do limiar de quebra de simetria $\mathcal{PT}$.

Palavras-chave: solitões, não-linearidade quadrática, potencial peridíco, potencial localizado, solitões de hiato, dinâmica não linear, simetria de espaço-tempo.

Contents

List of Figures

Chapter 1

Introduction

1.1 Solitons in $\chi^{(2)}$ media

Nowadays, nonlinear optics is a well established area of scientific research. It all started with the invention of the lasers in the early years of 1960s, where the powerful coherent light source allowed the experimental investigation of the nonlinear response of matter to a high intensity beam. One of the first observed effects was the Second Harmonic Generation (SHG). The effect consists in the emission of light of frequency $2\omega_1$, which in this thesis is referred as Second-Harmonic (SH), as a result of the interaction of a incident light with frequency ω_1, here referred as the Fundamental Field (FF), with an optical material, more commonly a crystal with a quadratic nonlinear response described by the coefficient $\chi^{(2)}$ which generally depends on frequency. The first experimental observation of SHG was done in [1] and followed by the development of the theory continuous SHG in [2].

In the period between late 1989 and early 1990s interest in SHG systems gained more attention after the works [3, 4]. The authors detected a nonlinearly induced phase shift in the light of a laser after propagating in a potassium titanyl phosphate crystal (KTP) as an effect of SHG in the crystal. The works demonstrated that under special conditions of large wave vector mismatch SHG can behave like system with cubic nonlinear response, i.e., $\chi^{(3)}$. This is of particular importance since it was discovered that $\chi^{(3)}$ system possess Localized Solutions (LS) [5, 6], commonly known as solitons. These stationary solutions remain lo-

calized in one or more dimensions during propagation in the spatial regime or light pulses which propagate without dispersion in the time domain.

The theoretical prediction of the existence of solitons in a system with quadratic nonlinearity was made in 1974, in the work [7]. The first observations of $\chi^{(2)}$ solitons in a experiment appeared much latter, in mid 1990s, in the works [8], where a bulk $\chi^{(2)}$ crystal was used and in [9], in a waveguide system.

The advent of new technologies such as low-pressure hydride vapor phase epitaxy [10] and molecular beam epitaxy using Si shadow masks [11] allows to construct a systems with modulated $\chi^{(2)}$. Other techninologies allows the fabrication of a system with modulated dielectric function, such as periodic one, using one or more techniques such as stacking of micromachined silicon wafers [12], holographic lithography [13, 14] and a combination of soft lithography and holographic lithography [15]. All these advancements in technology, along with the increasing power of personal computers increased the interest in the theoretical and numerical investigation various configurations of dielectric and $\chi^{(2)}$ modulations.

There is a growing interest in physical systems possessing the so-called $\mathcal{PT}$ (parity-time) symmetry [16] (See the review [17]), i.e., as a matter of fact, dissipative quantum systems with the antisymmetry between spatially separated gain and loss. If the strength of the gain-loss terms does not exceed a certain threshold value, the $\mathcal{PT}$-symmetric system has a purely real spectrum and its non-Hermitian Hamiltonians can be transformed into a Hermitian form [18]. Making use of the similarity of the quantum-mechanical Schrödinger equation to the parabolic propagation equation in optics it was proposed theoretically [19] and demonstrated experimentally [20] that the $\mathcal{PT}$-symmetry can be realized, in the purely classical context of the wave propagation, in optics, where it implies that a waveguide with the $\mathcal{PT}$-balanced gain and losses allows the transmission of wave modes, emulating the index-guiding transmission in ordinary (conservative) waveguides. These findings stimulated numerous additional studies of the linear wave propagation $\mathcal{PT}$-symmetric systems in the special issue [21]. Particular attention being focused on the periodic potentials [22] (see also review [23]).

It is relevant to mention that, as the $\mathcal{PT}$-symmetric systems is a special type of settings at the border between conservative and dissipative systems, the solitons

that exist in them may be naturally compared not only to their counterparts in conservative models (as mentioned above, concerning the relation to GSs in the conservative $\chi^{(2)}$ systems), but also to solitons in generic dissipative systems, with unbalanced gain and loss. The crucial difference of the dissipative solitons from their conservative counterparts is that they exist, as isolated attractors of the system, at a single value of the propagation constant, rather than continuous families parametrized by an arbitrary propagation constant [24, 25]. In particular, as concerns GSs, 1D and 2D dissipative gap solitons in the complex Ginzburg-Landau equations with periodic potentials were reported in Ref. [26, 27]. In this sense nonlinear $\mathcal{PT}$-symmetric systems, being not conservative and thus requiring the balance between dissipation and gain, but still allowing for existence of the continuous families of the solutions (what is the generic property of the such system provided the nonlinearity obey the same symmetry as the linear part [28]) occupy an intermediate position between the conservative and dissipative systems, and reduced to the former ones when the gain-loss coefficient becomes zero or the the later ones when appears unbalance between gain and loss.

Nonlinear systems with $\mathcal{PT}$-symmetry have been also investigated and it has been found that system with a periodic $\mathcal{PT}$-symmetric potential with $\chi^{(3)}$ nonlinearity [29, 30, 31] and systems with combined cubic and quintic nonlinearity [32] support stable solitons.

In addition to pure theoretical interest in the existence, properties and particularities of solitons in $\mathcal{PT}$-symmetric systems, the possibility of experimental realization of such systems using modern techniques actually stimulates theoretical and numerical studies like the ones in this thesis with the objective to find new relevant phenomena. The study of existence of solitons and their properties in such systems take a great portion of this thesis.

1.2 The problems investigated in this thesis

We consider trough this thesis a one-dimensional model of propagation of light on a medium. The medium itself is allowed to have modulations on the dielectric function and nonlinear $\chi^{(2)}$ coefficient. The modulations are considered to be transverse to the light propagation direction.

The first investigation had results published in [33]. The setup considers a periodic dielectric function in the presence of gain and loss in a special configuration which satisfies simultaneously parity and time reversal operations, a $\mathcal{PT}$-symmetric system. Here the quadratic nonlinearity is considered to be spatially invariant. In this problem the model is introduced and three types of bifurcations of solitons are discussed in detail. Each one has distinct limits for the FF and SH in the limit of small amplitudes. We investigate the linear properties of the gaps of the structure and discuss which type of bifurcation occurs in determinate regions of the bands of the system. Finally we discuss the existence of solitons in several forbidden propagation regions, i.e., band-gaps and their stability is discussed with a linear model valid for small perturbations and direct simulations of full equations. The Chapter 4 is dedicated to this problem.

The second investigation to be presented is a system with periodic modulations of the dielectric function and nonlinear coefficient $\chi^{(2)}$ in a lossless medium. The result of this investigation was published as an article in [34]. In this system we suggest a physical structure that is feasible to laboratory experimentation. We present asymptotic properties of the system that allows to use a shooting algorithm. We discuss the symmetry of solitons and find the position relative to the modulation where solitons can be centered. Families of solitons are found and their stability are studied with linear analysis and direct simulations of perturbed initial conditions. We also derive an effective Nonlinear Schrödinger Equation (NLS) that successfully predicts when bifurcations occurs. The solutions of the effective model is compared with the numerical solutions. In this thesis the system is discussed in Chapter 5.

The last problem is about a $\mathcal{PT}$-symmetric system where the dielectric permittivity modulation is localized and $\chi^{(2)}$ considered constant is presented on Chapter 6. The results of this investigation were published in [35]. In this problem we investigate the types of bifurcations from localized modes of the linear system. Branches are presented and their stability is studied. The new results are discussed in detail and in special a model for bifurcations with small amplitude limit of the FF in the presence of a finite localized SH is introduced.

In all the three different configurations the main object of study will be localized solutions. Their existence, dynamics and stability will be considered in

detail. A significant amount of numerical schemes were developed by the author to find numerical solutions. The development of such methods usually evolves about the careful analysis of symmetry properties and asymptotic behavior of solitons.

1.3 The thesis structure

In this thesis the Chapter 2 is a revision of the subject of LS in $\chi^{(2)}$ media. The equations which are used along all the investigated problems are presented and their dimensionless representation is presented. The state of the art on the subjected is presented.

The Chapter 3 is devoted to the presentation of the methods used in this thesis. It consists mainly in numerical methods. Sections about shooting method and Newton-Raphson are presented. The purpose of both methods is to find LS. A split-step method is presented. It is used in the study of the evolution of LS in the dynamical problem.

The Chapter 4 is dedicated to the study of solitons in $\chi^{(2)}$ media with $\mathcal{PT}$-symmetric periodic potential. The Chapter 5 concerns the study of gap solitons in nonlinear periodic $\chi^{(2)}$ media. The study of localized modes in $\chi^{(2)}$ media with $\mathcal{PT}$-symmetric localized potential is presented in 6.

Finally the final considerations and conclusions are made about the most important results in Chapter 7.

Chapter 2

Localized modes in $\chi^{(2)}$- media: a revision

We consider the FF and SH having respectively frequencies ω_1 and $2\omega_1$ and wave vectors k_1 and k_2. The wave vectors are allowed to have a mismatch $\delta k = k_2 - 2k_1$. The mismatch is assumed to be small, i.e., $|\delta k/k_{1,2}| \ll 1$. Both waves propagate in a nonlinear medium along z direction and are assumed have a non-vanishing component only in the y direction Maxwell equation is in the present case

$$\frac{\partial^2 E_y}{\partial x^2} + \frac{\partial^2 E_y}{\partial z^2} - \frac{\epsilon}{c^2}\frac{\partial^2 E_y}{\partial t^2} = \frac{4\pi}{c^2}\frac{\partial^2 P_{NL}}{\partial t^2}. \tag{2.1}$$

The y component of the electric field is written as

$$E_y(x,z,t) = E_1(x,z)\exp\left[i\left(k_1 z - \omega_1 t\right)\right] + E_2(x,z)\exp\left[i\left(k_2 z - 2\omega_1 t\right)\right] + c.c., \tag{2.2}$$

where E_1 (E_2) are the envelopes of the FF (SH). The medium is assumed to be modulated in the direction transverse to the direction of propagation, i.e. x, direction with characteristic size l, which can be the period of the modulation or the size, in the case of a localized modulation. Respectively, for the dielectric permittivity the definition

$$\epsilon(x, \beta\omega_1) \equiv \epsilon_\beta(x) = \epsilon_{\beta 0} + \epsilon_{\beta 1}(x), \quad \beta = 1, 2, \tag{2.3}$$

applies (See Fig.2.1). The symbol β refers to quantities calculated for the FF ($\beta = 1$) or the SH ($\beta = 2$). It will be used in all thesis with the same meaning. In above $\epsilon_{\beta 0}$ is a constant which may be considered the average of ϵ_β in the case of periodic modulations or an extreme value of ϵ_β in the case of a localized modulation. Here $\epsilon_{\beta 1}$ describes the modulation and is allowed to have complex values. A $\mathrm{Im}(\epsilon_{\beta 1}(x)) > 0$ represents a gain at a given x and a $\mathrm{Im}(\epsilon_{\beta 1}(x)) < 0$ represents a loss.

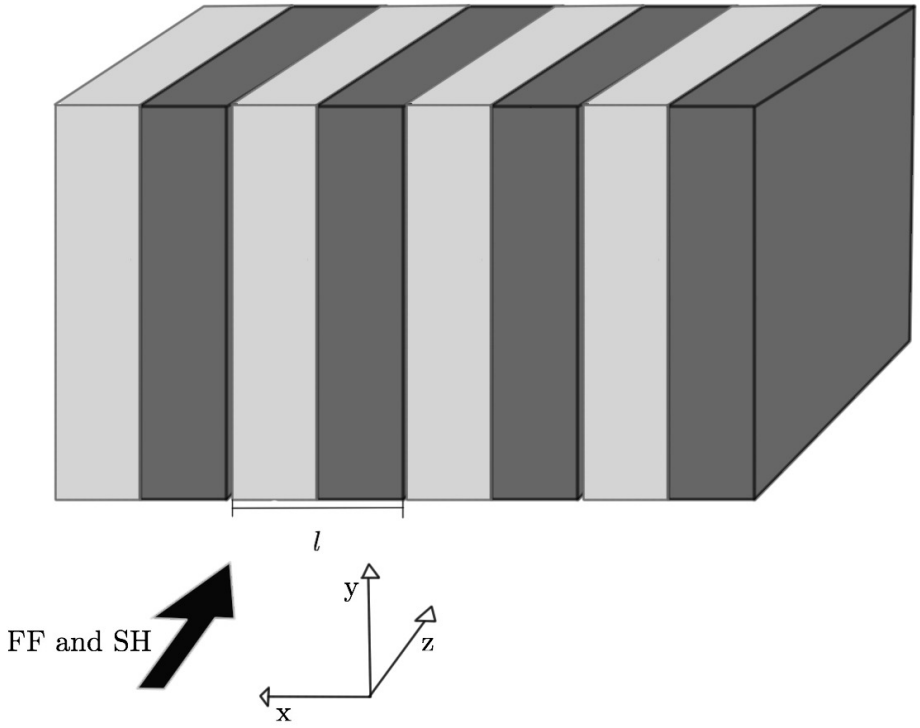

Figure 2.1: Schematics of a system with a periodic modulation of the dielectric permittivity. Dark gray and light gray regions denote regions of high and low values of the dielectric permittivity. The period is given by l.

The term $P_{NL} = \chi^{(2)} E_y^2$ represents the non-linear response of the medium. The envelopes are considered to be slowly varying in the z direction, i.e., we assume here that, after inserting (2.2) in (2.1), terms containing $\partial^2/\partial z^2$ can be neglected. We also take in consideration only resonant terms, i.e., terms resonant with the FF containing $e^{-i\omega_1 t}$ and terms resonant with the SH, containing $e^{-2i\omega_1 t}$, when expanding P_{NL} using (2.2). Let $\chi_1(x) \equiv \chi^{(2)}(x, \omega_1; 2\omega_1, -\omega_1)$ and $\chi_2(x) \equiv \chi^{(2)}(x, 2\omega_1; \omega_1, \omega_1)$ with $\chi_\beta(x)$ standing for the second-order susceptibilities at FF and SH frequencies. The propagation equations reads (see e.g. [36, 37, 38])

$$2ik_1 \frac{\partial E_1}{\partial z} + \frac{\partial^2 E_1}{\partial x^2} + \left(\frac{\omega_1^2}{c^2} \epsilon_{11}(x) + \frac{\omega_1^2}{c^2} \epsilon_{10} - k_1^2 \right) E_1 + 8\pi \frac{\omega_1^2}{c^2} \chi_1(x) \bar{E}_1 E_2 e^{i\delta k z} = 0 \tag{2.4a}$$

$$2ik_2 \frac{\partial E_2}{\partial z} + \frac{\partial^2 E_2}{\partial x^2} + \left(4\frac{\omega_1^2}{c^2} \epsilon_{21}(x) + 4\frac{\omega_1^2}{c^2} \epsilon_{20} - k_2^2 \right) E_2 + 4\pi \frac{\omega_1^2}{c^2} \chi_2(x) E_1^2 e^{-i\delta k z} = 0 \tag{2.4b}$$

where the bar denotes the complex conjugation, and c denotes the speed of light in vacuum.

The wave-vectors k_β are related to the frequencies $\beta\omega_1$ trough the dispersion relation. Here we assume a linear one

$$k_\beta^2 = \frac{\beta^2 \omega_1^2 \epsilon_{0\beta}}{c^2}. \tag{2.5}$$

Then (2.4) reduces to

$$2ik_1 \frac{\partial E_1}{\partial z} + \frac{\partial^2 E_1}{\partial x^2} + \frac{\omega_1^2}{c^2} \epsilon_{11}(x) E_1 + 8\pi \frac{\omega_1^2}{c^2} \chi_1(x) \bar{E}_1 E_2 e^{i\delta k z} = 0 \tag{2.6a}$$

$$2ik_2 \frac{\partial E_2}{\partial z} + \frac{\partial^2 E_2}{\partial x^2} + 4\frac{\omega_1^2}{c^2} \epsilon_{21}(x) E_2 + 4\pi \frac{\omega_1^2}{c^2} \chi_2(x) E_1^2 e^{-i\delta k z} = 0 \tag{2.6b}$$

From now on we will work on (2.6) in dimensionless form. To this end we make clear that all the transformed parameters below are dimensionless. The coordinates are written as

$$\xi = \frac{2\pi}{l} x, \quad \zeta = \frac{2\pi^2}{k_1 l^2} z. \tag{2.7}$$

The dimensionless envelopes $u_{1,2}$ are given by

$$u_1 = \frac{l^2\omega_1^2}{\pi c^2}\sqrt{\frac{\chi_{10}\chi_{20}}{2}}\left(\frac{\epsilon_{01}}{\epsilon_{02}}\right)^{\frac{1}{4}} E_1, \tag{2.8a}$$

$$u_2 = \frac{l^2\omega_1^2\chi_{10}}{\pi c^2} E_2 e^{-i\delta k z}. \tag{2.8b}$$

In above $\chi_{\beta 0}$ are the characteristic strengths of the nonlinearity, which can be the amplitude of nonlinear modulations in the case of periodic $\chi_{1,2}$ or the constant values of $\chi_{1,2}$ when nonlinear modulations are absent.

The substitution of (2.7) and (2.8) leads to the equations

$$i\frac{\partial u_1}{\partial \zeta} + \frac{\partial^2 u_1}{\partial \xi^2} + \mathcal{V}_1(\xi)\, u_1 + 2 f_1(\xi)\overline{u}_1 u_2 = 0, \tag{2.9a}$$

$$i\frac{\partial u_2}{\partial \zeta} + \sigma\frac{\partial^2 u_2}{\partial \xi^2} + 2\left(\mathcal{V}_2(\xi) + q\right) u_2 + f_2(\xi)\, u_1^2 = 0. \tag{2.9b}$$

In above

$$q = \frac{l^2 k_1}{4\pi^2}\delta k, \quad \sigma = k_1/k_2 = \frac{1}{2}\left(1 + \frac{\delta k}{2k_1}\right)^{-1} \tag{2.10}$$

Finally optical potentials are given by

$$\mathcal{V}_1(\xi) = \frac{\omega_1^2}{c^2}\frac{l^2}{4\pi^2}\epsilon_{11}\left(\frac{l}{2\pi}\xi\right), \tag{2.11a}$$

$$\mathcal{V}_2(\xi) = \left(1 + \frac{\delta k}{2k_1}\right)^{-1}\frac{l^2}{4\pi^2}\frac{\omega_1^2}{c^2}\epsilon_{21}\left(\frac{l}{2\pi}\xi\right) \tag{2.11b}$$

and the nonlinear functions are defined as $f_\beta(\xi) = \chi_\beta\left(\frac{l^2}{k_1}\xi\right)/\chi_{\beta 0}$.

This thesis focuses mainly on solutions that are localized in the ξ direction. The solution is searched in the form

$$u_\beta(\xi,\zeta) = w_\beta(\xi)e^{i\beta b\zeta}, \quad \beta = 1, 2. \tag{2.12}$$

In above the propagation constant of the FF is given by b and dimensionless stationary envelopes $w_{1,2}$ are required to satisfy $w_{1,2} \to 0$ as $|\xi| \to \infty$. The

substitution of (2.12) in (2.9) results in the nonlinear equations

$$\frac{d^2w_1}{d\xi^2} + (\mathcal{V}_1(\xi) - b)\, w_1 + 2f_1(\xi)\overline{w}_1 w_2 = 0, \tag{2.13a}$$

$$\sigma\frac{d^2w_2}{d\xi^2} + 2(\mathcal{V}_2(\xi) + q - b)\, w_2 + f_2(\xi)\, w_1^2 = 0. \tag{2.13b}$$

2.0.1 The $\mathcal{PT}$-symmetric systems

In this thesis we consider in addition to real potentials, complex valued $\mathcal{V}_1$ which satisfy the $\mathcal{PT}$-symmetry requirements that we describe below.

Consider a linear Schrödinger equation

$$\mathcal{L}_1 w_1 = b w_1, \quad \mathcal{L}_1 = \frac{d^2}{d\xi^2} + \mathcal{V}_1(\xi). \tag{2.14}$$

It is well known that if $\mathcal{V}_1(\xi)$ is a real function the eigenvalues b are real valued. If the potential is considered to have a period l, i.e. $\mathcal{V}_1(\xi + l) = \mathcal{V}_1(\xi)$, (2.14) becomes the well known Hill equation [39], with forbidden regions in the spectrum of b called band-gaps (BG). A localized potential, i.e., $\mathcal{V}_1 \to 0$ as $|\xi| \to \infty$ can have discrete eigenvalues with localized eigenfunctions w_1 [40].

Considering $\mathcal{V}_1(\xi)$ to be a complex function usually results in complex b. However in [16, 17] it was found that the class of $\mathcal{PT}$-symmetric potentials may have only real eigenvalues. The $\mathcal{PT}$-symmetry stands for the operator being simulaneously symmetric in respect to the parity operator $\mathcal{P}$ and the time-reversal operator $\mathcal{T}$. In the present case the operator $\mathcal{L}_1$ is $\mathcal{PT}$-symmetric when $\mathcal{V}_1(\xi) = \bar{\mathcal{V}}_1(-\xi)$.

2.1 The state of the art

The physics of nonlinear wave processes in periodic media and their optical applications attracted a great deal of attention during the last years [41, 42]. Numerous studies were focused on the band-gap materials with Kerr-type and $\chi^{(2)}$ nonlinearities (for the recent reviews see e.g. [38, 43, 44, 45]). In particular, solitons

in quadratically nonlinear optical media with shallow and deep periodic modulations of the dielectric permittivity were investigated in Refs. [46] and [47, 48, 49], respectively. The structure and stability of spatially localized and periodic stationary field patterns in optical parametric amplifiers and oscillators with periodically modulated dielectric permittivity have been addressed in [50, 51, 52]. Such type of materials can be important for the design of optical transistors and switchers [38, 53]. Recently, the attention has been turned to study of solitonic structures in materials with periodic modulations of the $\chi^{(2)}$ nonlinearity. In [54] optical solitons in a two-dimensional quasi-phase-matched geometry involving two concurrent non-collinear quadratic processes have been investigated. It was found that such system can support a class of localized modes with a large domain of stability. Nonlinear photonic crystals, whose existence in a form of a two-dimensional triangular lattice was suggested in [55], were experimentally implemented in [56]. It was shown that the phase matching resonances are given by a nonlinear Bragg law, what opens possibilities for the generation of new type of solitons and multiple beam second harmonic generation.

There have been also reported studies of structures where both linear and nonlinear modulations of $\chi^{(2)}$ arrays are taken into account. These studies were performed for thin layers with $\chi^{(2)}$ nonlinearity embedded into linear optical media [57]. Such system can be described by the discrete $\chi^{(2)}$ lattices, where discrete breathers of the different symmetries have been investigated in [58]. Bright soliton solutions in the second band gap in media with quadratic nonlinearity with a deep Bragg grating are investigated in the work [59] in the framework of the coupled-mode theory approximation. It was shown that only the difference from the shallow grating case [38] is a reduction of the peak intensity of the gap soliton (GS). Recently in [34] solitons with linear periodic modulations of the refractive index and nonlinearity were investigated and were found to have bistability. In [60] a system with periodic modulations in the refractive index imprinted with the use of thermo-optic heaters was proposed and effects of adiabatic changes in the modulation, such as defects and transverse displacement of the periodic modulation, on the soliton mobility was presented.

Due to optical applications, additional interest has been recently attracted by nonlinear $\mathcal{PT}$-symmetric optical systems with periodic modulation of the re-

fractive index [29, 31, 32, 61] which demonstrated that stable solitons can be supported by the combination of the Kerr nonlinearity and periodic complex potentials, whose spatially odd imaginary part accounts for the balanced gain and loss. The stability of such solitons was rigorously analyzed in Ref. [62]. Solitons can also be naturally found in linearly-coupled dual-core systems with balanced gain and loss in the two cores and intrinsic Kerr (cubic) nonlinearity in each one [63], and discrete solitons were predicted in coupled chains of $\mathcal{PT}$-symmetric elements [64] and in general network of coupled $\mathcal{PT}$-symmetric oligomers (dimers, quadrimers, etc) [65]. In addition to introducing the usual Kerr nonlinearity, the $\mathcal{PT}$-symmetric part of the system can be made nonlinear too, by introducing mutually balanced cubic gain and loss terms [66].

Properties of solitons in $\mathcal{PT}$-symmetric systems may differ significantly from what is known about usual solitons in conservative models. In particular, different families of solutions bifurcating from different linear modes may merge in a single family, exhibiting increased stability [67]. On the other hand, the increase of the gain-loss coefficient in the $\mathcal{PT}$-symmetric Kerr-nonlinear coupler leads to shrinkage of the stability areas for $\mathcal{PT}$-symmetric and antisymmetric solitons, until they vanish when this coefficient becomes equal to the inter-core coupling constant. We also mention recent intensive activity in study of the combined effect of linear and nonlinear $\mathcal{PT}$ [68, 69] on existence and stability of optical solitons.

A particularly interesting realization of a $\mathcal{PT}$-symmetric modulation of the refractive index is when losses and gain are localized in space, giving rise to a $\mathcal{PT}$-symmetric localized impurity. Such impurities allow for existence of localized (defect) modes. In the linear theory such modes were studied for exactly integrable models in [70, 71]. Linear scattering by a $\mathcal{PT}$-symmetric inhomogeneity and emerging of the related spectral singularities was described in [72]. The effect of two and various randomly distributed $\mathcal{PT}$-symmetric impurities on the lattice dynamics was addressed in [73]. In [29] there was the first report of solitons in a system with cubic nonlinearity. Several works on solitons with cubic nonlinearity followed. Solitons supported by other $\mathcal{PT}$-symmetric defects were also reported for focusing [74] and defocusing [30] media. Switching of solitons in a unidirectional coupler using $\mathcal{PT}$-symmetric defects was suggested in [75]. Nonlinear modes in even more sophisticated, double well $\mathcal{PT}$-symmetric potentials were studied re-

cently [76]. Solitons in quadratic nonlinear media with conservative defects were investigated in [77, 78], where it was shown that solutions are dynamically stable in the case of attractive impurities. Recently the soliton dynamics in $\chi^{(2)}$ materials was considered in the presence of a $\mathcal{PT}$-symmetric localized impurity [35], it was found that stable solutions can exist well above the $\mathcal{PT}$-symmetry breaking threshold. In [33] quadratic solitons in $\mathcal{PT}$-symmetric periodic medium was investigated and stable fully localized embedded solitons were found.

Chapter 3

The methods

One of the fundamental objectives in this thesis is the search of stationary solutions of the system of nonlinear differential equations (2.13). However analytical solutions are not expected to be found easily due to the complexity of the problem. It is then necessary to use numerical methods in order to find solutions in a computer.

The first method we use to find solutions is the shooting method, a method that allows the systematic search of localized solutions of (2.13) using previous knowledge about asymptotic properties of solutions and symmetries of the system. The accuracy of the method is generally good enough to use as a initial seed for the Newton-Raphson method, a iterative method to find solutions of a system of nonlinear equations that can obtain high accuracy in little computational time if the initial seed is good enough.

The next step is to study the behavior of localized profiles when solutions of (2.13) are used as initial conditions at $\zeta = 0$ in the full dynamical problem presented by the system of partial differential equations (2.9). Since in any real world physical applications imperfections are always present, it is necessary to study the stability of stationary solutions when subjected to perturbations. We use the split-step method, as it provides efficient computational evaluation, very good accuracy in the case of integration of smooth functions, and energy conservation, properties that are specially useful in the study of the appearance of instabilities, that can require a large propagation distance to have visible effects.

In the next sections we present all described methods directly applied to the

problems of this thesis.

3.1 Shooting method

In this thesis we consider several types of potentials $\mathcal{V}_\beta$ when searching for solutions of (2.13), but a simple distinction can be made between them, the simplest form we consider is $\mathrm{Im}(V_\beta) = 0$, i.e. purely real potentials without a imaginary part representing gain and loss. Furthermore we consider in this thesis localized and periodic $\mathcal{V}_\beta$. In both cases the real part of $\mathcal{V}_\beta$ will always be considered even functions, i.e. $\mathcal{V}_\beta(\xi) = \mathcal{V}_\beta(-\xi)$. In this thesis only $f_{1,2}(\xi) = f_{1,2}(-\xi)$ are considered.

In this thesis we consider only solutions of (2.13) with definite symmetry, of which two types can exist if real and even $\mathcal{V}_\beta$ and $f_{1,2}$ are used [34, 52],

$$\{w_1(\xi), w_2(\xi)\} = \{\pm w_1(-\xi), w_2(-\xi)\}. \tag{3.1}$$

This means that while w_2 is always an even function, w_1 can be even or odd. The solutions are valid when $f_{1,2}$ are even. The case when $f_{1,2}$ is odd results in odd w_2, but it will not be considered in this thesis. The symmetry (3.1) is useful in constructing a numerical method to find localized solutions as described below.

When considering solutions with symmetries like (3.1) it is enough to consider only $\xi \geq 0$, in which case the localized boundary conditions are

$$\left.\frac{dw_{1,2}}{d\xi}\right|_{\xi=0} = 0, \quad w_{1,2}(\xi) \to 0 \text{ as } \xi \to \infty \tag{3.2}$$

for $w_{1,2}(\xi) = w_{1,2}(-\xi)$ or

$$w_1(0) = 0, \qquad \left.\frac{dw_2}{d\xi}\right|_{\xi=0} = 0, \quad w_{1,2}(\xi) \to 0 \text{ as } \xi \to \infty \tag{3.3}$$

for odd w_1 and even w_2.

The shooting method consists in transforming the boundary value problems (3.2) or (3.3) into an initial value problem. To effect, consider that a $\xi_f \gg 1$ suitable asymptotic approximations can be used. In this thesis we use the

shooting method only with a real, even $\mathcal{V}_1$ with period l_0. We first consider the asymptotic behavior of the FF. For a large ξ_f, the nonlinear term in (2.13a) can always be neglected in the case of LS. The resulting equation, (2.14), is the well known Hill's equation ([39]). The Floquet theorem states that two linearly independent solutions exist for (2.14)

$$A_{1\pm}(\xi) = \phi_1(\pm\xi)e^{\pm\mu_1\xi}. \tag{3.4}$$

In above μ_1 is the real-valued characteristic exponent of (2.14) if the solutions are calculated for a b in a band gap. Also in (3.4), $\phi_1(\xi)$ is a function with period l_0, which is the period of $\mathcal{V}_\beta$ not to be confused with the period of $\epsilon_{\beta 1}$. The general solution of (2.14) is given by

$$A_1(\xi) = c_+A_{1+}(\xi) + c_-A_{1-}(\xi). \tag{3.5}$$

In order to find the value of μ_1 we need to solve the characteristic equation of (2.14) [39]

$$r^2 - \left(y_1(l_0) + \left.\frac{dy_2}{d\xi}\right|_{\xi=l_0} \right) + 1 = 0. \tag{3.6}$$

The functions $y_{1,2}(\xi)$ are two linearly independent solutions of (2.14) defined by the initial conditions

$$y_1(0) = 1, \quad (dy_1/d\xi)|_{\xi=0} = 0, \tag{3.7a}$$

$$y_2(0) = 0, \quad (dy_2/d\xi)|_{\xi=0} = 1. \tag{3.7b}$$

The characteristic exponent is related to the solutions $r_\pm$ of (3.6) through the expression

$$r_\pm = e^{\pm\mu_1}, \tag{3.8}$$

valid when $r_+ \neq r_-$.

The case we are interested in this thesis, with even $\mathcal{V}_{1,2}$, has solutions that

satisfy the following condition (See [39])

$$y_1(l_0) = \left.\frac{dy_2}{d\xi}\right|_{\xi=l_0}. \tag{3.9}$$

It is then possible to obtain the value of μ_1 substituting (3.9) into (3.6) and using (3.8) to obtain

$$\mu_1 = \frac{\ln\left(y_1(l_0) + \sqrt{y_1(l_0)^2 - 1}\right)}{l_0}. \tag{3.10}$$

Now we need to calculate $\phi_1(\xi)$. To this, just substitute the expression for A_{1+} in (3.4) into (2.14) to obtain

$$\frac{d^2\phi_1}{d\xi^2} + 2\mu_1\frac{d\phi_1}{d\xi} + \left(\mathcal{V}_1(\xi) + \mu_1^2 - b\right)\phi_1(\xi) = 0 \tag{3.11}$$

and solve the boundary value problem $\phi_1(0) = \phi_1(l_0)$. The asymptotic behavior of the SH in the case of periodic $\mathcal{V}_{1,2}$ is explained in the Appendix **??**.

From now on, in the description of the shooting algorithm, we denote

$$w_{1,2}(\xi_f) \approx C_{1,2}\mathcal{A}_{1,2}(\xi_f). \tag{3.12}$$

In above $\mathcal{A}_{1,2}$ are functions that describe the asymptotic behavior of the solutions, i.e. $w_{1,2} \to C_{1,2}\mathcal{A}_{1,2}(\xi)$ as $\xi \to \infty$. The localized solution is found if a pair $C_{1,2}$ leads to (3.2) or (3.3) when (2.13) is integrated in the interval $[0, \xi_f]$ starting from $\xi = \xi_f$.

A shooting algorithm is used to find pairs $C_{1,2}$. The shooting itself is composed of two shooting procedures running one within the other. The first step is to set a given C_1. It is generally useful to set a $|C_1| \ll 1$ if a solution of a fundamental branch, i.e., a branch with solutions satisfying $w_\beta \to 0$, is sought. Then the following algorithm finds a value of C_2 for which $dw_2/d\xi|_{\xi=0}$ is satisfied. The algorithm consists in the following steps:

1. Choose a small C_2, a small step $\delta C_2 \ll 1$ and a small tolerance $\varepsilon \ll 1$. Set

$$w_{1,2}(\xi_f) = C_{1,2}\mathcal{A}_{1,2}(\xi_f). \tag{3.13}$$

2. Integrate (2.13) from $\xi = \xi_f$ to $\xi = 0$.

3. Store
$$D_2^{(0)} = \left.\frac{dw_2}{d\xi}\right|_{\xi=0} \tag{3.14}$$

4. Set $C_2 \to C_2 + \delta C_2$, evaluate steps 1 and 2.

5. Store
$$D_2^{(1)} = \left.\frac{dw_2}{d\xi}\right|_{\xi=0}. \tag{3.15}$$

6. If $D_2^{(0)} D_2^{(1)} > 0$ then the derivative has not changed sign between steps. Make the change $D_2^{(0)} = D_2^{(1)}$ and repeat steps in sequence 4,1, 2, 5 and 6. Else if $D_2^{(0)} D_2^{(1)} < 0$, i.e., the derivative has changed sign between steps. Set $C_2^{(0)} = C_1 - \delta C_2$, $C_2^{(1)} = C_2$ and $C_2 = (C_2^{(0)} + C_2^{(1)})/2$, i.e., calculate the new constant C_2 between the last two iterated values of C_2.

7. Evaluate steps 1 and 2 and store
$$D_2 = \left.\frac{dw_2}{d\xi}\right|_{\xi=0}. \tag{3.16}$$

8. If $D_2 D_2^{(1)} < 0$ then the derivative has changed signs in the interval $[C_2, C_2^{(1)}]$ and substitutions $C_2 \to (C_2 + C^{(1)})/2$ and $D_2^{(0)} = D_2$ are made. If the contrary happens, $D_2 D_2^{(1)} > 0$ then the derivative has changed sign in the interval $[C_2^{(0)}, C_2]$ and the substitutions $C_2 \to (C_2 + C^{(0)})/2$ and $D_2^{(1)} = D_2$ are made.

9. Evaluate $C_2 = (C_2^{(0)} + C_2^{(1)})/2$.

10. Repeat evaluations of 1, 2, 7, 8 and 9 until the tolerance $C_{error} < \varepsilon$, where $C_{error} = |C_2^{(1)} - C_2^{(0)}|$, is attained. This means that the solution is within the interval $[C_2^{(0)}, C_2^{(1)}]$.

See the Fig. 3.1 for a flow chart of the algorithm.

The algorithm described was used to find solutions of (2.13b) with $dw_2/d\xi|_{\xi=0}$ at a good accuracy, i.e., $dw_2/d\xi|_{\xi=0} \sim O(10^{-8})$, for a given C_1. Next it is necessary

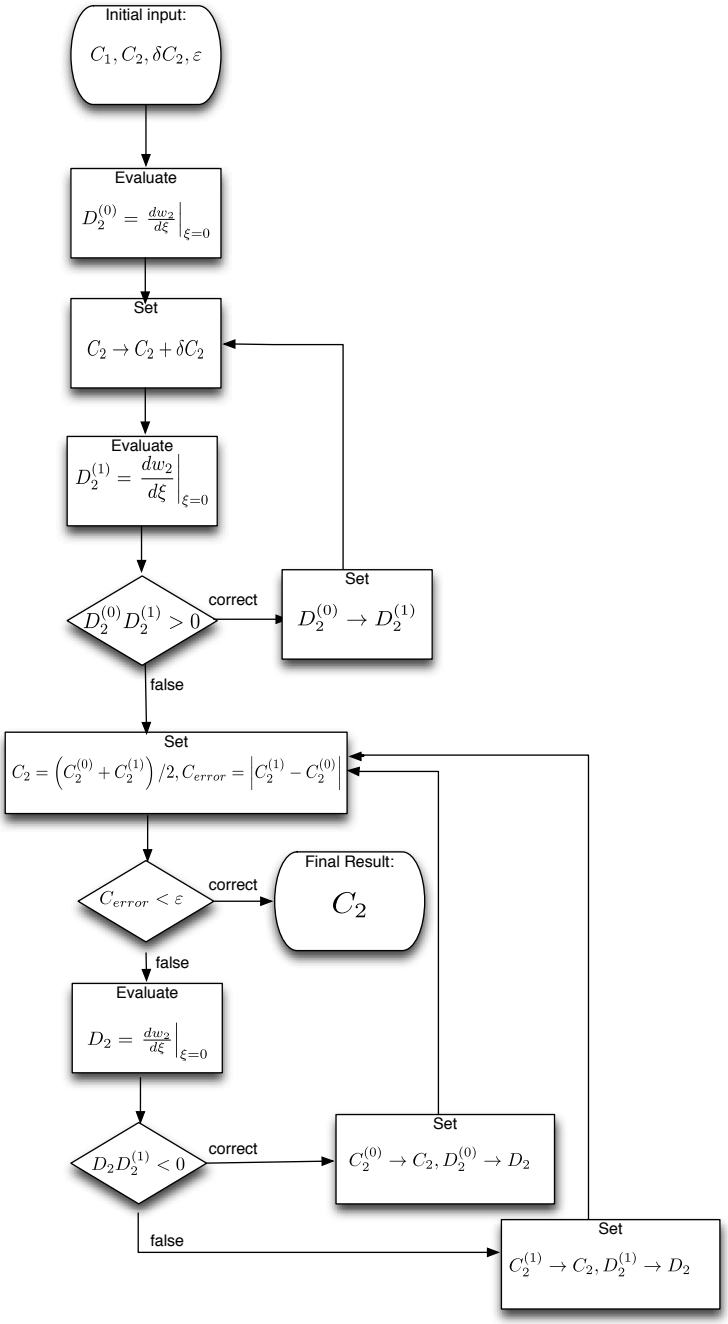

Figure 3.1: Flowchart for the shooting algorithm to find C_2. Each arrow denotes an integration of the initial value problem at $\xi = \xi_f$ using (3.12).

to develop an shooting algorithm in order to find C_1 to satisfy the boundary conditions (3.2) or (3.3). The algorithm is the same, the only difference is that is necessary to substitute C_2, $C_2^{(0,1)}$, D_2 and $D_2^{(0,1)}$ by C_1, $C_1^{(0,1)}$, D_1 and $D_1^{(0,1)}$. The iteration parameters D_1 and $D_1^{(0,1)}$ can be the evaluation of $dw_1/d\xi|_{\xi=0}$ if even w_1 are sought or $w_1(0)$ the search is for odd w_1.

We used integration routine ODE45 of MATLAB® [79] to calculate the initial value problems for (2.13a). The routine is based on the Dormand-Prince method (DOPRI) [80]. The DOPRI method consists on evaluation of Runge-Kutta integrations of order 4 and 5. The error in the step is approximated as the maximal value of the difference between the two integrations. If the error is greater than the specified accuracy the step is reduced iteratively until the tolerance is achieved.

The integration is based in two alternating steps. First integrate (2.13a) starting from the initial point $\xi = \xi_f$ using (3.12), denoted by ${w_{1,2}^*}^{(0)} = w_{1,2}(\xi_f)$, in a small step h keeping w_2 fixed and a temporary $w_1^{*(1)} \approx w_1(\xi+h)$ is stored. Second (2.13b) is integrated using the previous temporary value $\widetilde{w}_1^{(1)}$ in the nonlinear term to find the temporary value of $w_2^{*(1)} \approx w_2(\xi + h)$. Integrations of (2.13a) using $w_1^{*(0)}$ as a initial condition and using $w_1^{*(0)}$ and $w_2^{*(1)}$ in the nonlinear term followed by integrations of (2.13b) using a linear interpolation of values $w_1^{*(0)}$ and $w_1^{*(1)}$ and $w_2^{*(1)}$ as a initial condition, are repeated until $\max\{|w_1^{*(1)} - w_1^{*(0)}|, |w_2^{*(1)} - w_2^{*(0)}|\}$ is lower than the specified tolerance. Note the small step h is not the internal step of in ODE45 routine, where it has the role of integration interval, within the routine the step used is allowed to vary, only the result after integration in the interval h is used.

We mention that the presented shooting method was used extensively to obtain localized solutions in this thesis, it is accurate enough that its use as a seed in the iterative method to be presented in the section below resulted in accurate solutions in very few, usually between 2 to 4, iterations.

3.2 Newton-Raphson method

The method to be described in this section is used to find localized solutions of (2.13). It is used in this thesis in two ways: One is to increase accuracy of

solution obtained with the shooting method. The other use is to obtain solutions of a given branch of solutions by changing slightly b and iteratively obtaining the desired number of solutions within a specified range in b.

It is convenient to write the functions

$$F_1(w_1, w_2, \overline{w}_1, \overline{w}_2) = \frac{d^2 w_1}{d\xi^2} + (\mathcal{V}_1(\xi) - b)\, w_1 + 2 f_1(\xi) \overline{w}_1 w_2, \tag{3.17a}$$

$$F_2(w_1, w_2, \overline{w}_1, \overline{w}_2) = \sigma \frac{d^2 w_2}{d\xi^2} + 2\,(\mathcal{V}_2(\xi) + q - b)\, w_2 + f_2(\xi)\, w_1^2. \tag{3.17b}$$

It follows that if a given solution $\{w_1, w_2, \overline{w}_1, \overline{w}_2\}$, satisfies simultaneously the system of equations

$$F_1(w_1, w_2, \overline{w}_1, \overline{w}_2) = 0, \quad F_2(w_1, w_2, \overline{w}_1, \overline{w}_2) = 0, \tag{3.18}$$

The first step to solve numerically the system (3.17) is discretize the system in a grid with a sufficiently large number N of discretization points

$$\xi^{(n)} = (n-1)L/(N-1) - L/2, \quad n = 1, 2, \ldots N \tag{3.19}$$

in a large interval $[-L/2, L/2]$, with $L \gg 1$, and obtain the discrete versions of $F_{1,2}$

$$\mathcal{F}_1(\mathbf{y}) = 0, \quad \mathcal{F}_2(\mathbf{y}) = 0. \tag{3.20}$$

The following definitions are used

$$\begin{aligned}
\mathbf{y} &= \left(w_1^{(1)}, \ldots, w_1^{(N)}, w_2^{(1)}, \ldots, w_2^{(N)}, \overline{w_1^{(1)}}, \ldots, \overline{w_1^{(N)}}, \overline{w_2^{(1)}}, \ldots, \overline{w_2^{(N)}}\right)^T, \\
\mathcal{F}_{1,2} &= \left(\mathcal{F}_{1,2}^{(1)}, \mathcal{F}_{1,2}^{(2)}, ..., \mathcal{F}_{1,2}^{(N)}\right)^T, \\
\mathbf{w}_{1,2} &= \mathrm{diag}\left(w_{1,2}^{(1)}, w_{1,2}^{(2)}, ..., w_{1,2}^{(N)}\right), \quad w_{1,2}^{(n)} = w_{1,2}\left(\xi^{(n)}\right), \\
\mathbf{f}_{1,2} &= \mathrm{diag}\left(f_{1,2}^{(1)}, f_{1,2}^{(2)}, ..., f_{1,2}^{(N)}\right), \quad f_{1,2}^{(n)} = f_{1,2}\left(\xi^{(n)}\right).
\end{aligned} \tag{3.21}$$

In above T denotes the matrix transpose. The functions $\mathcal{F}_{1,2}$ will be defined

below. The discrete version of the condition $w_{1,2} \to 0$ as $|\xi| \to \infty$ is given by

$$w_{1,2}^{(1)} = w_{1,2}^{(N)} = 0. \tag{3.22}$$

It is convenient to define the vectorial function

$$\begin{aligned} \mathbf{F}(\mathbf{y}) &= \left(\mathcal{F}_1^{(1)}, ..., \mathcal{F}_1^{(N)}, \mathcal{F}_2^{(1)}, ..., \mathcal{F}_2^{(N)}, \overline{\mathcal{F}_1^{(1)}}, ..., \overline{\mathcal{F}_1^{(N)}}, \overline{\mathcal{F}_2^{(1)}}, ..., \overline{\mathcal{F}_2^{(N)}}\right)^T \\ &= \left(\mathcal{F}^{(1)}, \mathcal{F}^{(2)}, \ldots, \mathcal{F}^{(4N)}\right)^T. \end{aligned} \tag{3.23}$$

A solution of (3.20) is equivalent to a solution of $\mathbf{F}(\mathbf{y}) = 0$.

The second order derivatives in (3.17) are approximated by second order central finite differences

$$\left.\frac{d^2 w_{1,2}}{d\xi^2}\right|_{\xi=\xi^{(n)}} \approx \frac{w_{1,2}^{(n+1)} - 2w_{1,2}^{(n)} + w_{1,2}^{(n-1)}}{h^2} \tag{3.24}$$

in (3.20). Thus we have

$$\mathcal{F}_1^{(n)} = \frac{w_1^{(n+1)} - 2w_1^{(n)} + w_1^{(n-1)}}{h^2} + \left(\mathcal{V}_1\left(\xi^{(n)}\right) - b\right) w_1^{(n)} + 2f_1\left(\xi^{(n)}\right) \overline{w_1^{(n)}} w_2^{(n)}, \tag{3.25a}$$

$$\mathcal{F}_2^{(n)} = \sigma \frac{w_2^{(n+1)} - 2w_2^{(n)} + w_2^{(n-1)}}{h^2} + 2\left(\mathcal{V}_2\left(\xi^{(n)}\right) + q - b\right) w_1^{(n)} + f_2\left(\xi^{(n)}\right)\left(w_1^{(n)}\right)^2. \tag{3.25b}$$

The above definitions are valid for the equally spaced discretization (3.19), i.e., $h = \xi^{(n)} - \xi^{(n-1)}$, as defined in (3.19). Note that the boundary condition (3.22) allows one to calculate $\mathcal{F}_{1,2}^{(N)}$ and $\mathcal{F}_{1,2}^{(1)}$ if we set the extensions $w_{1,2}^{(N+1)} = w_{1,2}^{(0)} = 0$.

Now expand the function $\mathbf{F}$ in Taylor series

$$\mathbf{F}(\mathbf{y} + \delta\mathbf{y}) = \mathbf{F}(\mathbf{y}) + \sum_{n'=1}^{4N} \frac{\partial \mathbf{F}}{\partial y_{n'}} \delta y_{n'} + O(\delta \mathbf{y}^2). \tag{3.26}$$

In above $y_{n'}$ are the coordinates of $\mathbf{y}$ as arranged in (3.21). The matrix of partial derivatives in (3.26) is the Jacobian matrix $\mathbf{J} = [J_{n'',n'}]_{4N\times 4N}$. Its matrix elements

are written here as

$$J^{(n'',n')} \equiv J_{n'',n'} \equiv \frac{\partial \mathbf{F}^{(n'')}}{\partial y_{n'}}. \tag{3.27}$$

Next write (3.26) in matrix notation

$$\mathbf{F}(\mathbf{y} + \delta\mathbf{y}) = \mathbf{F}(\mathbf{y}) + \mathbf{J} \cdot \delta\mathbf{y} + O(\delta\mathbf{y}^2). \tag{3.28}$$

Neglect terms of order $\delta\mathbf{y}^2$ and higher and set $\mathbf{F}(y + \delta\mathbf{y}) = 0$ results in the set of linear equations for the corrections $\delta\mathbf{y}$

$$\delta\mathbf{y} = -J^{-1} \cdot \mathbf{F}(\mathbf{y}). \tag{3.29}$$

We use the eig routine from MATLAB® to calculate the inverse matrix J^{-1}. The routine itself takes in account wether the matrix is real symmetric, Hermitian or more generally, complex and non-Hermitian to choose automatically which algorithm it uses. In this thesis the most general case the system (3.29) has a complex valued non-Hermitian matrix J^{-1}. The routine used in this case is ZGGEV [81].

Finally the corrections are added to the solution vector $\mathbf{y}_{\text{old}}$

$$\mathbf{y}_{\text{new}} \to \mathbf{y}_{\text{old}} + \delta\mathbf{y}, \tag{3.30}$$

and the corrected solution vector $\mathbf{y}_{\text{new}}$ is obtained. The routine (3.30) is repeated until the desired accuracy in the solution is obtained. The explicit form of J in the present problem is

$$\mathbf{J} = \begin{pmatrix} L_1 & 2\mathbf{f}_1\overline{\mathbf{w}}_1 & 2\mathbf{f}_1\mathbf{w}_2 & 0 \\ 2\mathbf{f}_2\mathbf{w}_1 & L_2 & 0 & 0 \\ 2\bar{\mathbf{f}}_1\overline{\mathbf{w}}_2 & 0 & \overline{L}_1 & 2\bar{\mathbf{f}}_1\mathbf{w}_1 \\ 0 & 0 & 2\bar{\mathbf{f}}_2\overline{\mathbf{w}}_1 & \overline{L}_2 \end{pmatrix}. \tag{3.31}$$

We have, for the non-zero components of the matrices $L_{1,2}$,

$$\begin{aligned} L_1^{(n,n)} &= -\frac{2}{h^2} + \mathcal{V}_1(\xi^{(n)}) - b, & L_1^{(n,n+1)} &= \frac{1}{h^2}, & L_1^{(n,n-1)} &= \frac{1}{h^2} \\ L_2^{(n,n)} &= -\sigma\frac{2}{h^2} + 2\left(\mathcal{V}_2(\xi^{(n)}) - b\right), & L_2^{(n,n+1)} &= \frac{\sigma}{h^2}, & L_2^{(n,n-1)} &= \frac{\sigma}{h^2}. \end{aligned} \tag{3.32}$$

3.3 Split-step method

In previous sections the tools used to obtain stationary solutions of (2.13) were discussed. The next step is to develop a method to study the dynamics of stationary solutions in the partial nonlinear differential equations (2.9).

The method we use in all numerical simulations of this thesis is the split-step Fourier method. The main ideia of the method is to split the system of nonlinear evolution equations into several steps, which are integrated separately in sequence. The successive integration of each steps can then lead to the evolution of the full system. The main idea of the method appeared in [82] and [83]. In the last years it became popular and used to study dynamics of several physical systems[84, 85].

The main advantage of the method is that integrations of some steps of the evolution equations, such as second-order spatial derivatives such as the one that appears in (2.9), can be performed rapidly in a computer with great accuracy using Fourier transforms. Other steps can generally be integrated by other numerical integration method as Runge-Kutta method.

Today, numerical routines are readily available in books like [86] and also can be used directly in commercial software like MATLAB® and free software like OCTAVE. So here we describe the method and how it is applied it to (2.9). See [87] for several split-step method implementations with MATLAB® code.

Here we assume that after the use of shooting method or Newton-Raphson, a stationary solution $\{w_1, w_2\}$ has been obtained. Next we study the evolution of the initial condition $u_{1,2}(\xi, 0) = w_{1,2}$ in the sytem (2.9). It is convenient to rewrite (2.9) as

$$\frac{\partial u_1}{\partial \zeta} = i\frac{\partial^2 u_1}{\partial \xi^2} + \mathcal{N}_1\left(u_1, u_2\right), \quad \frac{\partial u_2}{\partial \zeta} = i\sigma\frac{\partial^2 u_2}{\partial \xi^2} + \mathcal{N}_2\left(u_1, u_2\right). \tag{3.33}$$

In above

$$\mathcal{N}_1\left(u_1,u_2\right)=i\mathcal{V}_1(\xi)u_1+2if(\xi)\bar{u}_1u_2,\quad \mathcal{N}_2\left(u_1,u_2\right)=2i\left(\mathcal{V}_2(\xi)+q\right)u_2+if(\xi)u_1^2. \tag{3.34}$$

The objective is to integrate Eqs.(3.33) in a small interval $\delta\zeta$ along the ζ direction. We do this in two steps for each equation. The first is to consider of dispersion alone

$$\frac{\partial u_1}{\partial\zeta}=i\frac{\partial^2u_1}{\partial\xi^2},\quad \frac{\partial u_2}{\partial\zeta}=i\sigma\frac{\partial^2u_2}{\partial\xi^2}. \tag{3.35}$$

The field components in a given ζ coordinate are then represented by the values $u_{1,2}^{(n)}$ in the equally spaced grid through the vectors $\mathbf{u}_{1,2}=(u_{1,2}^{(1)},u_{1,2}^{(2)},...,u_{1,2}^{(N)})^T$.

The method we use to integrate (3.35) is based on the discrete Fourier transform (DFT), defined as

$$\tilde{u}_{1,2}^{(K)}=\sum_{n=1}^{N}u_{1,2}^{(n)}\exp\left[(-2\pi i)\left(n-1\right)\left(K-1\right)/N\right], \tag{3.36}$$

and the inverse discrete Fourier transform (IDFT) defined as

$$u_{1,2}^{(n)}=(1/N)\sum_{K=1}^{N}\tilde{u}_{1,2}^{(K)}\exp\left[(2\pi i)\left(n-1\right)\left(K-1\right)/N\right]. \tag{3.37}$$

The question now is how to evaluate the terms of the form $\frac{\partial^2u_{1,2}}{\partial\xi^2}$ in (3.35). The differentiation must be performed on the trigonometric interpolation polynomial of the sets of data points $\{u_{1,2}^{(1)},u_{1,2}^{(2)},...,u_{1,2}^{(N)}\}$, which is defined as

$$p_\beta(\xi)=\frac{1}{N}\left[\tilde{u}_\beta^{(1)}+\sum_{1<K'<N/2+1}\left(\tilde{u}_\beta^{(K')}e^{\frac{2\pi i(K'-1)\xi}{L}}+\tilde{u}_\beta^{(N-K')}e^{-\frac{2\pi i(K'-1)\xi}{L}}\right)\right] \tag{3.38}$$

which approximates the functions $u_{1,2}$ in the continuous interval $[-L/2,L/2]$ and valid for odd N. The form (3.38). Is the minimal band interpolation of $\{u_{1,2}^{(1)},u_{1,2}^{(2)},...,u_{1,2}^{(N)}\}$, i.e., (3.38) has only $|K'|<N/2+1$, which means it has the minimal amount of oscillations between any points $[\xi^{(n)},\xi^{(n+1)}]$ [88].

The second derivative in respect to ξ can be evaluated from (3.38)

$$\frac{\partial^2 p_\beta}{\partial \xi^2} = -\frac{4\pi^2}{NL^2}\left[\sum_{K'=2<N/2+1} (K'-1)^2 \left(\tilde{u}_\beta^{(K')} e^{\frac{2\pi i (K'-1)\xi}{L}} + \tilde{u}_\beta^{(N-K')} e^{-\frac{2\pi i (K'-1)\xi}{L}}\right)\right]. \tag{3.39}$$

Note that (3.39) is obviously independent of ζ. Additonaly the second derivative in respect to ξ of each fourier component evaluated at $\xi^{(n)}$ is equivalent to the multiplication of each component of the original expansion (3.37) by the correspondent component of the vector $\boldsymbol{\kappa}$, where $\boldsymbol{\kappa} = (\kappa_1, \kappa_2, ..., \kappa_N)^T$ and its components defined as

$$\kappa_K = \begin{cases} \left[\frac{2\pi}{L}(K-1)\right]^2 & \text{if } K < N/2 \\ \left[\frac{2\pi}{L}(K-1-N)\right]^2 & \text{if } N/2 < K \leq N. \end{cases} \tag{3.40}$$

The evolution in ζ of the dispersion term in the interval $\delta\zeta/2$ is easily evaluated on the components

$$\tilde{u}_1^{(K)}(\zeta+\delta\zeta/2) = \tilde{u}_1^{(K)}(\zeta)\exp\left(\frac{i\kappa_K \delta\zeta}{2}\right), \quad \tilde{u}_2^{(K)}(\zeta+\delta\zeta/2) = \tilde{u}_2^{(K)}(\zeta)\exp\left(\frac{i\sigma\kappa_K \delta\zeta}{2}\right). \tag{3.41}$$

To obtain the solution in the ξ coordinate it is necessary just to calculate (3.37) using (3.41) to obtain

$$u_{1,2}^{(n)}(\zeta+d\zeta/2) = (1/N)\sum_{K=1}^{N} \tilde{u}_{1,2}^{(K)}(\zeta+d\zeta/2)\exp\left[2\pi i\,(n-1)\,(K-1)\,/(N)\right]. \tag{3.42}$$

The spectral solutions with discrete spatial coordinates given by (3.42) of the partial differential equations (3.35) have spectral accuracy[84, 89], i.e., the error decays at a rate that depends only on the smoothness of the solution.

Now we turn attention to the steps represented by the equations

$$\frac{\partial u_1}{\partial \zeta} = i\mathcal{N}_1(u_1, u_2), \quad \frac{\partial u_2}{\partial \zeta} = i\mathcal{N}_2(u_1, u_2). \tag{3.43}$$

We use the fourth order Runge-Kutta method (see [86]) to obtain the evolu-

tion of (3.43) through an interval $\delta\zeta$. The envelopes after the nonlinear evolution are

$$\mathbf{u}_{1,2}(\zeta+\delta\zeta)=\mathbf{u}_{1,2}(\zeta)+\frac{1}{6}\left(R^{(0)}_{1,2}+2R^{(1)}_{1,2}+2R^{(2)}_{1,2}+R^{(3)}_{1,2}\right), \tag{3.44}$$

with

$$\begin{aligned}
R^{(0)}_1&=\delta\zeta\mathcal{N}_1(\mathbf{u}_1,\mathbf{u}_2),\\
R^{(1)}_1&=\delta\zeta\mathcal{N}_1(\mathbf{u}_1+R^{(0)}_1/2,\mathbf{u}_2),\\
R^{(2)}_1&=\delta\zeta\mathcal{N}_1(\mathbf{u}_1+R^{(1)}_1/2,\mathbf{u}_2),\\
R^{(3)}_1&=\delta\zeta\mathcal{N}_1(\mathbf{u}_1+R^{(2)}_1/2,\mathbf{u}_2),
\end{aligned} \tag{3.45}$$

and

$$\begin{aligned}
R^{(0)}_2&=\delta\zeta\mathcal{N}_2(\mathbf{u}_1,\mathbf{u}_2),\\
R^{(1)}_2&=\delta\zeta\mathcal{N}_2(\mathbf{u}_1,\mathbf{u}_2+R^{(0)}_2/2),\\
R^{(2)}_2&=\delta\zeta\mathcal{N}_2(\mathbf{u}_1,\mathbf{u}_2+R^{(1)}_2/2),\\
R^{(3)}_2&=\delta\zeta\mathcal{N}_2(\mathbf{u}_1,\mathbf{u}_2+R^{(2)}_1/2).
\end{aligned} \tag{3.46}$$

In (3.44) we assume that the nonlinear operator $\mathcal{N}_1$ acts only on $\mathbf{u}_1$ and $\mathcal{N}_2$ acts only on $\mathbf{u}_2$.

Now we describe how all previous considerations combine in a multi-step scheme. We use a symmetric second order split method for the $\mathbf{u}_1$ by evaluating the sequence (3.36), (3.41) and (3.37), the dispersion step. Then we evaluate (3.44) for the (3.43), the nonlinear part step. Note that only formulas related to $\mathbf{u}_1$ are evaluated. After, repeat the sequence for the dispersion step and obtain the evolution at the intermediate step $\delta\zeta$. The next step is to make the same procedure, i.e., calculate the dispersion step, followed by the nonlinear step and another dispersion step, considering changes in $\mathbf{u}_2$ only, to obtain $\mathbf{u}_{1,2}(\zeta+2\delta\zeta)$. Finally, the method is repeated to calculate $\mathbf{u}_{1,2}(\zeta+4\delta\zeta)$ and so on.

Chapter 4

Localized modes in $\chi^{(2)}$ media with $\mathcal{PT}$-symmetric periodic potential

4.1 introduction

The objective of the present Chapter is to introduce a generic one-dimensional (1D) system with the $\mathcal{PT}$-symmetric periodic complex potential and conservative $\chi^{(2)}$ nonlinearity, and construct stable solitons in it. The realization of such a system in the spatial domain is quite possible in optics, using appropriately juxtaposed gain and loss elements, like in Ref. [20], inserted into a $\chi^{(2)}$ medium. We here focus on the search for gap solitons (GSs) in the system with the periodic potential, i.e., localized solutions whose propagation constant belongs to regions of the forbidden propagation (*gaps*) in the underlying linear spectra. Similarly to the usual $\chi^{(2)}$ systems (which do not include gain and loss) [90], the quadratic nature of the nonlinearity makes the interplay between the gaps of the fundamental-frequency (FF) and second-harmonic (SH) fields a fundamental factor affecting GS families. In particular, the generic mechanism of the creation of the families via bifurcations from edges of the bandgaps [87] can work in the FF or SH component, or in both [35]. We here analyze all these possibilities.

The Chapter is organized as follows. The model is introduced in Sec. 4.2. In

Sec. 4.3 results are reported for soliton families found in the model, including the analysis of their stability, using both direct simulations and linearized equations for small perturbations. Some special cases are separately considered in Sec. 4.4 and in Sec. 4.5. The Chapter is concluded by Sec. 4.6.

4.2 The model

We consider the $\chi^{(2)}$ system, based on the evolution equations for the FF and SH components, $u_1(\xi,\zeta)$ and $u_2(\xi,\zeta)$, including the periodic $\mathcal{PT}$-symmetric potential, with an imaginary component of amplitude α, which is assumed to act only onto the FF field:

$$i\frac{\partial u_1}{\partial \zeta} = \frac{\partial^2 u_1}{\partial \xi^2} + \left[V_1\cos(2\xi) + i\alpha\sin(2\xi)\right]u_1 + 2\bar{u}_1 u_2, \tag{4.1a}$$

$$i\frac{\partial u_2}{\partial \zeta} = \frac{1}{2}\frac{\partial^2 u_2}{\partial \xi^2} + 2\left[V_2\cos(2\xi) + q\right]u_2 + u_1^2. \tag{4.1b}$$

Note that the conservative version of model (4.1), with $\alpha = 0$, was studied in Refs. [34, 50], where stable solitons were found.

Basic results are reported below for the situation that corresponds to the periodic potential induced by a material grating etched into the $\chi^{(2)}$ waveguide. We consider $V_1 = V_2$ in Eqs. (4.1).

A *virtual grating* can made by means of the electromagnetically-induced-transparency mechanism in a three-level atomic medium in a planar hollow-core photonic crystal waveguide, see, e.g., Ref. [91, 92]. In this case, the effective periodic potential is resonant, acting only in a narrow spectral interval. It is then reasonable to consider the system with $V_1 \neq 0$ and $V_2 = 0$, when the potential does not affect the SH field, which is far detuned from the resonance, and the opposite case, with $V_2 \neq 0$ and $V_1 = 0$. To illustrate similarities and differences between the different settings, some results for the systems with $V_2 = 0$ (the virtual grating) and $V_1 = V_2 = 0$ (the purely imaginary periodic potential) are presented in Sections 4.4 and 4.5, respectively.

As concerns the loss and gain terms, they may be naturally assumed resonant

(e.g., if both are induced by resonant dopants, with the inverted and uninverted populations in the gain and loss regions, respectively). For this reason, it is natural to assume that these terms are present only in the FF equation, as adopted in the system based on Eqs. (4.1). The opposite situation, with the imaginary potential acting on the SH field, is possible too; it will be considered elsewhere.

We look for LS with propagation constant b in the form of (2.12) where complex functions $w_{1,2}(\xi)$ obey the stationary equations,

$$\frac{d^2w_1}{d\xi^2} + [V_1\cos(2\xi) + i\alpha\sin(2\xi) - b]\,w_1 + 2\overline{w}_1 w_2 = 0, \tag{4.2a}$$

$$\frac{1}{2}\frac{d^2w_2}{d\xi^2} + 2\,[V_2\cos(2\xi) + q - b]\,w_2 + w_1^2 = 0. \tag{4.2b}$$

Generally speaking, Eqs. (4.2) allow for solutions obeying one of the following symmetries: $\{w_1(\xi), w_2(\xi)\} = \{\overline{w}_1(-\xi), \overline{w}_2(-\xi)\}$ or $\{w_1(\xi), w_2(\xi)\} = \{-\overline{w}_1(-\xi), \overline{w}_2(-\xi)\}$. Note also that, in the well-known cascading limit, $|q| \to \infty$ [90], Eq. (4.2b) yields $w_2 \approx -w_1^2/(2q)$, and Eq. (4.2a) amounts to the equation with the cubic nonlinearity,

$$\frac{d^2w_1}{d\xi^2} + [V_1\cos(2\xi) + i\alpha\sin(2\xi) - b]\,w_1 - q^{-1}\,|w_1|^2\,w_1 = 0. \tag{4.3}$$

As mentioned above, solitons in the $\mathcal{PT}$ system based on Eq. (4.3) were recently studied in Refs. [29, 62].

4.3 Gap-soliton families

It is well known that $\chi^{(2)}$ equations have particular solutions with the vanishing FF component, $w_1 \to 0$, while the SH part may either vanish or remain finite [41, 49, 50]. These solutions are usually subject to the parametric instability [90], but they may be stabilized by an additional cubic nonlinearity [93], by an external trapping potential either [94], or by a $\mathcal{PT}$-symmetric localized defect [35].

To identify bifurcations which give rise to GSs from edges of bandgaps, it is also necessary to analyze the situation for $w_1 \to 0$. Generally speaking, one

should then deal with three different cases [35], as shown below.
Case 1: both components are of the same order,

$$w_2 = \mathcal{O}(w_1), \quad w_1 \to 0. \tag{4.4}$$

Case 2: The SH field remains finite:

$$w_2 = \mathcal{O}(1), \ w_1 \to 0. \tag{4.5}$$

Case 3: The SH amplitude scales as the square of the FF amplitude:

$$w_2 = O(w_1^2), \ w_1 \to 0. \tag{4.6}$$

Below, particular features of these three cases are considered separately.

4.3.1 Bifurcation of the nonlinear modes from the linear spectrum

In the limit case defined as per condition (4.4), the nonlinear terms in both equations (4.2) can be neglected, which, at the leading order, results in the system of decoupled linear equations:

$$\frac{d^2A_1}{d\xi^2} + [V_1\cos(2\xi) + i\alpha\sin(2\xi) - b]\,A_1 = 0, \tag{4.7a}$$

$$\frac{d^2A_2}{d\xi^2} + 4\,[V_2\cos(2\xi) + q - b]\,A_2 = 0. \tag{4.7b}$$

We notice that while Eq. (4.7b) is the well known Mathieu equation the linear spectral problem (4.7a) with the $\mathcal{PT}$-symmetric periodic potential was also thoroughly studied in literature [17, 22, 95]. In particular, it is known that subject to constraint $|\alpha| \leq V_1$, equation (4.7a) gives rise to the pure real spectrum. Now we turn to the *combined* bandgap spectrum of Eqs. (4.7), i.e. to the values of the propagation constant b which belong to the spectra of the both spectral problems. We denote by $b_{\beta,k}^{(m)}$ the propagation constant with wave-vector k in the m-th band ($m = 0, 1, 2...$) band for the FF ($\beta = 1$) and SH ($\beta = 2$) components,

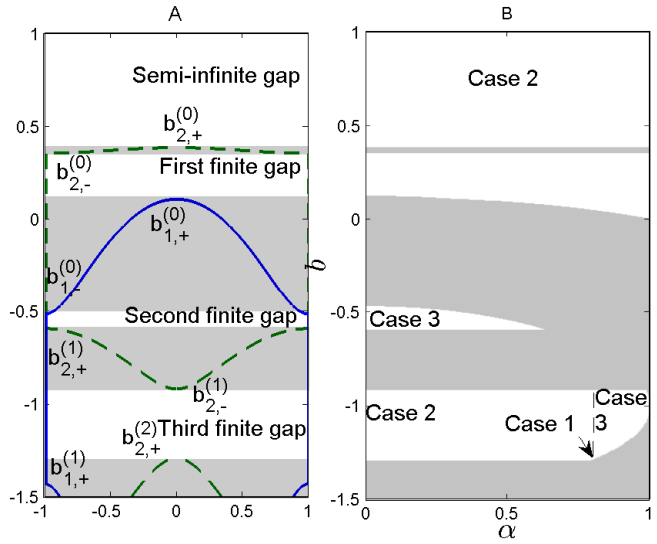

Figure 4.1: Panel A: the spectrum of potential (4.7) with $\alpha = 0.4$. The blue (solid) and green (dashed) curves correspond to the FF and SH components, respectively. Regions of FF- and SH-bands are shaded. The total gap correspond to white domains, as indicated in the figure. Panel B: Propagation constant *vs* the gain-loss coefficient. Edges of the total gap determined by the SH component are identifiable by horizontal lines, as they do not depend on α. The other edges are imposed by the FF component. The other parameters are $V_1 = V_2 = 1$ and $q = 0$.

the latter being computed for $q = 0$ (then propagation constants of the SH with $q \neq 0$ are given by $b_{2,k}^{(m)} - q$). The upper $(+)$ or lower $(-)$ band edges are defined represented by $b_{\beta,\pm}^{(m)}$. Accordingly, the sequence of finite gaps is defined as $\Sigma_\beta^{(m+1)} = \left(b_{\beta,+}^{(m+1)}, b_{\beta,-}^{(m)}\right)$ and the semi-infinite gap is interval $\Sigma_\beta^{(0)} = (b_{\beta,+}^{(0)}, \infty)$. A *total gap* is the intersection of gaps of both components, as illustrated in panel A of Fig. 4.1.

Condition (4.4) requires that in Eqs. (4.7), b is a band edge for the FF and SH components simultaneously (this situation is illustrated in the right panel of Fig. 4.2) because otherwise one linear modes of (4.7) would decay with a rate faster than the other, invalidating (4.4) for large ξ.. Since the band edges of the FF and the SH are in general independent, to let case (4.4) occur, and hence to let a branch bifurcate from the band edge $b_{1,\pm}^{(m)}$ of the FF, we have to impose the

following condition,

$$b_{1,s}^{(m)} = b_{2,s}^{(m')} - q, \quad s = \pm \tag{4.8}$$

where m' can be any band of the SH. Note, however, that only edges of the same type allow the existence of the bifurcation we are dealing with, which justifies the same sign, + or −, on both sides of Eq. (4.8). Indeed, as one can see in panel A of Fig. 4.1, the individual gaps are located directly above (below) the band edges $b_{\beta,+}^{(m)}$ ($b_{\beta,-}^{(m)}$).

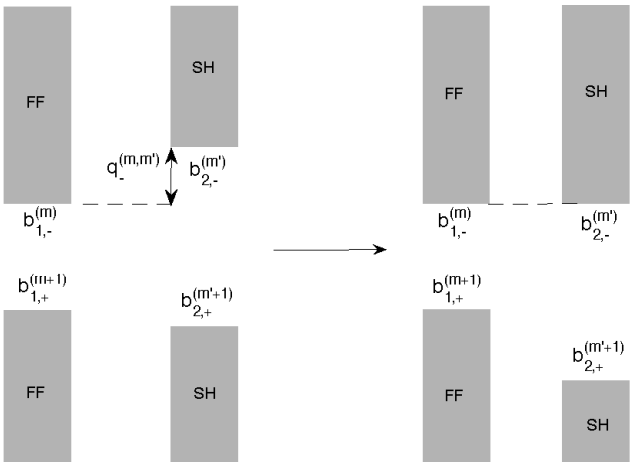

Figure 4.2: A schematic diagram illustrating matching the band edges of the FF and SH for configuration of the Case 1. The left part of the figure represents the system without mismatch ($q = 0$). The arrow in the middle shows to what configuration the band structure is transfered when the mismatch $q = q_{-}^{(m,m')}$, resulting in the existence of the total gap, is imposed.

Once we impose condition (4.8), we force individual gaps to have at least one common edge. Then the total gap only exists if this edge is either the lower or upper one for the both bands simultaneously, as illustrated by Fig. 4.2.

Condition (4.8) imposes constraints on the design of the periodic structure. Typically, V_β would be fixed, and one could change the concentration of the dopant, which amounts to varying the amplitude of the imaginary part of the potential, α, or mismatch q. Accordingly, for given values values of $b_{1,s}^{(m)}$ and $b_{2,s}^{(m')}$, which are determined by the real part of the potential, it is possible to

satisfy Eq. (4.8) by setting $q = q_s^{(m,m')}$, where

$$q_s^{(m,m')} = b_{1,s}^{(m)} - b_{2,s}^{(m')}, \quad s = \pm. \tag{4.9}$$

All edges of the FF and the SH bands may be, in principle, matched with $q = q_s^{(m,m')}$. Additionally it is possible to match the edges by tuning α alone, as can be seen in the third gap of panel B in Fig. 4.1 for $q = 0$. It is also possible to see that Case 1 in the semi-infinite gap cannot be realized solely through adjusting α.

4.3.1.1 Solitons in the semi-infinite gap

Here and in the rest of the Chapter, localized solutions satisfying zero boundary conditions were calculated numerically using the shooting method described in

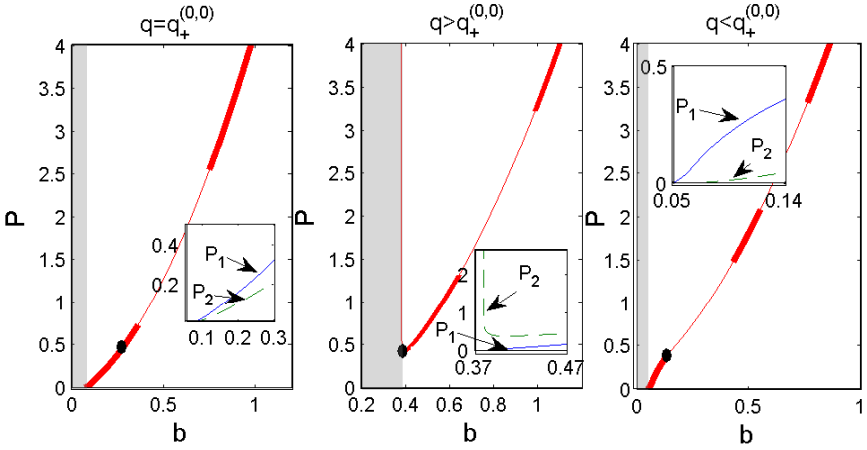

Figure 4.3: Branches of fundamental solitons for $\alpha = 0.7$ and different values of q, found in the semi-infinite gap. The left, central, and right panels correspond to cases 1, 2, and 3, with values $q = q_+^{(0,0)} = -0.316$, $q = 0$ and $q = -0.5134$ respectively [see Eqs. (4.4), (4.5), and (4.6)]. Insets show power components P_1 (line) and P_2 (dashed line) close to an edge of the semi-infinite total gap. Here and below, thick and thin lines represent stable and unstable solutions, respectively. Shaded regions denote bands of the FF and/or SH. Parameters are $V_1 = V_2 = 1$ and $\alpha = 0.7$.

detail in Section 3.1 for the conservative case, $\alpha = 0$, which will be described

in the Chapter 5, and then extended to given $\alpha > 0$ by means of the Newton-Raphson method. In Fig. 4.3, we display branches of the fundamental solitons,

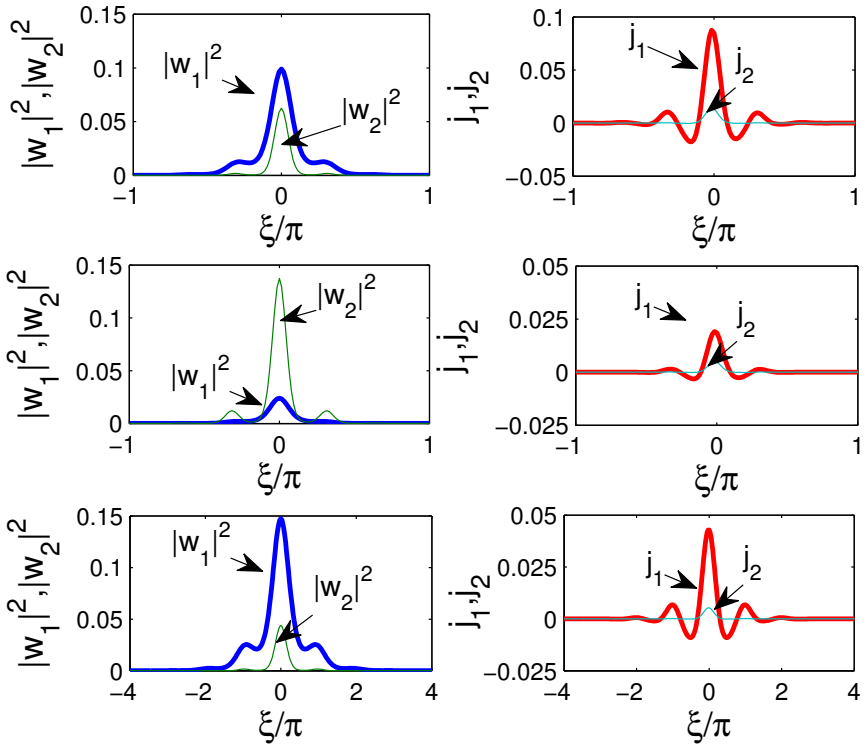

Figure 4.4: Examples of stable fundamental solitons found in the semi-infinite gap pertaining to all the three cases, which are indicated by black circles in Fig. 4.3. The upper panels correspond to case 1, with $b = 0.25$ and band-edge matched with $q = q_+^{(0,0)} = -0.316$. The middle panels correspond to case 2, with $b = 0.43$ and $q = 0$. Lower panels show a solution of case 3 with $b = 0.21$ and $q = -0.5134$. The parameters are $V_1 = V_2 = 1$ and $\alpha = 0.7$.

found numerically in the Case 1 in the semi-infinite gap, using matching $q = q_+^{(0,0)}$. The branches are presented in the plane (b, P), where the total power P is given by

$$P = P_1 + P_2, \quad P_\beta \equiv \beta \int_{-\infty}^{\infty} |w_\beta|^2 d\xi. \tag{4.10}$$

Examples of fundamental soliton solutions, i.e. the energy flows in each component as well as the currents are defined as

$$j_\beta(\xi) = |w_\beta|^2 \frac{d\theta_\beta}{d\xi}, \qquad \theta_\beta(\xi) = \arg\, w_\beta(\xi), \tag{4.11}$$

corresponding to the total power $P = 0.5$ are shown in Fig. 4.4. We observe, that while the currents having maximum in the center and domains with alternating sign, have very similar shapes of the spatial profiles, the power density is mainly concentrated in the FF and SH in the Cases 3 and 2, respectively and is approximately equally split between the two components in the Case 1 (as this is expected due to (4.4)). In all three cases the real valued FF current j_1 has a significantly higher amplitude than the current of the SH, j_2, i.e. the balance between gain and losses is accomplished mainly due to the FF.

4.3.1.2 Solitons in the third finite gap

The main focus of this Chapter is on the effects of the gain-loss coefficient α on branches of the fundamental solitons. To concentrate on this point, in what

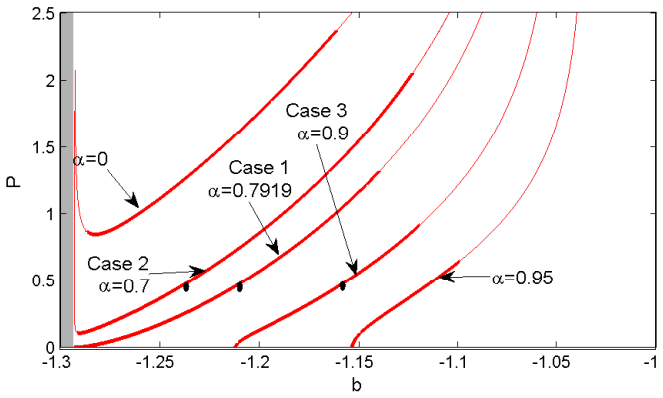

Figure 4.5: Branches of fundamental GSs found in the third finite gap for several values of amplitude α of the imaginary part of the periodic potential. All the three cases, 1, 2, and 3, which are defined as per Eqs. (4.4), (4.5), and (4.6), respectively, are presented. The gray region denotes the band of the SH component. The parameters are $V_1 = V_2 = 1$, $q = 0$.

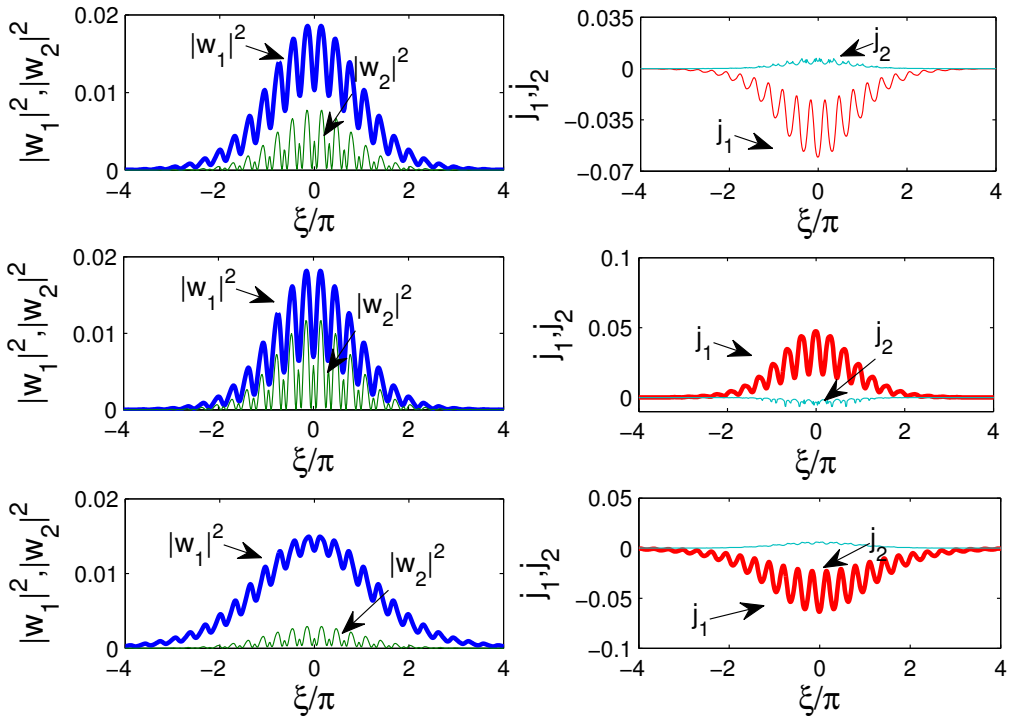

Figure 4.6: Examples of stable fundamental gap solitons in the third finite gap pertaining to all the three cases, which are indicated by black circles in Fig. 4.5. The upper panels corresponds to Case 1, with $b = -1.207$ and band-edge matched with $\alpha = 0.7919$. The middle panels correspond to Case 2, with $b = -1.234$ and $\alpha = 0.7$. Lower panels shows a solution of Case 3 with $b = 1.553$ and $\alpha = 0.9$. The total power of all the three solitons is $P = 0.5$. The parameters are $V_1 = V_2 = 1$, $q = 0$.

follows we set $q = 0$. For this choice it turns out possible to obtain the matching condition $b^{(1)}_{1,+} = b^{(2)}_{2,+} = 1.29$ only in the third finite gap at $\alpha = 0.792$ (the value indicated by an arrow in Fig. 4.1B). In this context the consideration of the third gap becomes particularly relevant, as one can examine all three cases using only small deviations in parameter α.

The respective modifications of the branches subject to variation of the amplitude of the imaginary part of the potential α are illustrated Fig. 4.5. Examples of the profiles of the respective gap solitons are shown in Fig. 4.6, where all three

presented solutions have the same energy flow: $P = 0.5$. The most significant distinction with the situation observed in Fig. 4.4 for the solitons in the semi-infinite gap is that (i) now the intensity of the FF is always bigger than the intensity of the SH and (ii) the energy currents of the FF and SH are counter propagating and having constant signs (the current j_1 is negative while j_2 positive).

4.3.2 Stability analysis

The stability of the solutions found as outlined above was tested in direct simulations using the split-step method described in Section 3.3, as well as within the framework of the linear stability analysis as described in Appendix B. Turning

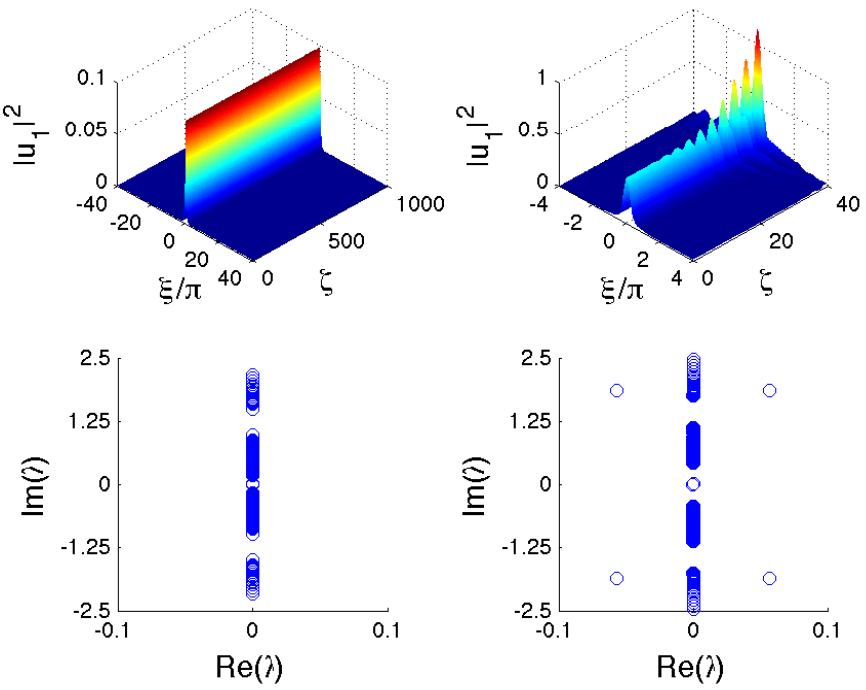

Figure 4.7: Top plots: The evolution of two GS solutions with 10% of amplitude random perturbations in Case 1 [see Eq. (4.4)] in the semi-infinite gap. Left panel has $b = 0.25$ and is stable. The right panel corresponds to unstable evolution of a solution with $b = 0.5$. The corresponding eigenvalues of small perturbations are shown in the lower panels. The parameters of the structure are $V_1 = V_2 = 1$, $\alpha = 0.7$ and $q = q_+^{(0,0)} = -0.316$.

now to the stability properties of branches located in the semi-infinite gap, we obtain that the fundamental branches may have one or more instability intervals (see Fig. 4.3). The lengths of these intervals increase with α approaching the $\mathcal{PT}$-symmetry breaking point. This is a feature observed in all the cases considered below for semi-infinite gaps.

In Fig. 4.7 we show examples of the evolution of stable and unstable localized solutions. The observed oscillatory instability is due to a quartet of complex λ and instability develops as amplitude oscillations that increase with ζ.

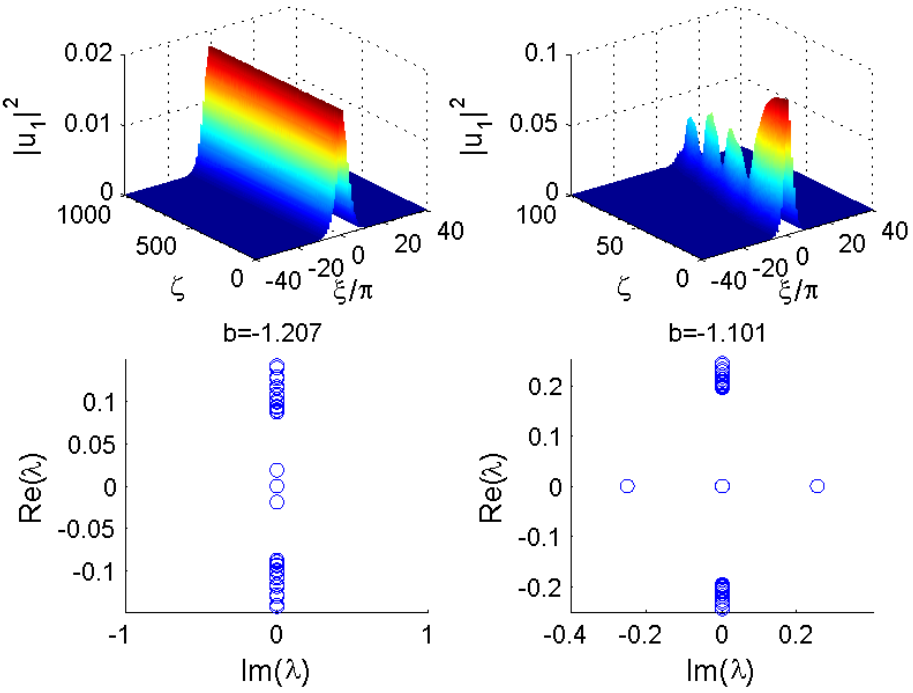

Figure 4.8: Top plots: The evolution of two GS solutions with 10% of amplitude random perturbations in Case 1 [see Eq. (4.4)] in the third finite gap. Left panel has $b = -1.207$ and is stable. The right panel corresponds to unstable evolution of a solution with $b = -1.101$. The corresponding eigenvalues of small perturbations are shown in the lower panels. The parameters of the structure are $V_1 = V_2 = 1$, $\alpha = 0.7919$ and $q = q_+^{(0,0)} = 0$.

Stability of the solitons of the fundamental branches in the third finite gap (Case 1 with $\alpha = 0.792$) is shown in Fig. 4.5. We observe an interval of stability

which starts at the bifurcation point $b = b^{(1)}_{1,+} = b^{(2)}_{1,+} = 1.29$, the rest of the branch corresponding to unstable solutions.

Explicit examples of the direct propagation compared with the linear stability analysis are shown in Fig. 4.8. Stable and unstable GSs with slightly modified b belonging to the third finite gap are shown in the left and right columns, respectively. The two eigenvalues of the stable solution collide when b is varied and assume purely imaginary values. It can be seen in the upper right panel that the perturbed solution decays very rapidly.

4.3.3 Nonlinear modes without linear limit

Now we turn to numerical studies of solutions satisfying condition (4.5), in the vicinity of the total gap, which coincides with an m-th SH gap edge, i.e. with $b^{(m)}_{2,s}$. While FF component is vanishing in this case, i.e. $w_1 \to 0$ as $b \to b^{(m)}_{2,s}$, the amplitude of the SH w_2 persists finite while its width increases (i.e. the SH in this limit becomes delocalized).

In particular, the effect of the delocalization is responsible for the grows of the total power, i.e. divergence of P, at $b \to b^{(0)}_{2,+}$ and $\alpha = 0.7$ shown in the central panel of Fig. 4.3 and at $b \to b^{(2)}_{2,+}$ shown in Fig. 4.5 for the branches with $\alpha = 0$ and $\alpha = 0.7$. Note that, in branches of Case 2 represented in Fig. 4.5 for both $\alpha = 0$ and $\alpha = 0.7$, P diverges at the same $b = b^{(2)}_{2,+}$, as the spectrum of Eq. (4.7b) is independent of α. Similar results for the conservative system, with $\alpha = 0$, were previously obtained in Refs. [34, 50]. On the other hand, no delocalization of the SH component was observed for the branches satisfying condition (4.5) in Ref. [35], where a $\mathcal{PT}$-symmetric localized potential was considered, since the bifurcation of the second harmonic in that case departed from the localized defect state. The SH amplitude, we denote it by $C_2 = \max|w_2|$, of a solution with b close to $b^{(m)}_{2,s}$, i.e., at $|b - b^{(m)}_{2,s}| \ll 1$, depends on the phase mismatch and on the gain-loss coefficient.

This is illustrated in the left panel of Fig. 4.9, where we display plots C_2 *vs.* α, calculated at the SH edge $b = b^{(1)}_{2,+}$ which coincides with the edge of the third finite gap (like this is illustrated in the panel A of Fig. 4.1) for fixed $q = 0$. In the right panel of Fig. 4.9 we show dependence of C_2 on the mismatch q at the

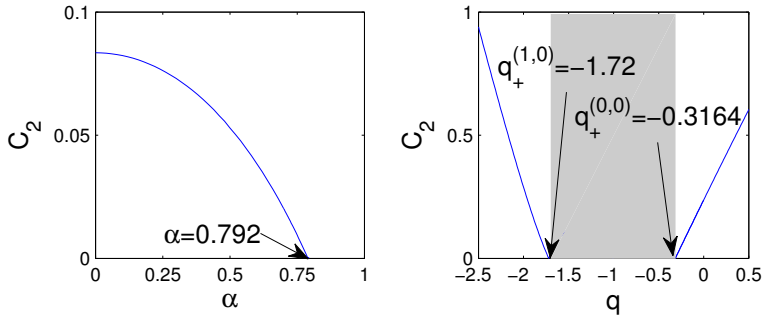

Figure 4.9: Left panel: C_2 *vs.* α at the SH edge $b = b^{(1)}_{2,+} = -1.293$ of the third finite gap for $q = 0$. $C_2 = 0$ at $b^{(1)}_{1,+} = b^{(1)}_{2,+}$. Right panel: C_2 *vs.* q for $\alpha = 0.7$, at the edge $b = b^{(0)}_{2,+} = 0.3784$. The shaded region represents the interval where $b = b^{(0)}_{2,+} + q$ falls inside the band $[b^{(0)}_{1,-}, b^{(0)}_{1,+}]$. $C_2 = 0$ at $q = q^{(0,0)}_{+}$ and $q = q^{(1,0)}_{+}$. The parameters are $V_1 = V_2 = 1$.

SH edge $b = b^{(0)}_{2,+}$ coinciding with the semi-infinite gap edge for fixed $\alpha = 0.7$.

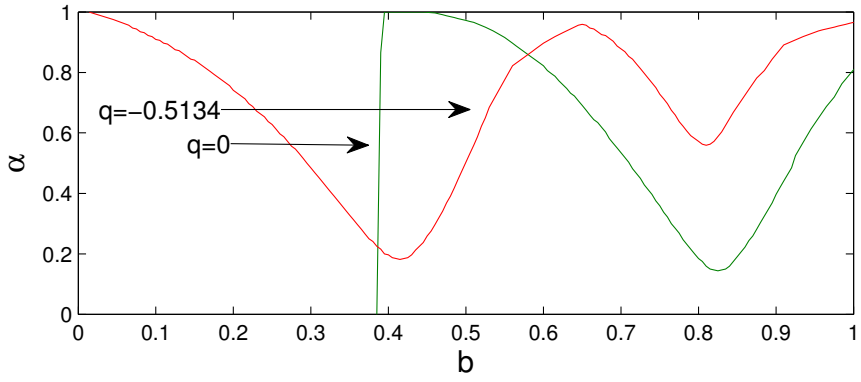

Figure 4.10: The boundary between stable (below the curves) and unstable (above the curves) gap-soliton solutions in the plane of (b, α) obtained from the linear-stability analysis. The curve with $q = 0$ represents a Case 2 branch bifurcating from $b^{(0)}_{2,+} = 0.3786$ and the curve with $q = -0.5134$ represents a Case 3 branch bifurcating from $b^{(0)}_{1,+}$. Note that while $b^{(0)}_{2,+}$ can be identified easily in the Case 2 curve as the point where the curve goes to $\alpha = 0$, $b^{(0)}_{1,+}$ is not fixed because it depends on α (See panel B of Fig. 4.1). The parameters are $V_1 = V_2 = 1$.

We found that $C_2 \to 0$ in the $C_2(\alpha)$ and $C_2(q)$ depends on the specific value

of the gain-loss coefficient: at $\alpha \approx 0.7919$ and $q = q_+^{(m,0)}$ respectively. In respect to values in which $C_2(q) \to 0$ we obtain this whenever q just adjusts the edge of the SH band-edge, which in the present analysis is $b = b_{2,+}^{(0)}$, to be located exactly of an edge of the FF of the same type (in the figure this means it is a edge of upper type, +), exactly as described by formula (4.9). In Fig. 4.9 we show only the values $q = q_+^{(0,0)}$ and $q = q_+^{(1,0)}$, which translates to the matching of edges $b_{1,+}^{(0)} = b_{2,+}^{(0)} + q_+^{(0,0)}$ and $b_{1,+}^{(1)} = b_{2,+}^{(0)} + q_+^{(1,0)}$. In respect to the left panel of Fig. 4.9, $C_2(\alpha)$ vanishes at the given value of the gain-loss coefficient corresponding to the situation when the edges of the FF and SH gaps coalesce (i.e. $b_{1,+}^{(1)} = b_{2,+}^{(2)}$). Thus,

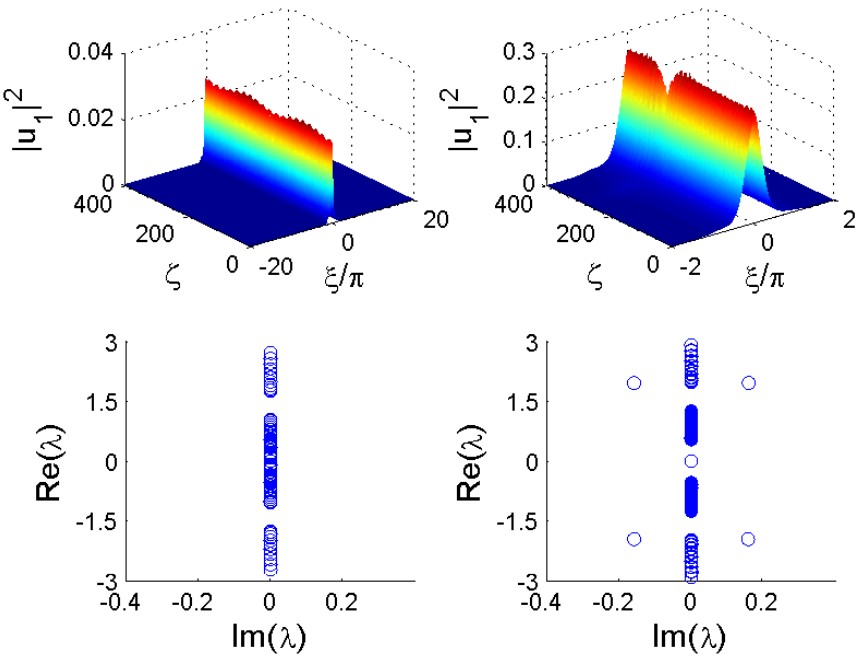

Figure 4.11: Top plots: The evolution of two GS solutions with 20% of amplitude random perturbations in Case 2 [see Eq. (4.5)] in the semi-infinite gap. Left panel has $b = 0.4$ and is stable. The right panel corresponds to unstable evolution of a solution with $b = 0.6$. Note that the linearly unstable solution remains localized. The corresponding eigenvalues of small perturbations are shown in the lower panels. The parameters of the structure are $V_1 = V_2 = 1$, $\alpha = 0.7$ and $q = 0$.

whenever $C_2 \to 0$ is attained by a proper choice of α or q, both the FF and SH components emerge with infinitely small amplitudes $w_{1,2}$ when condition (4.8) is

met, i.e., when Case 2 merges with Case 1.

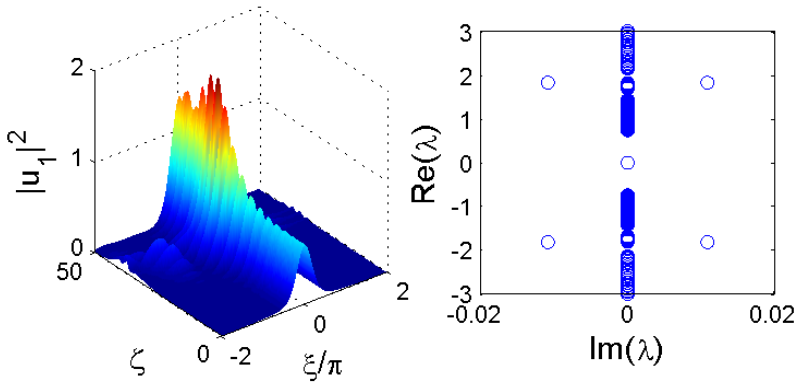

Figure 4.12: Left plot shows the evolution of an unstable localized solution with $b = 0.8$ added by 10% of amplitude random perturbations in Case 2 [see Eq. (4.5)] in the semi-infinite gap. The right plot shows the corresponding eigenvalues of small perturbations. The parameters of the structure are $V_1 = V_2 = 1$, $\alpha = 0.7$ and $q = 0$.

Examples of field profiles $w_{1,2}$ pertaining to the fundamental GS branches in the semi-infinite and in the third finite bandgap are displayed in middle panels of Figs. 4.4 and 4.6, respectively. In both figures the solutions are in the region close to the respective SH band edges $b_{2,+}^{(0)}$ and $b_{2,+}^{(1)}$ where (4.5) is satisfied.

As concerns the stability of the GSs, Case 2 has one notable difference in the semi-infinite and in the third finite gaps in comparison with Case 1, whenever a given branch satisfying (4.5) bifurcates from a SH edge $b_{2,s}^{(m)}$, a small unstable region close to $b_{2,s}^{(m)}$ that persists even when $\alpha = 0$ exists. In Fig. 4.10 the curves separating stable and unstable solutions of the fundamental branch values of $q = 0$ and $q = -0.5134$ are shown in the plane (b, α). The Case 2 branch is the curve with $q = 0$ in the semi-infinite gap, where can be seen stability threshold abruptly decays to zero. The other curve with $q = -0.5134$ a Case 1 bifurcation, it do not share this property. In both curves is possible to see that, as we reported in the previous section, there may be one or more unstable intervals with lenghts that increase with α.

Examples of the propagation of stable and unstable solutions with variations

in b in the semi-infinite gap are shown in Fig. 4.11. Instability appear due to the collision of internal modes with the band edges of the spectrum of (B.3) resulting in four complex eigenvalues λ. The propagation however shows that the perturbed solution can remain localized despite amplitude oscillations as is possible to see in the upper left panel of Fig. 4.11. At about $\zeta = 300$ there is an emission of energy from the localized field region but the structure quickly regains energy and remains localized. However not all linearly unstable solutions have this behaviour. In Fig. 4.12 we show an unstable solution that rapidply

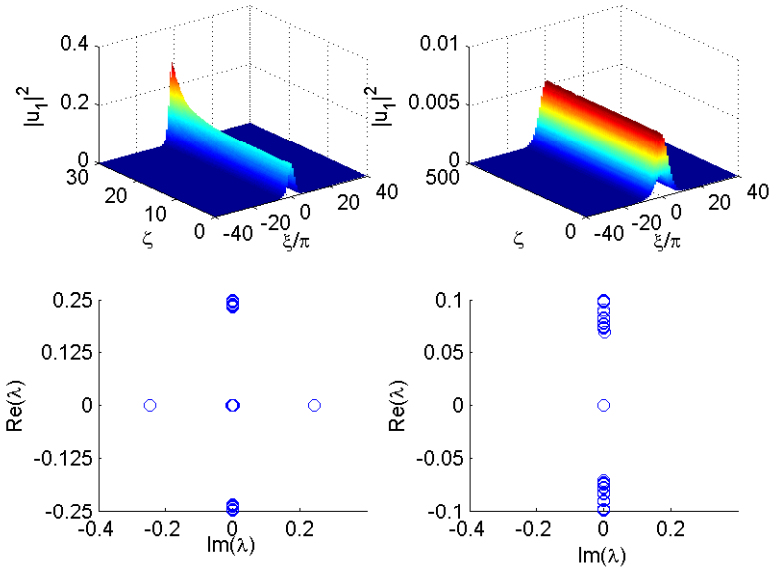

Figure 4.13: Top plots: The evolution of two GS solutions with 10% of amplitude random perturbations in Case 2 [see Eq. (4.5)] in the third finite gap. Left panel has $b = -1.11$ and is unstable. The right panel corresponds to stable evolution of a solution with $b = -1.268$. The corresponding eigenvalues of small perturbations are shown in the lower panels. The parameters of the structure are $V_1 = V_2 = 1$, $\alpha = 0.7$ and $q = 0$.

decays.

Examples of solutions in the third finite gap with slightly different b are shown in Fig. 4.13. Unstable eigenvalue with positive λ appear when b is slightly bigger than $b = -1.268$ of the stable solution. Instability develops as a rapid increase

of the amplitudes of the intensities $|w_{1,2}|^2$ with propagation.

4.3.4 Modes with negligible second-harmonic

Finally, we consider GS branches generated by bifurcations which obey condition (4.6) satisfied in a vicinity of the FF edge of the total gap, $b = b_{1,s}^{(m)}$. The branch

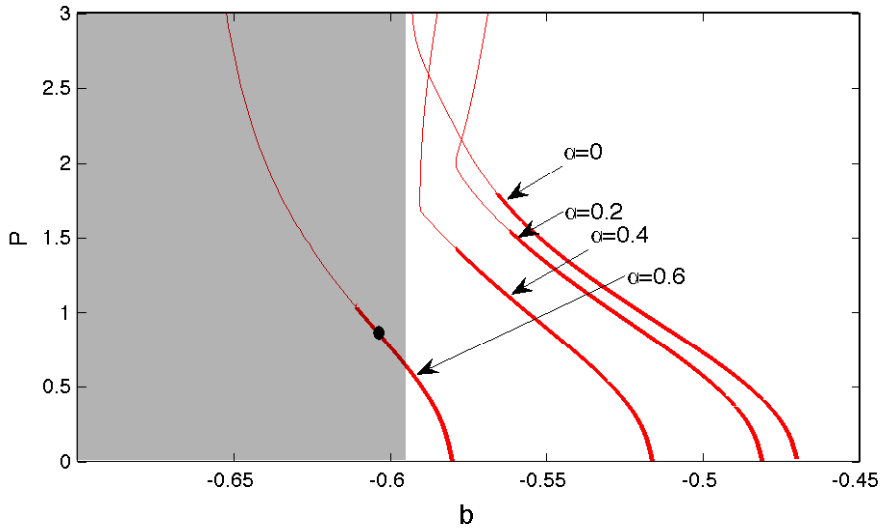

Figure 4.14: Branches of fundamental GSs for several values of α in the second finite gap. The bifurcations are of the Case 3 type. The shaded region denotes the band of the SH component. The branches extend into the SH band, as *embedded solitons*, atr $\alpha > 0.41$. Thick and thin lines represent stable and unstable solutions, respectively. The parameters are $V_1 = V_2 = 1$, $q = 0$.

of the fundamental GS solutions pertaining to Case 3 is displayed in the right panel of Fig. 4.3 for the semi-infinite gap.

An example of GS solution is displayed in the lower panels Fig. 4.4. It can be seen that $|w_1|^2$ has a much higher amplitude than $|w_2|^2$. Fundamental branches of Case 3 are also represented by the branches with $\alpha = 0.9$ and $\alpha = 0.95$ in Fig. 4.5 for the third gap. An example of the respective field profiles for the GS branch in the third finite bandgap, bifurcating from $b_{1,+}^{(1)}$, is shown in the lower panels of Fig. 4.6. Also in the same figure, can be noted that while $|w_1|^2$ is strictly positive, j_1 is strictly negative. The current j_2 is strictly positive.

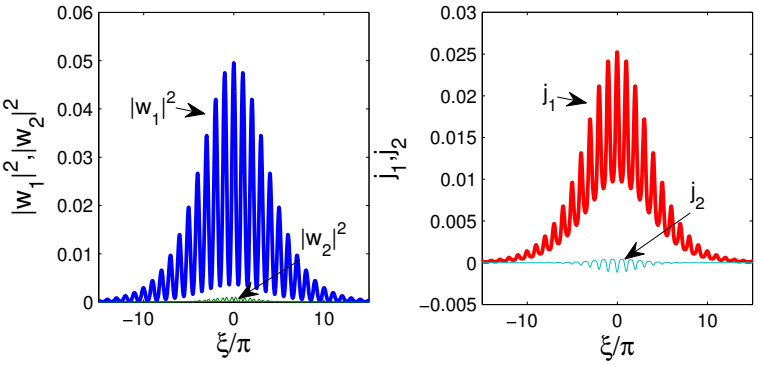

Figure 4.15: An example of a stable *embedded soliton* with $b = -0.6$, indicated by the black circle in Fig. 4.14 inside the SH band. This solution belongs to the branch of fundamental solitons that bifurcates from $b^{(0)}_{1,-}$ in the second finite gap. The parameters are $\alpha = 0.6$, $V_1 = V_2 = 1$ and $q = 0$.

We observe in Fig. 4.14, where branches for several values of α are found in the second finite gap, that the branch which bifurcates from $b^{(0)}_{1,+}$ at $\alpha = 0.6$ goes into the band of the SH, where it becomes a family of *embedded solitons* (ESs) [96, 97], i.e., those existing inside (*embedded into*) the continuous spectrum. The existence of such solitons is explained by fact that their decaying asymptotic tails at $|\xi| \to \infty$ follow relation (4.6), hence the SH equation is *non-linearizable* for the decaying tails, invalidating the standard argument for the non-existence of solitons whose propagation constant falls into the band. We have found that the GS branches extend into the SH band for $\alpha > 0.41$. In Fig. 4.15 we show a typical example of stable ES. In particular is possible to see that both $|w_{1,2}|^2$ decay rapidly despite being in the SH band. Note that no ESs were found for the conservative version of the present system, with $\alpha = 0$ [34, 50]. Embedded solitons were found in Ref. [97] in the conservative model without the potential ($V_1 = V_2 = 0$), but with cubic nonlinear terms added to the equations, otherwise only *quasi-solitons* can be found, with non-vanishing tails at $|\xi| \to \infty$ [98]. Furthermore, in the conservative system the ESs were found only at discrete values of b. A noteworthy feature of ESs in the present system is that a part of their family is stable, as seen in Fig. 4.14 and in the left panels of Fig. 4.16 while in the conservative system the isolated ES is *semi-stable* (in Ref. [97], the ES was stable against

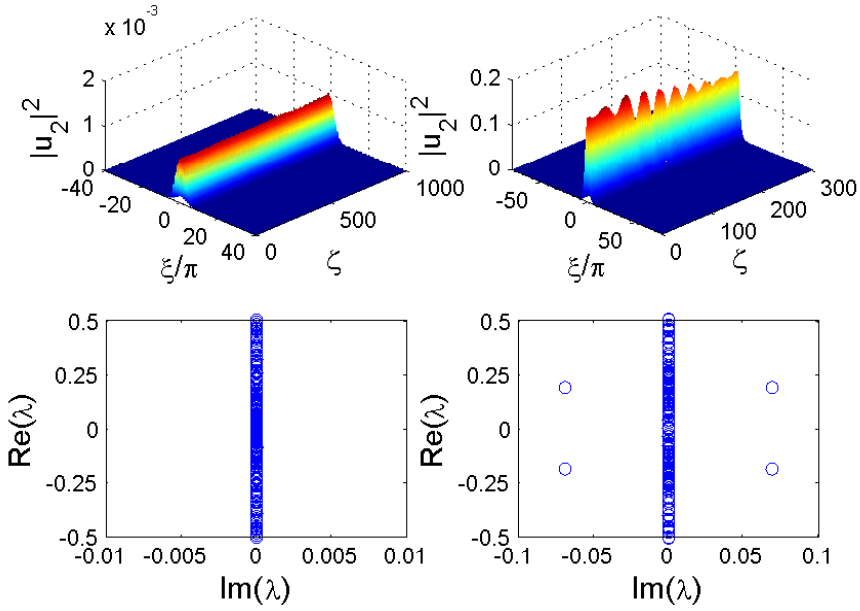

Figure 4.16: Top plots: The evolution of two GS solutions with 10% of amplitude random perturbations in Case 3 in the second finite gap. Left panel has $b = -0.6$ and is stable. The right panel corresponds to unstable evolution of a solution with $b = -0.65$. The corresponding eigenvalues of small perturbations are shown in the lower panels. The parameters of the structure are $V_1 = V_2 = 1$, $\alpha = 0.6$ and $q = 0$.

perturbations that increased the total power, but unstable against those which decreased it). The unstable perturbations in the semi-stable conservative system grow *sub-exponentially* [in fact, as ζ^2, rather than as $\exp(\text{const} \cdot \zeta)$]. In our system, the gain component supplies the power and helps to stabilize perturbed solitons, see Fig. 4.17. Instability, when it appears, is due to the emergence of quartets of complex eigenvalues, as is possible to see in the right panels of Fig. 4.17. The propagation of perturbed unstable solution revealed that the decay is oscillatory (See right panels of 4.16). We also mention that in Ref. [99] continuous families of ESs in a system with a cubic nonlinearity were found for moving solitons in the plane of (v, b), where v is the soliton's velocity. However, the ES solutions still formed discrete sets for any given v, including the case of the quiescent solitons, $v = 0$, considered here. To the best of our knowledge, the

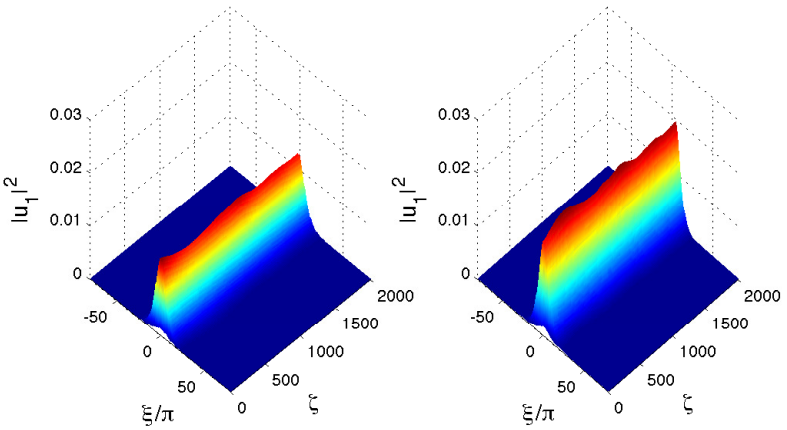

Figure 4.17: An example of the stable evolution of the GS with $b = -0.6$, indicated by the black circle in Fig. 4.14, inside the SH band pertaining to the fundamental branch that bifurcates from $b^{(1)}_{1,+}$, in the third finite gap. In the left panel the initial condition is $u_{1,2}(\xi, 0) = 0.95 \cdot w_{1,2}(\xi)$ and in the right panel it is $u_{1,2}(\xi, 0) = 1.05 \cdot w_{1,2}(\xi)$. In both cases, the soliton is stable. The parameters are $\alpha = 0.6$, $V_1 = V_2 = 1$ and $q = 0$.

present system furnishes the first example a continuous branch of ESs in a system with a purely quadratic nonlinearity, a part of the branch being stable. In the semi-infinite gap, the behavior of solitons in Case 3 is similar to that in Case 1, outlined above, with one or more alternating stable and unstable intervals, whose lengths depend on the gain-loss strength, α. In Fig. 4.18 we show examples of stable and unstable evolutions in the semi-infinite gap. The linear stability analysis shows four complex eigenvalues in the case of the unstable solution. Dynamics shows that instability develops as increasing amplitude oscillations.

In all the finite gaps, we have found two regions, one stable, starting at the bifurcation point, and the other unstable, as one can see in Fig. 4.3 for values $\alpha = 0.9$ and $\alpha = 0.95$ and Fig. 4.14. In Fig. 4.19 we show examples of stable and unstable solutions in the second-finite gap. The linear stability analysis shows that in the unstable solution the eigenvalues responsible for the instability are purely real. Dynamics shows that the amplitude of the perturbed unstable solution grows without oscillations.

Lastly, stable solutions have never been found for $|\alpha| > V_1$. This conclusion

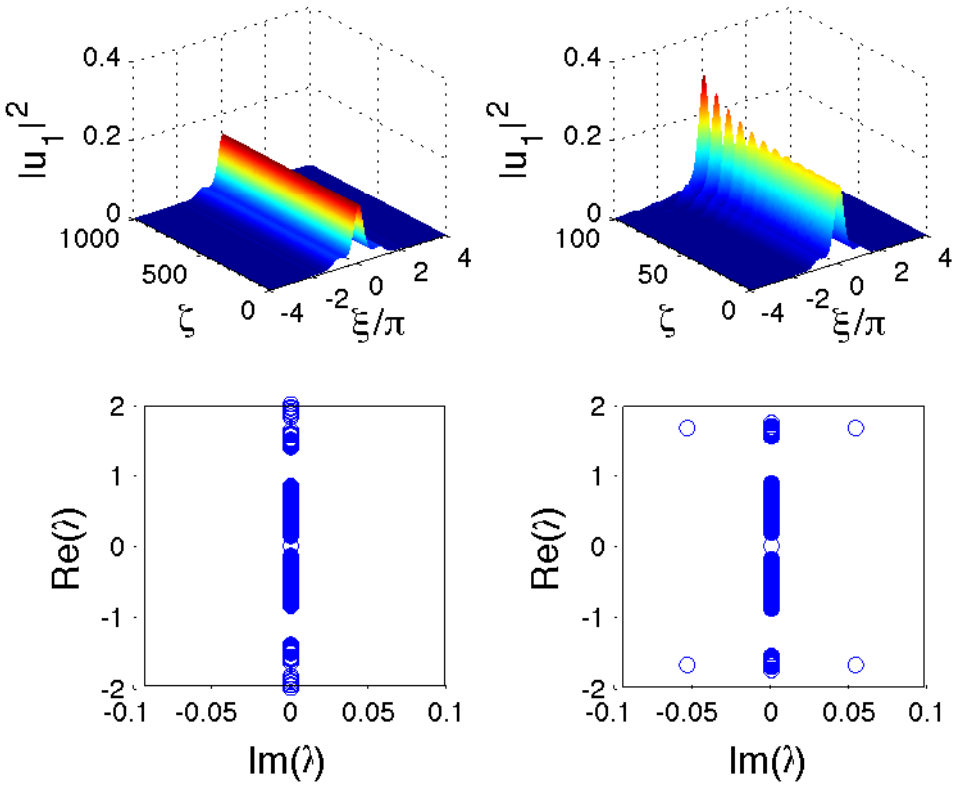

Figure 4.18: Top plots: The evolution of two GS solutions with 10% of amplitude random perturbations in Case 3 [see Eq. (4.6)] in the semi-infinite gap. Left panel has $b = 0.21$ and is stable. The right panel corresponds to unstable evolution of a solution with $b = 0.25$. Note that the linearly unstable solution remains localized. The corresponding eigenvalues of small perturbations are shown in the lower panels. The parameters of the structure are $V_1 = V_2 = 1$, $\alpha = 0.7$ and $q = -0.5134$.

is qualitatively similar to that made in other nonlinear $\mathcal{PT}$-symmetric systems, where solitons do not exists above a critical level of the gain-loss coefficient [29, 63].

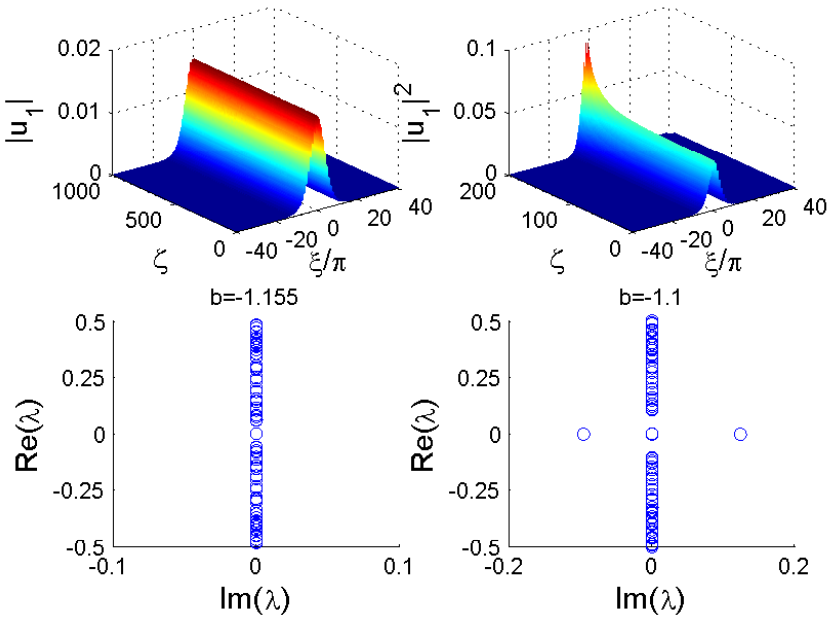

Figure 4.19: Top plots: The evolution of two GS solutions with 20% of amplitude random perturbations in Case 3 [see Eq. (4.6)] in the third finite gap. Left panel has $b = -1.155$ and is stable. The right panel corresponds to unstable evolution of a solution with $b = -1.1$. Note that the linearly unstable solution remains localized. The corresponding eigenvalues of small perturbations are shown in the lower panels. The parameters of the structure are $V_1 = V_2 = 1$, $\alpha = 0.9$ and $q = 0$.

4.4 The system with the "virtual grating"

Here we consider the case of $V_2 = 0$, i.e. the periodic potential acting only on the FF component. A typical example of a stable GS, found as solutions to Eqs. (4.2a) and (4.2b) in the absence of the periodic potential acting on the SH, is displayed in Fig. 4.20. It is seen that its shape is conspicuously different from that of the solitons found above in the system with $V_2 = V_1$, cf. Fig. 4.6.

The analysis of the stability of solitons in Eqs. (4.1a) and (4.1b) in the case of $V_2 = 0$ reveals a stability boundary, shown in in Fig. 4.21, which is qualitatively similar to its counterparts presented above for the system with $V_2 = V_1$, cf. Fig. 4.10. It particular, the instability area appears for values of α above a certain

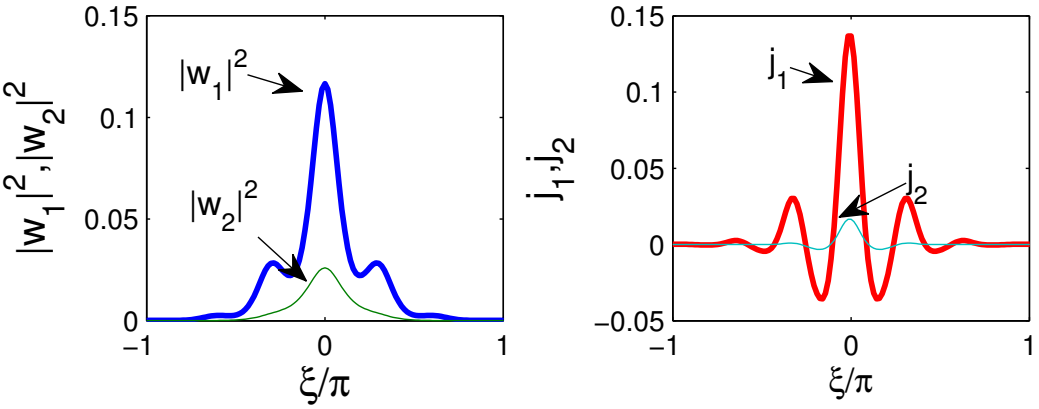

Figure 4.20: The intensities $|w_{1,2}|^2$ and currents $j_{1,2}$ of a stable GS solution with propagation constant $b = 0.2$ pertaining to the semi-infinite gap. The parameters of the system are $V_1 = 1, V_2 = 0$, $q = 0$ and $\alpha = 0.9$.

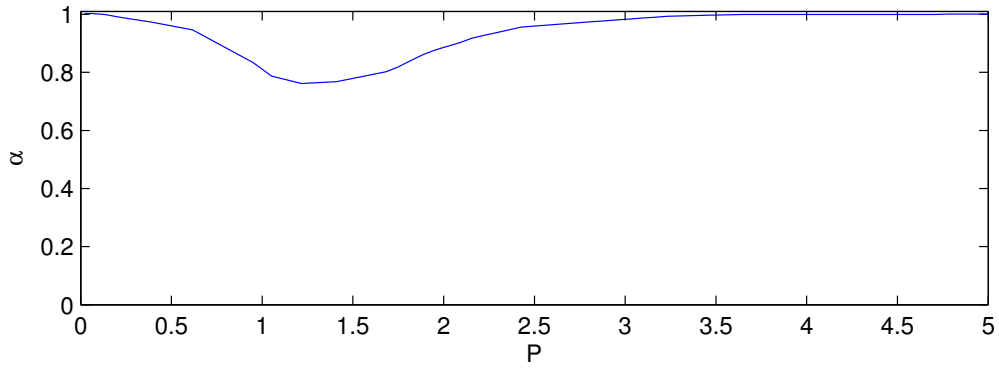

Figure 4.21: The stability boundary in the plane of (P, α), in the system with $V_1 = 1$ and $V_2 = 0$. The instability area is located above the boundary.

threshold. However, the difference is that only one instability interval exists in this case, and the threshold for its appearance, $\alpha \approx 0.75$, is higher than in the system where the periodic potential acts on both components.

4.5 The case of a purely imaginary potential

Here we consider the limit case of the system when the potential in Eq. (4.1a) is purely imaginary, and no potential appears in Eq. (4.1b), i.e., $V_1 = V_2 = 0$. A

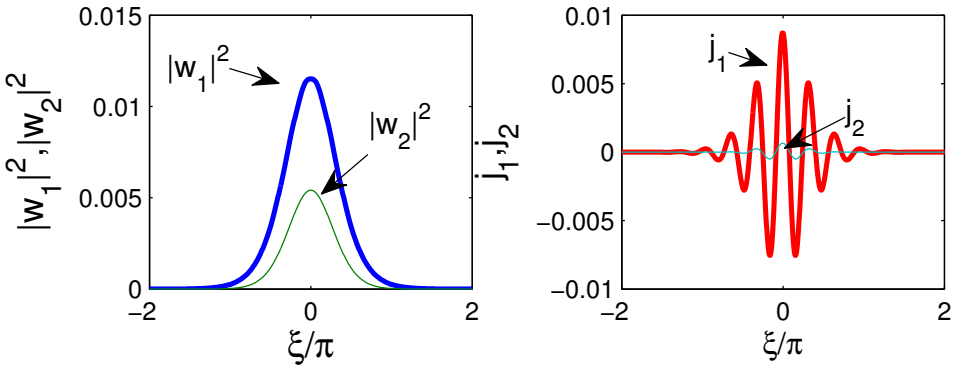

Figure 4.22: The intensities $|w_{1,2}|^2$ and currents $j_{1,2}$ of a GS with $b = 0.06$, in the system with $V_1 = V_2 = 0$ (no real potential) and $q = 0$, $\alpha = 0.5$.

typical example of the soliton found in this case is shown in Fig. 4.22. In this case, all the solitons are unstable at $\alpha > 0$. The respective instability growth rate being rather small, Fig. 4.23 shows that the growth of the instability in direct simulations starts abruptly, as the instability eigenvalues are purely imaginary, see Appendix B.

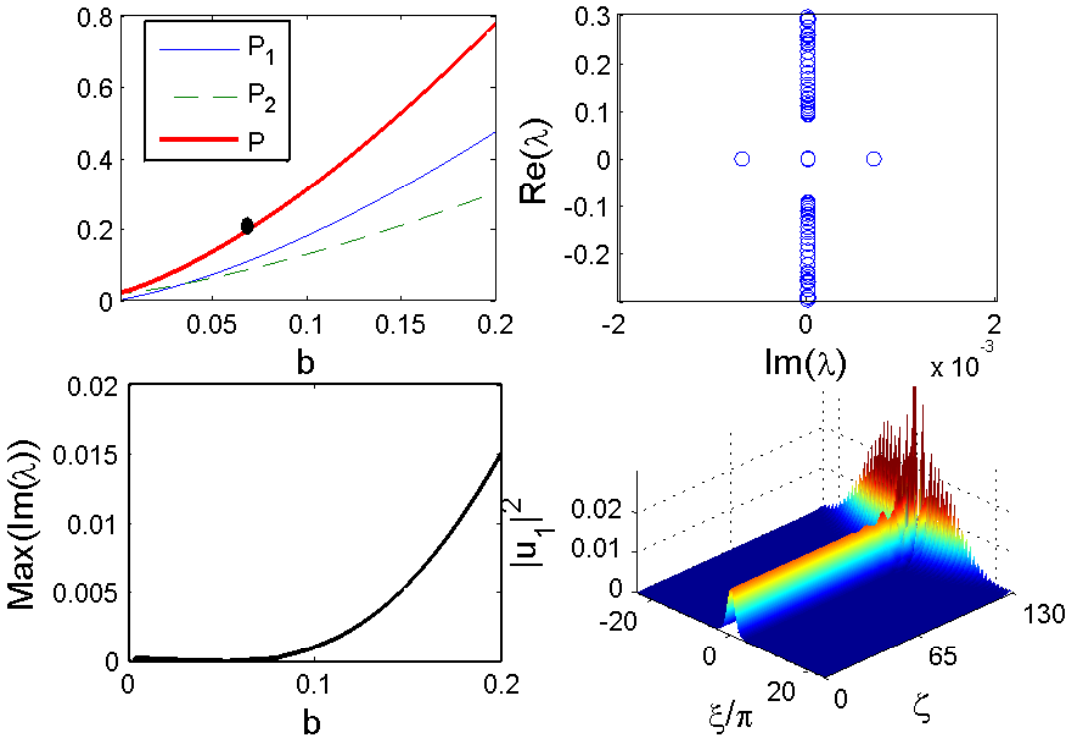

Figure 4.23: Solitons in the system with $V_1 = V_2 = q = 0$ and $\alpha = 0.5$. The upper left panel: The power-vs.-propagation-constant (b) branch. The lower left panel: The instability eigenvalue, λ, with the largest imaginary part, as a function of b. The upper right panel: Stability eigenvalues for the soliton with $b = 0.06$, the instability being accounted for by a pair of small purely imaginary eigenvalues. The lower right panel: The unstable propagation of the soliton randomly perturbed at the 1% amplitude level.

4.6 Conclusions

In this Chapter we considered a system with a $\mathcal{PT}$-symmetric periodic potential acting on the FF and a real potential acting on the SH. We studied numerically three types of bifurcations of solitons with $w_1 \to 0$ at the edge of a total gap which happens to be an edge of a gap of the FF, SH or both. We found that part of the branch in all considered cases is stable, with exception of the case of a purely imaginary potential, where no solutions stable solutions were found.

The main concern in this Chapter was to study the effect of gain and loss parameter on the system. The total-gap structure was found to depend on it, even being responsible for the disappearance of total gaps for values of gain and loss coefficient below $\mathcal{PT}$-symmetry breaking threshold. The stable regions was found to depends on the gain and loss parameter. The limit in amplitude of the solutions approaching the edge of the SH was found to depend on gain and loss parameter. Stable *embedded solitons* may exist as a part of a fundamental branch that bifurcates from an edge of the FF. Their appearance depends on values of the gain and loss parameter above some threshold.

Chapter 5

Gap solitons in nonlinear periodic $\chi^{(2)}$- media

5.1 Introduction

In the present chapter we consider a system with simultaneous spatially periodic modulations of linear and nonlinear properties. The nonlinearity is considered to have the same spatial distribution as the linear refractive index. We focus on alternating layers of dielectric materials possessing quadratic nonlinearity and address localized mode such systems.

The organization of this chapter is as follows. In Section 5.2 the physical model is described. The asymptotic properties of stationary solutions are studied in Section 5.3 and a numerical scheme for solution of the system of equations for $\chi^{(2)}$ media is described. In Section 5.4 the physical implementation of nonlinear quadratic media periodically modulated parameters is given. The LS branches of solutions and their stability are discussed in Sections 5.5.1, 5.5.2 and 5.5.3. The main results are summarized in the conclusion.

5.2 The model

In this chapter we consider a perfectly matched fundamental field and the second-harmonic having respectively the frequencies ω_1 and $2\omega_1$ and wave vectors k_1 and

$k_2 = 2k_1$. The both waves propagate along z direction. The medium is considered periodically modulated in the transverse, i.e. x, direction with the spatial period l. Respectively, for the dielectric permittivity (2.3) is used and $\epsilon_{1\beta}(x) = \epsilon_{1\beta}(x+l)$ describes the periodic modulation. The following considerations will be restricted to lossless media with same period l of the dielectric permittivity, such that $\chi_2 = \chi_1/2$ is assumed to be satisfied (See [36]) along with $\chi_{1,2}(x) = \chi_{1,2}(x+l)$. Here the coefficient $\chi_{10} = \max(\chi_1^{(2)}) - \min(\chi_1^{(2)})$ is the amplitude of the nonlinear coefficient modulation. It follows that the amplitude of nonlinear modulation of the SH satisfies $\chi_{20} = \chi_{10}/2$. The evolution equations (2.9) are written as

$$i\frac{\partial u_1}{\partial \zeta} + \frac{\partial^2 u_1}{\partial \xi^2} + \mathcal{V}_1(\xi)u_1 + 2f(\xi)\bar{u}_1 u_2 = 0, \tag{5.1a}$$

$$i\frac{\partial u_2}{\partial \zeta} + \frac{1}{2}\frac{\partial^2 u_2}{\partial \xi^2} + 2\mathcal{V}_2(\xi)u_2 + f(\xi)u_1^2 = 0. \tag{5.1b}$$

In above the index of f_β was dropped since $f_{1,2}(\xi) = f(\xi)$. From (2.7) is possible to see that $\mathcal{V}_\beta(\xi) = \mathcal{V}_\beta(\xi + 2\pi)$. The model (5.1) corresponds to (2.9) with $\sigma = k_1/k_2 = 1/2$ and $q = 0$.

System (5.1) where only the linear lattice is present, i.e. where $f(\xi) \equiv$const, was considered in [50, 52], while in the presence of only nonlinear lattice, i.e. at $\mathcal{V}_{1,2}(\xi) \equiv$const, it was studied in the recent paper [54].

Solutions of (5.1) conserve the Hamiltonian

$$H = \int_{-\infty}^{\infty} \left(-\left|\frac{\partial u_1}{\partial \xi}\right|^2 - \frac{1}{2}\left|\frac{\partial u_2}{\partial \xi}\right|^2 + \mathcal{V}_1|u_1|^2 + 2\mathcal{V}_2|u_2|^2 + f\bar{u}_1^2 u_2 + f u_1^2 \bar{u}_2 \right) d\xi \tag{5.2}$$

and the total power (4.10).

5.3 Asymptotic properties of stationary solutions

In this section the interest in asymptotic properties, i.e., properties of localized field envelopes $u_{1,2}$ for a large distance $|x| \to \infty$. Stationary localized solutions are searched in the form (2.12) where $w_\beta(\xi) \to 0$ at $\xi \to \pm\infty$. Following the

arguments of [52], it is possible to prove that for exponentially localized solutions, $w_{1,2}(\xi)$ have constant phases, and thus can be chosen real, and consequently satisfying the equations

$$\frac{d^2w_1}{d\xi^2} + (\mathcal{V}_1(\xi) - b)\, w_1 + 2f(\xi)w_1w_2 = 0, \tag{5.3a}$$

$$\frac{1}{2}\frac{d^2w_2}{d\xi^2} + 2\,(\mathcal{V}_2(\xi) - b)\, w_2 + f(\xi)w_1^2 = 0. \tag{5.3b}$$

It follows from (5.3) that the localized stationary solutions obey the integral relation

$$\int_{-\infty}^{\infty} \left(\frac{d\mathcal{V}_1}{d\xi} w_1^2 + 2\frac{d\mathcal{V}_2}{d\xi} w_2^2 - \frac{df}{d\xi} w_1^2 w_2 \right) d\xi = 0. \tag{5.4}$$

Below in this chapter we focus the modulations having well defined symmetry. More specifically we consider them to be even functions, i.e. $\mathcal{V}_{1,2}(\xi) = \mathcal{V}_{1,2}(-\xi)$ and $f(\xi) = f(-\xi)$ (see Fig. 5.1 and its description below). Taking into account the symmetry of the periodic medium, we search the solutions of the stationary problem (5.3) which are either even or odd functions, i.e. which satisfy the relations $w_{1,2}^2(\xi) = w_{1,2}^2(-\xi)$.

Assuming that $w_2(-\xi) = -w_2(\xi)$, it is deduced from Eq. (5.3b) that $f(\xi)w_1^2(\xi)$ is either a odd function, or zero. Since the first possibility is ruled out by the above suppositions about the parity of the nonlinear modulation $f(\xi)$, we conclude that nonlinear localized modes can exist only with an even field of the SH, i.e. with $w_2(\xi) = w_2(-\xi)$. Meantime Eq. (5.3a) may support both even and odd profiles of the FF $w_1(\xi)$.

Since $fw_2 \to 0$ at $\xi \to \pm\infty$, the last term in Eq. (5.3a) decays faster than other ones and thus in the asymptotic region this equation becomes effectively linear. This means that

$$w_1(\xi) \to C_1 A_{1\pm}(\xi), \quad \xi \to \pm\infty \tag{5.5}$$

where C_1 is a constant and $A_{1\pm}$ are the solutions of the linear Hill equation (2.14) (See[39]) decaying at $\pm\infty$ respectively. In above we remind that $\mathcal{L}_1$ was defined in (2.14). The Floquet theorem assures that these two linearly independent solutions can be expressed in the form (3.4). Here $\phi_1(\xi)$ is a 2π-periodic function, and the

real Floquet exponent μ_1 is defined by the location of the propagation constant b inside a gap of the spectrum of the operator $\mathcal{L}_1$ defined in (2.14) through (3.10). Denoting the set of the gaps of (2.14) by Σ_1, thus the formulated conditions can be written as $b \in \Sigma_1$.

Passing now to the asymptotic of Eq. (5.3b), it can be treated as an inhomogeneous linear equation for w_2 satisfying the conditions $dw_2(0)/d\xi = 0$ (recall that the mode $w_2(\xi)$ must be necessarily even) and $w_2(\pm\infty) = 0$, with w_1 considered as given. Then the asymptotic behavior of w_2 depends on the relation between the asymptotics of the solution of the linear equation

$$\mathcal{L}_2 A_{2\pm} = 2bA_{2\pm}, \quad \mathcal{L}_2 = \frac{1}{2}\frac{\partial^2}{\partial\xi^2} + 2\left(\mathcal{V}_2(\xi) + q\right). \tag{5.6}$$

and on the decay of w_1^2 defined by (3.4), i.e. by the exponent $2\mu_1$. In other words, the asymptotic of w_2 depends on the position of a given b with respect to the spectrum of Eq. (5.6). In the present chapter we concentrate only on the cases where b belongs also to a gap of the spectrum of Eq. (5.6), i.e., a total gap (See Section 4.3.1). We require b to be considered to be in a gap of (5.6), where can again use the Floquet theorem and represent its solutions as

$$A_{2\pm}(\xi) = \phi_2(\pm\xi)e^{\pm\mu_2\xi}, \tag{5.7}$$

where $\mu_2 > 0$ and $\phi_2(\xi)$ is a 2π-periodic function.

The asymptotic of (5.3b) is given using the particular solution of the inhomogeneous equation (5.3b) with localized boundary conditions. Using the Green function

$$G(\xi,\xi') = \begin{cases} A_{2+}(\xi)A_{2-}(\xi') & \text{for } \xi < \xi', \\ A_{2+}(\xi')A_{2-}(\xi) & \text{for } \xi > \xi' \end{cases} \tag{5.8}$$

Eq. (5.3b) can be rewritten in the integral form

$$w_2(\xi) = -\frac{2}{W}\int_{-\infty}^{\infty} G(\xi,\xi')f_2(\xi')w_1^2(\xi')d\xi'. \tag{5.9}$$

The Wronskian is given by $W = A_{2+}dA_{2-}/d\xi - A_{2-}dA_{2+}/d\xi$.

One can distinguish two asymptotic regimes in (5.9). In the first case, when

$2\mu_1 > \mu_2$, from (5.5) we conclude that the integral

$$C_+ = \int_0^\infty (A_{2+} + A_{2-})\, f w_1^2 d\xi' \tag{5.10}$$

exists. This allows us to write (5.9) as

$$\begin{aligned} -\frac{W}{2} w_2 = A_{2+}(\xi) \int_\xi^\infty A_{2-} f_2 w_1^2 d\xi' - \\ - A_{2-}(\xi) \int_\xi^\infty A_{2+} f_2 w_1^2 d\xi' + C_+ A_{2-}. \end{aligned} \tag{5.11}$$

The both terms containing integrals in this expression decay faster than $C_+ A_{2-}$ as $\xi \to \infty$. Thus the total solution decays with exponent μ_2 and we have

$$w_2(\xi) \to \begin{cases} C_+ A_{2-}(\xi) & \text{for } \xi \gg 1, \\ C_+ A_{2+}(\xi) & \text{for } \xi \ll -1. \end{cases} \tag{5.12}$$

The second case corresponds to $2\mu_1 < \mu_2$. For some $\xi = \xi_f$ far enough from the origin, one can approximate $w_1(\xi_f) \approx C_1 A_{1-}(\xi_f)$ and obtain

$$-\frac{W}{2} w_2 \approx C_1^2 \int_\xi^\infty \phi_2(-\xi') A_{1-}^2 [\phi_2(\xi) e^{-\mu_2(\xi'-\xi)} + \phi_2(-\xi) e^{-\mu_2(\xi'+\xi)}] d\xi' + C_- \phi_2(-\xi), \tag{5.13}$$

where

$$C_- = \int_{-\xi_f}^{\xi_f} \phi_2(\xi) e^{-\mu_2(\xi_f - \xi)} f_2(\xi) w_1^2(\xi) d\xi. \tag{5.14}$$

We notice that the described situation resembles the cases of free-tail and tail-locked cases considered in [100] for the three-wave gap solitons in quadratic media.

In order to obtain the localized modes in this chapter we use the shooting method described in Sec. 3.1. Here the shooting parameters are C_1 and C_+ for the $2\mu_1 > \mu_2$ case or C_1 and C_- for the $2\mu_1 < \mu_2$. The shooting parameters $C_\pm$ plays the role of C_2. The asymptotic formula (5.5) is used for $\mathcal{A}_1$ and (5.12) or (5.13) for $\mathcal{A}_2$.

The shooting method allowed us to obtain solutions which when used in evaluation of (3.20) are of $O(10^{-4})$. In order to increase the accuracy further we em-

ployed the solution obtained using the shooting method as a seed for a Newton-Raphson solver. The final accuracy of the obtained solutions was of order of 10^{-10}.

5.4 A periodic structure

In order to proceed with numerical construction of particular solutions, it is necessary to specify the layered structure, i.e. to introduce particular forms of the functions $\mathcal{V}_\beta$ and f. To this end we consider a structure consisting of alternating slabs of two different materials alternating periodically and denoted below by "a" and "b". This structure is different from Chapter 4, where a continuous modulation with cosine form was used, but results used in previous section for the asymptotic behavior of solutions still can be used in the case $\alpha = 0$. Respectively we have for one period

$$\mathcal{V}_\beta(\xi) = \begin{cases} V_{\beta \mathrm{a}} & \text{for } |\xi| < \pi/2, \\ V_{\beta \mathrm{b}} & \text{for } \pi/2 < |\xi| < \pi \end{cases} \tag{5.15}$$

where $V_{\beta \mathrm{a}}$ and $V_{\beta \mathrm{b}}$ are constants, and

$$f(\xi) = \begin{cases} f_0 + 1/2 & \text{for } |\xi| < \pi/2, \\ f_0 - 1/2 & \text{for } \pi/2 < |\xi| < \pi. \end{cases} \tag{5.16}$$

In the numerical studies reported below we the use for slabs a and b respectively an orientation-patterned Gallium Arsenide (OP-GaAs) [10] and the alloy $\mathrm{Al}_{0.125}\mathrm{Ga}_{0.875}\mathrm{As}$ [101]. This structure, possessing the required modulation of both dielectric permittivity and of the nonlinear susceptibility, can be fabricated with the combination of techniques suchs as low-pressure hydride vapor phase epitaxy [10] for the χ_1 modulation and molecular beam epitaxy using Si shadow masks [11]. The both materials are transparent when $k_1^{-1} = 3.18\mu$m. Their dielectric constants are $\epsilon_{1\mathrm{a}} = \epsilon_{2\mathrm{a}} = 10.9$ and $\epsilon_{1\mathrm{b}} = \epsilon_{2\mathrm{b}} = 10.28$ respectively. Here $\epsilon_{\beta \mathrm{a}}$ ($\epsilon_{\beta \mathrm{b}}$) represents the dielectric constant of the "a" ("b") layer on the FF ($\beta = 1$) or SH ($\beta = 2$). One has in this case $\epsilon_{10} = 10.59$. We choose the period of the structure to be $l = 1.63\mu$m. The modulus of the nonlinear susceptibilities are

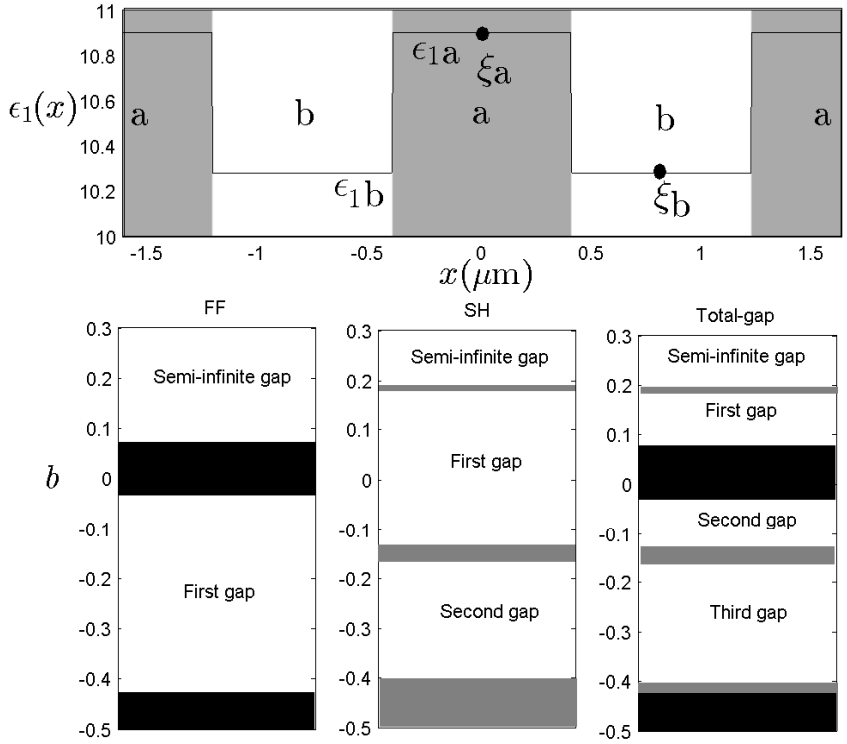

Figure 5.1: Upper panel: Schematic presentation of the periodic structure considered in the present chapter. The two black circles indicate the coordinates of two symmetry axes (i.e. $\xi_{\rm a} = 0$ and $\xi_{\rm b} = \pi$) which are located in the slabs respectively with lower (white) and higher (gray) refractive indexes. Lower panels: The left panel shows gaps (white) and bands (black) for the FF. Middle panel shows gaps (white) and bands (gray). Right panel shows the resulting total gaps (white) and bands.

$\chi_{1\rm a} = 2\chi_{2\rm a} = 94$pm/V and $\chi_{1\rm b} = 2\chi_{2\rm b} = -94$pm/V [102]. The constant $\chi_{\beta\rm a}$ ($\chi_{\beta\rm b}$) is the nonlinear suscetibility in the "a" ("b") layer at the FF ($\beta = 1$) or SH ($\beta = 2$). The axis of the GaAs and $Al_{0.125}Ga_{0.875}As$ are inverted in respect to another, such that the second-order susceptibility changes sign from layer to layer. Thus we have $\chi_{10} = 188$pm/V. This particular structure corresponds to $f_0 = 0$, $V_{1a} = V_{2a} = 0.31$ and $V_{1b} = V_{2b} = -0.31$ in dimensionless form and is schematically illustrated in Fig. 5.1.

We notice that the structure has two symmetry axes passing through the centers of the layers of each type, i.e. through the points $\xi_a = 0$ and $\xi_b = \pi$ (See

the the black circles in the upper panel of Fig. 5.1).

5.5 Gap Solitons

5.5.1 Bifurcation of branches from continuum spectrum

Since we are interested in gap solitons belonging to one of the total gaps it becomes relevant whether such gaps have edges coinciding with edges of the FF bands or with edges of the SH bands as we previously discussed in Section 4.3. For the layered structure at hand one observes from Fig. 5.1, that the total semi-infinite gap is limited by the upper branch of the SH, while the first highest total gap has the upper boundary from the band spectrum of the SH and the lower boundary coinciding with the boundary for the semi-infinite gap for the FF. As we will see below these facts have direct implications on the existence of small amplitude gap solitons.

In order to clarify this last point we now turn to the analysis of the small amplitude limit, i.e., the Case (4.6), and more specifically we address the possibility of having families of the gap solitons bifurcating from the continuum spectrum (i.e. from the linear Bloch states). In the general analysis performed below we exclude the possibility of two coinciding edges of bands of the FF, i.e., Case (4.4) since this case does not exist in the structure subjected to analysis in this Chapter. From (5.3) we deduce the conclusion that no branches can bifurcate from the edge of the total gap which is originated by the spectrum of the SH, i.e., the Case (4.5). Indeed, assuming the opposite we should have w_2 tending to zero, i.e. to the linear spectrum of the problem (5.6), while $w_1(\xi)$ for the respective propagation constant, having nonzero detuning to a gap of the spectrum of the linear problem (5.6), should have zero limit. This obviously contradicts to Eq. (5.3b), which in the described case should have the first two terms much smaller than the last one.

In other words, a branch of solutions (if any) can bifurcate only from the boundary of the total gap coinciding with the boundary of a gap of the FF. This is however is only a necessary condition for the existence of a bifurcating branch but not yet enough one. The second necessary condition comes from the

requirement of the instability of the Bloch states bordering the respective gap edge. This issue can be addressed withing the framework of the multiple scale expansion [103]. Indeed, when a branch bifurcates from a gap-edge of the FF, then w_1 is small. If at the same time w_2 is not small, since in this case it does not border any gap-edge of the SH, we again arrive at the contradiction because now Eq. (5.3b) in the leading order becomes linear. This means that no small amplitude limit with $w_1 = O(w_2)$ is possible. This is what would happen in the case $2\mu_1 > \mu_2$. In the case $2\mu_1 < \mu_2$, however, one can require w_2 to be much smaller than w_1. Then Eq. (5.3b) may have a small amplitude solution which obeys the scaling (4.6). Thus to find (approximately) such solution we have to explore the expansions in the form

$$u_1 = \eta u_1^{(1)}\left(\xi_0, \xi_1, ..., \zeta_0, \zeta_1, ...\right) + \eta^2 u_1^{(2)}\left(\xi_0, \xi_1, ..., \zeta_0, \zeta_1, ...\right) + ..., \tag{5.17a}$$

$$u_2 = \eta^2 u_2^{(2)}\left(\xi_0, \xi_1, ..., \zeta_0, \zeta_1, ...\right) + ... \tag{5.17b}$$

where $\eta \ll 1$ is a formal small parameter and $\xi_j = \eta^j \xi$ and $\zeta_j = \eta^j \zeta$, with $j = 0, 1, 2, 3...$, are the scale variables, regarded as independent. In the vicinity of a given band-edge (let it be m_0-th band and k_0 stands for the wave vector at the reduced Brillouin zone) the leading order of the solution is searched in the form

$$u_1^{(1)}\left(\xi_0, \zeta_0\right) = U\left(\xi_1, \zeta_2\right) \phi_{1,k_0}^{(m_0)}\left(\xi_0\right) e^{i b_{1,k_0}^{(m_0)} \zeta_0} + c.c. \tag{5.18}$$

where $\phi_{1,k_0}^{(m_0)}\left(\xi_0\right)$ is the Bloch function at the m_0-th edge with wave vector $k_0 = 0, 1/2$ and propagation constant $b_{1,k_0}^{(m_0)}$ of the FF where the bifurcation is considered. Here $U\left(\xi_1, \zeta_2\right)$ is a slowly varying envelope. The further steps are standard, and therefore we only briefly outline them in the Appendix A. The resulting equation for the small amplitude reads

$$i\frac{\partial U}{\partial Z} = \frac{\partial^2 U}{\partial X^2} + S\left|U\right|^2 U. \tag{5.19}$$

In above X is a rescaled transverse coordinate and Z is a rescaled propagation

coordinate. The constant $S = \pm 1$ is defined in (A.7) in Appendix A. Bright solitons are known to exist when $S > 0$. The constant S depends on an effective nonlinearity, averaged over a product of band-edge functions of the FF and SH. It is of particular importance, since given a structure with fixed $\mathcal{V}_{1,2}$, the periodic nonlinear modulation f can effectively in change when a bifurcation satisfying (5.19) can occur. This is in stark contrast to a system without nonlinear modulation where only the band-edge functions of the FF and SH are relevant. Thus the second condition which must be satisfied for existence of a solitonic branch bifurcating from a gap-edge is that $S > 0$.

5.5.2 Branches of solutions

Turning to the discussion of the branches of the solution we notice that the symmetry of the structure implies the existence of two different families of solutions, corresponding to two different symmetry axes of the structure (see Fig. 5.1). We address the solitons which are centered either in a slab with lower refractive index, i.e. at $\xi_{\mathrm{a}} = 0$ (shown in Fig. 5.2) or in an optically more dense slab, i.e. in the point $\xi_{\mathrm{b}} = \pi$, (see Fig. 5.3).

As the first step, using (A.6) and (A.7) we computed S for all edges of the total gaps, coinciding with the gap-edges of the FF. It turns out that for the structure at hand only the edge defined by the propagation constant $b^{(0)}_{1,1/2} \approx -0.3573$ (i.e. at the boundary of the Brillouin zone, i.e. corresponding to a finite total gap) has $S = 1$. Hence this is the only edge where a branch of the gap soliton solutions can bifurcate from the linear spectrum. This precisely what the curves C, bifurcating from the upper edge of the second total gap, in Figs. 5.2 and 5.3 show. In the low intensity limit, the SH appears only as a small perturbation to the FF, what one can also observe in the second lower panels in Figs. 5.2 ($b = -0.044$) and Fig. 5.3 ($b = -0.48$). The comparison of these two figures reveals the first interesting phenomenon: the symmetry of the fundamental field is changed depending on the center location.

Since we are in the small amplitude limit, this change of the symmetry is understandable form the requirement for the light to concentrate in the waveguides with higher refractive index (the gray strips). This gives also the physical

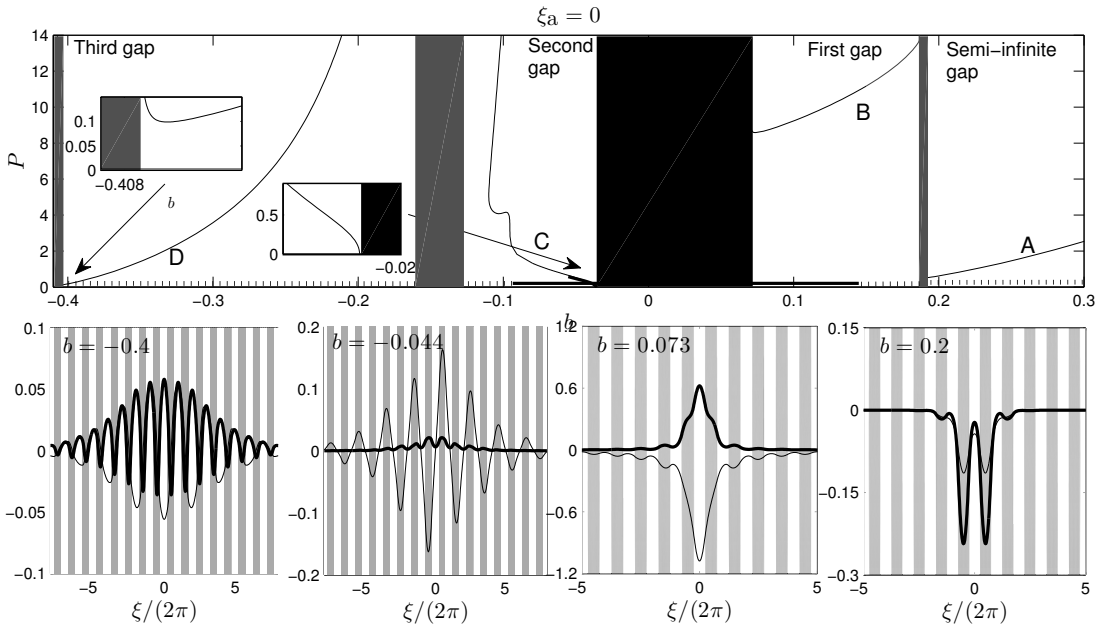

Figure 5.2: Upper panel: the lowest branches of the solutions centered at $\xi_a = 0$ which belong to the semi-infinite gap and to the three highest total gaps of the spectrum. Thick (thin) lines denote stable (unstable) solutions. Gray and black bars represent FF and SH bands, respectively. In the abscissa axis we use the thick (dotted) lines to indicate the range of the propagation constant where $2\mu_1 < \mu_2$ ($2\mu_1 > \mu_2$). Lower panels: examples of gap solitons for the branch of each total-gap starting from the semi-infinite total-gap on the right. Thick (thin) lines represent w_2 (w_1).

understanding for the observed stability of the modes. This is another important property, which can be interpreted as *bistability of gap solitons*, which manifests itself in existing two different branches of the solutions bifurcating from the same gap edge. The both branches C have overlapping intervals of the stability of the solutions.

It worth mentioning an example of the first total gap, where at the edge where $b_{1,0}^{(0)} = 0.0724$ (it coincides with the band-edge of the FF) one has $S = -1$ while the upper edge coincides with the band-edge of the SH. Therefore the lowest branch of the solutions (see curves B in Figs. 5.2 and 5.3) does not approach zero at any of the gap edges: at the lower edge because the NLS equation (5.19) does not possess bright solutions when $S = -1$, while at the upper edge because the

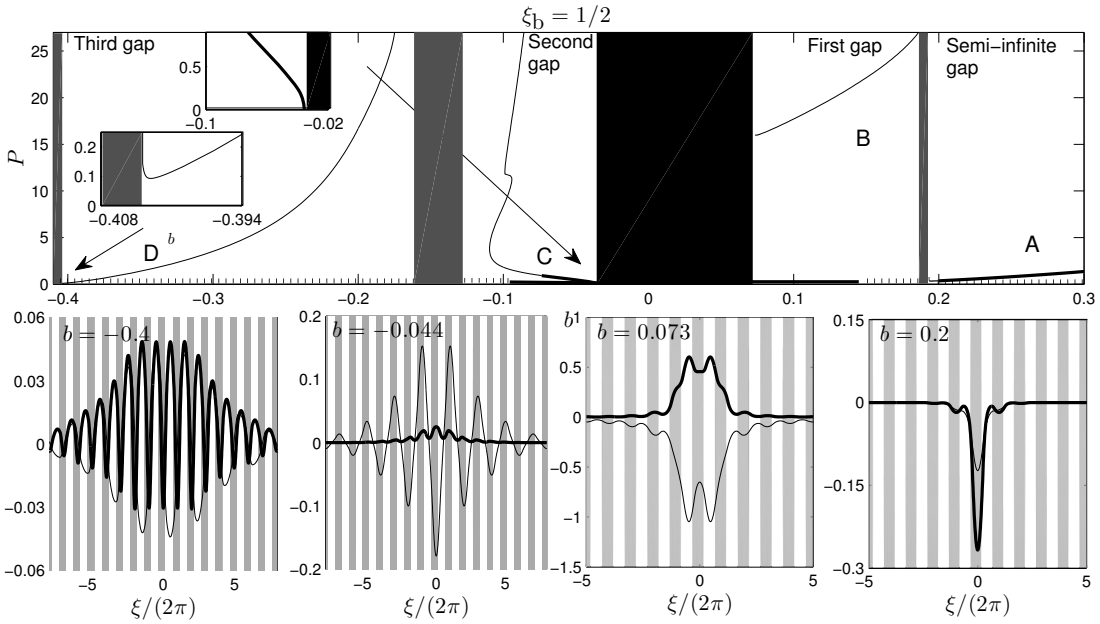

Figure 5.3: The same as in Fig. 5.2 but for the branches of solitons centered at $\xi_b = \pi$. Notice that here we introduced the π-shift in the coordinate ξ (with respect to the ξ-axis shown in Fig. 5.1), in order to place the soliton centers in the origin.

branch borders the SH edge.

In general we observe that Eq.(20), obtained by multiple-scale expansion gives the result which is in good agreement with the corresponding numerical solution of the system (5.3). This is illustrated in Fig. 5.4.

Localized modes may have the field concentrated in the slabs with lower refractive index. This observed in the third and first total gaps if the mode is centered in the waveguide with lower refractive index (respectively the first and third lower panels in Figs. 5.2 and 5.3). As it is expectable, such modes are unstable.

Probably the most important distinction of the modes centered in different domains is that while in the both cases one can find branches of solutions in the semi-infinite gap, only "one-hump" mode having its maximum in a slab with larger refractive index (the lower panel with $b = 0.2$ in Fig. 5.3) appears to be stable if the propagation constant exceeds some critical value (c.f. A – branches

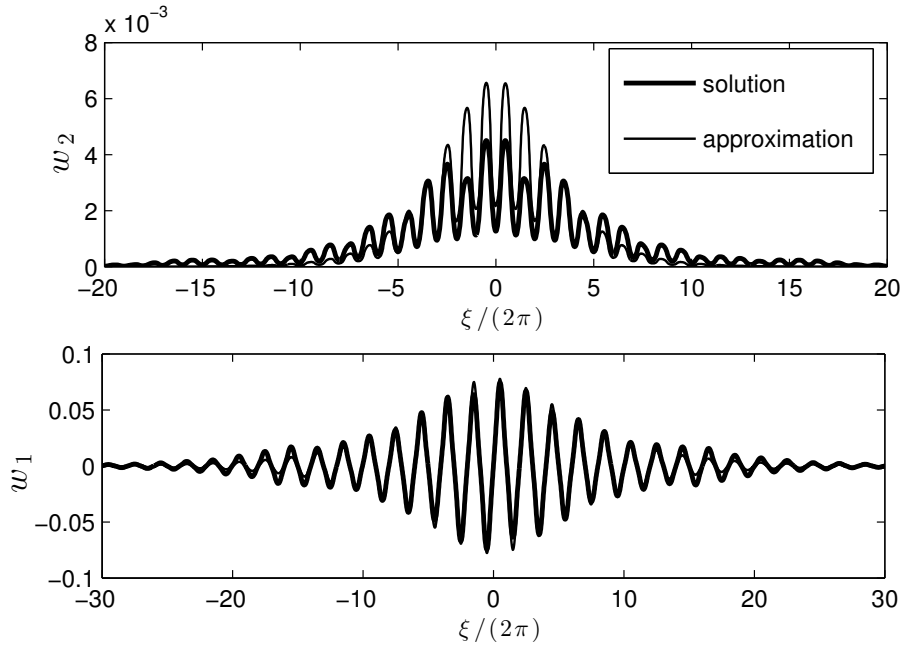

Figure 5.4: Panels shows comparison of approximated model with numerical solution with $\xi_a = 0$ and $b = -0.038$.

in the semi-infinite bands shown in Figs. 5.2 and 5.3).

In semi-infinite and third total-gaps (branches A and D in Fig.5.2 and Fig.5.3) both edges are from the SH gap. As we previously explained, the small amplitude limit is not possible in this case.

5.5.3 On dynamics of gap solitons

The stability of the modes discussed above has been checked both by the analysis of the linear stability and by the direct propagation using the split-step method described in Section 3.3. The results of this last test are illustrated in Fig. 5.5, where we show the propagation of randomly perturbed input beam corresponding to stable and unstable parts of the same branch of the solution.

Next we concentrate on possibilities of the exciting stationary gap solitons by an input field consisting of only FF. The respective dynamics, obtained by the direct numerical integration of Eq. (2.9), is shown in Fig. 5.6 where we used the

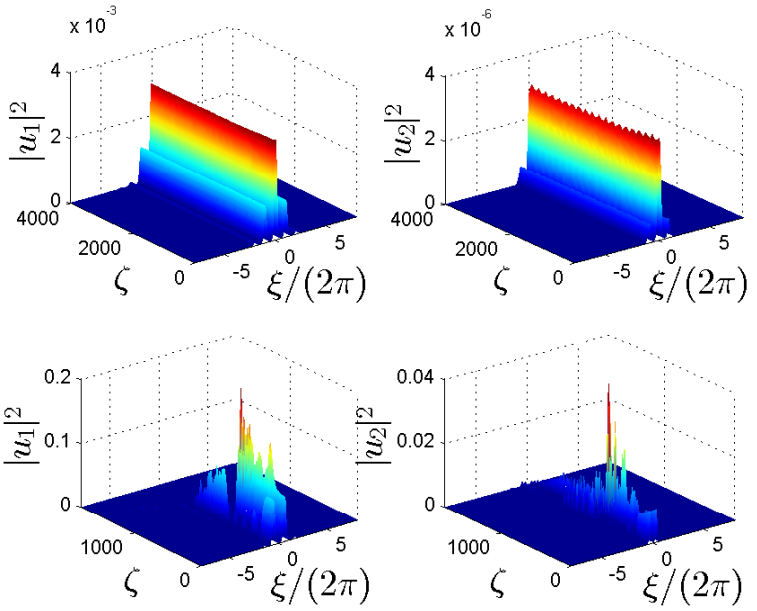

Figure 5.5: Upper panels: stable propagation of the soliton centered in $\xi_{\rm a} = 0$ and having $b = -0.05$ (curve C in Fig. 5.2), integrated up to $\zeta = 4000$. Lower panels: unstable propagation of a solution centered at $\xi_a = 0$ and having $b = -0.1$ (curve C in Fig. 5.2), integrated up to $\zeta = 2000$. In all simulations the input beam was perturbed by noise of order of 10% of the soliton amplitude.

initial conditions of the form $u_1(\xi, 0) = w_1(\xi)$ and $u_2(\xi, 0) = 0$. Dynamics of FF and SH is shown in the left and right panels, respectively. The both examples illustrate persisting localized solutions with almost all energy localized in the fundamental mode, and periodic exchange of relatively small amount of energy between the modes. The energy oscillations have a period ≈ 14 for the both examples.

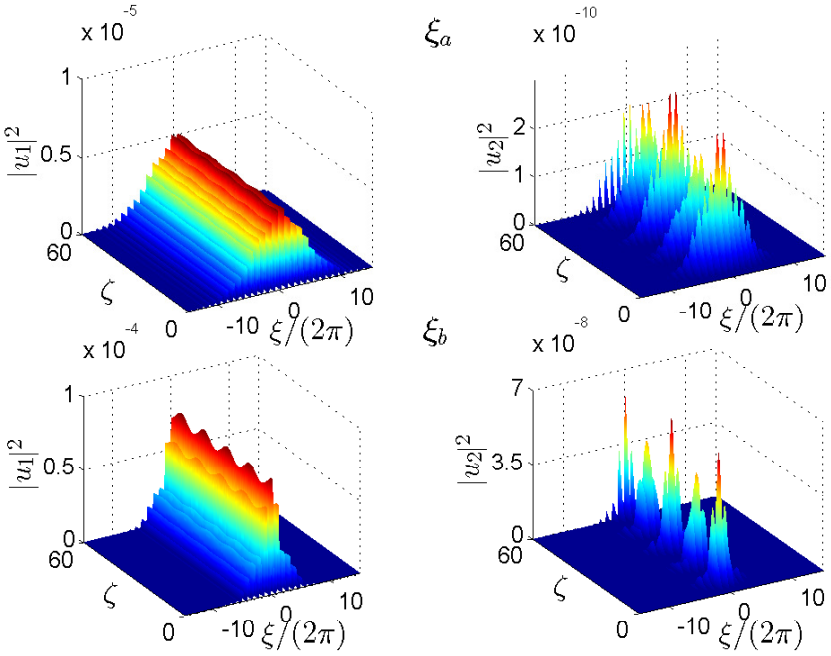

Figure 5.6: Upper (lower) panel shows evolution of the initial condition $u_1(\xi, 0) = w_1(\xi)$ and $u_2(\xi, 0) = 0$, where $w_1(\xi)$ is a solution of (5.3) with $b = -0.038$, corresponding to branch C and centered at ξ_a (ξ_b).

5.6 Conclusions

In this chapter we considered a model that describes solitons in a system with periodic modulations on the dielectric permittivity and nonlinearity. The system was considered to be lossless. We studied solitons with definite symmetry and their asymptotic properties, which were used in a shooting algorithm. A particular structure with realistic materials was proposed. Numerical solutions were obtained and stability of solitons were discussed. In particular it was found that two branches, characterized by their center of symmetry, which can be localized in regions of higher or lower dielectric permittivity, can exist. In both cases stable solutions were found, characterizing a type of bistability. We derived an effective NLS equation that describes solutions with small amplitude in the case of bifurcations of a FF band gap edge. The equation was found to be useful in describing when the limit of small amplitude exists.

Chapter 6

Localized modes in $\chi^{(2)}$ media with $\mathcal{PT}$-symmetric localized potential

6.1 Introduction

In the present chapter we study the existence of solitons in the media with quadratic nonlinearity and localized $\mathcal{PT}$-symmetric potentials. Such systems may be easier to realize physically than the periodic counterpart presented in Chapter 4. Analytical solutions were found in [70, 71] for linear waves, and it was found that localized modes exist in this system. It was found that a localized $\mathcal{PT}$-symmetric impurity can support solitons in the case of cubic nonlinearity [29]. Here the interest is to investigate solitons in a system with quadratic nonlinearity with localized dielectric permittivity modulations with gain and losses acting only on the FF.

The chapter is organized as follows. In Section 6.2 the model and statement of the problem are formulated. The properties of localized modes for different ratios between fundamental and second harmonics are studied in Sections 6.3, 6.4 and 6.5. The stability and dynamics of localized solutions are considered in Section 6.6. Conclusions are made in Section 6.7.

6.2 Statement of the problem

We consider the system (2.9) in the form

$$i\frac{\partial u_1}{\partial \zeta} + \frac{\partial^2 u_1}{\partial \xi^2} + V\left(\frac{1}{\cosh^2\xi} + i\alpha\frac{\sinh\xi}{\cosh^2\xi}\right)u_1 + 2\overline{u}_1 u_2 = 0, \tag{6.1a}$$

$$i\frac{\partial u_2}{\partial \zeta} + \frac{1}{2}\frac{\partial^2 u_2}{\partial \xi^2} + 2\left(\frac{V}{\cosh^2\xi} + q\right)u_2 + u_1^2 = 0 \tag{6.1b}$$

describing spatial second-harmonic generation in a $\chi^{(2)}$ material with localized modulation of the dielectric permittivity in the presence of gain and loss. The dielectric permittivity modulation is characterized by the amplitude V. This model is good for scientific investigation because the linear counterpart has analytical solutions for expressions for the localized modes [70, 71], which we use in important parts of this chapter.

We notice that experimentally the introduced model can describe a medium with active dopants, typically having rather narrow spectral resonances, i.e. affecting only a limited range of frequencies. In particular, such impurities can induce gain and dissipation, whose strengths is characterized by α, only for one of the field component, which in our case is the FF.

Before into the detail study of the system (6.1) we note, that in the standard way solitonic solutions can be found in the analytical form in the limit of large mismatch parameter $-q \gg 1$, when $u_2 \approx -u_1^2/(2q)$ and the system (6.1) reduces to the NLS equation with $\mathcal{PT}$-symmetric potential for the fundamental harmonic u_1, in the same way as we shown in (4.3),

$$i\frac{\partial u_1}{\partial \zeta} + \frac{\partial^2 u_1}{\partial \xi^2} + V\left(\frac{1}{\cosh^2\xi} + i\alpha\frac{\sinh\xi}{\cosh^2\xi}\right) - \frac{1}{q}|u_1|^2 u_1 = 0. \tag{6.2}$$

For $q < 0$ the bright soliton solution has the form [29]

$$u_1 = \sqrt{|q|A}\,\mathrm{sech}(\xi)\exp\left[i\frac{\alpha V}{3}\tan^{-1}(\sinh(\xi)) + i\zeta\right],$$

$$A = \left(2 - V + \frac{\alpha^2 V^2}{9}\right) \tag{6.3}$$

We are interested in LS in the form (2.12). We have

$$\frac{d^2w_1}{d\xi^2}+\left[V\left(\frac{1}{\cosh^2\xi}+i\alpha\frac{\sinh\xi}{\cosh^2\xi}\right)-b\right]w_1+2\overline{w}_1w_2=0, \tag{6.4a}$$

$$\frac{1}{2}\frac{d^2w_2}{d\xi^2}+2\left(V\frac{1}{\cosh^2\xi}+q-b\right)w_2+w_1^2=0. \tag{6.4b}$$

subject to the zero boundary conditions $w_{1,2}(\xi)\to 0$ as $|\xi|\to\infty$.

We restrict our consideration mainly to solutions bifurcating from the linear limits, (4.4), (4.5) and (4.6) which is understood as a limit where at least one of the harmonics vanishes.

6.3 Modes with negligible second harmonic in the linear limit

Let us start with the conditions necessary for (4.6) to occur. In this limit the nonlinear term in (6.4a) can be neglected and in the leading order we have the eigenvalue problem (2.14) with

$$\mathcal{L}_1=\frac{d^2}{d\xi^2}+V\left(\frac{1}{\cosh^2\xi}+i\alpha\frac{\sinh\xi}{\cosh^2\xi}\right). \tag{6.5}$$

Eq. (2.14) with (6.5) has been studied before. Therefore below we only briefly outline the features necessary for our analysis, referring to [70, 71] for more details. For $V>0$ Eq. (6.5) possesses localized solutions. When α is below the $\mathcal{PT}$-symmetry breaking threshold

$$\alpha<\alpha_{cr}=1+\frac{1}{4V}, \tag{6.6}$$

the spectrum of Eq. (6.5) has discrete real eigenvalues given by [104]

$$b_{1,n}=(n-\eta_1)^2,\quad n=0,1,...<\eta_1, \tag{6.7}$$

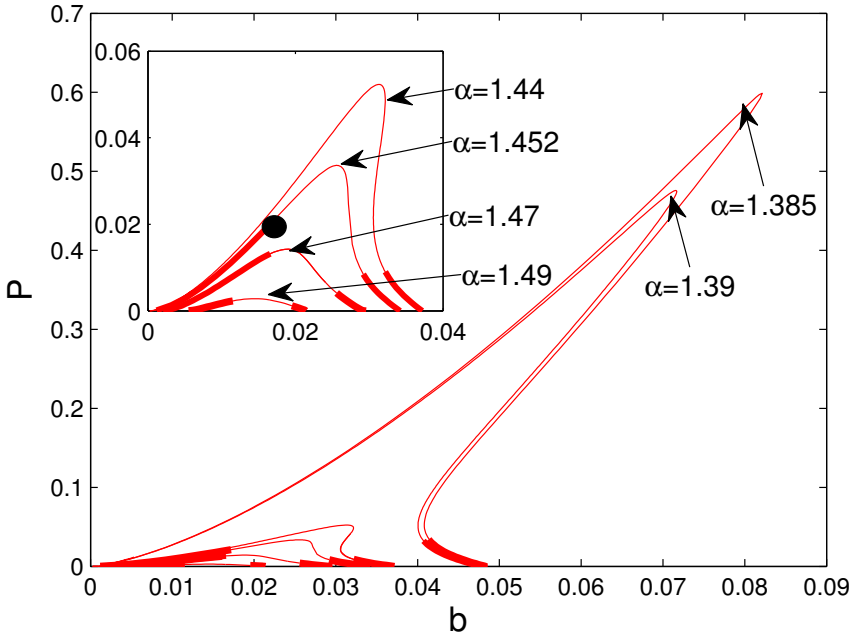

Figure 6.1: Families of the solutions bifurcating from $b_{1,0} = \eta_1^2$ in the case (4.6) for several values of α. Thick (thin) lines represent stable (unstable) solutions. Insertion shows the branches for larger values of α. The black circles represent solutions studied in text. The parameters of the structure are $V = 1/2$ and $q = 0$ and $\alpha_{cr} = 1.5$.

where

$$\eta_1 = \frac{1}{2}\left(\sqrt{V(\alpha_{cr} - \alpha)} + \sqrt{V(\alpha + \alpha_{cr})} - 1\right). \tag{6.8}$$

Above the symmetry breaking point ($\alpha > \alpha_{cr}$) the eigenvalues of the bound states are complex valued. We notice here that no fundamental branch satisfying condition (4.6) with $\alpha > \alpha_{cr}$ was found. Therefore from now on we concentrate only on the results for $\mathcal{PT}$-symmetry preserving case (6.6). Moreover, our consideration will be limited to nonlinear modes that bifurcate from the ground state of defect potential in Eq. (6.5), i.e. $n = 0$. The respective eigenstate of the linear problem (6.5) reads [70, 71]

$$w_{1l}(\xi) = W_1 \mathrm{sech}^{\eta_1}(\xi) \exp\left[\frac{i}{2}\Theta \tan^{-1}(\sinh \xi)\right] \tag{6.9}$$

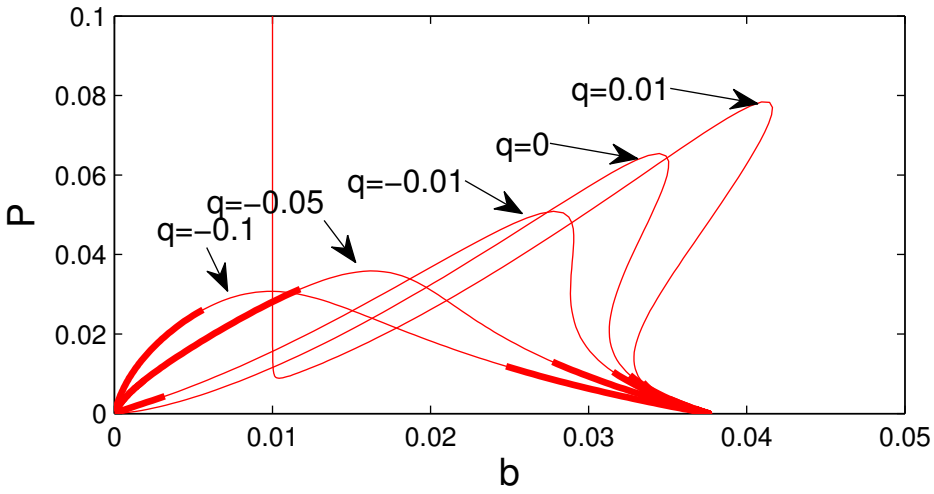

Figure 6.2: Families of the solutions bifurcating from $b_{1,0} = \eta_1^2$ and corresponding to the case (4.6) for several values of q. Thick (thin) lines represent stable (unstable) solutions. The parameters of the structure are $V = 1/2$ and $\alpha = 1.44$.

where W_1 is a constant and

$$\Theta = \sqrt{V(\alpha_{cr} - \alpha)} - \sqrt{V(\alpha + \alpha_{cr})}. \tag{6.10}$$

Passing to (6.4b), in the small amplitude limit one can look for a solution with $w_1 \approx w_{1l}$, which plays the role of the inhomogeneous term in the linear equation for w_2. However, to obtain the complete families of solutions one has to consider both Eqs. (6.4). We did this using relaxation Newton-Raphson method using the described linear solutions as the initial ansatz.

Fig. 6.1 shows the dependence of the total power P as defined in (4.10) on the propagation constant with several values of α. We observe that the fundamental branches shown in Fig. 6.1 have a maximal in power P_M, $P \leq P_M$. The value of P_M is decreasing as α increases. We also observed that $P_M \to 0$ as $\alpha \to \alpha_{cr}$, i.e. the fundamental branch disappears. For a given α, the position of P_M in respect to b approaches $b = 0$ as q decreases, as one can see in Fig. 6.2. The position of P_M moves to the right in the case $q > 0$. One can also see in Fig. 6.2 that in this case the branch ends in $b = -q$ because the mismatch shifts the position of the continuum spectrum of the linear part of (6.4b) and w_2 becomes delocalized.

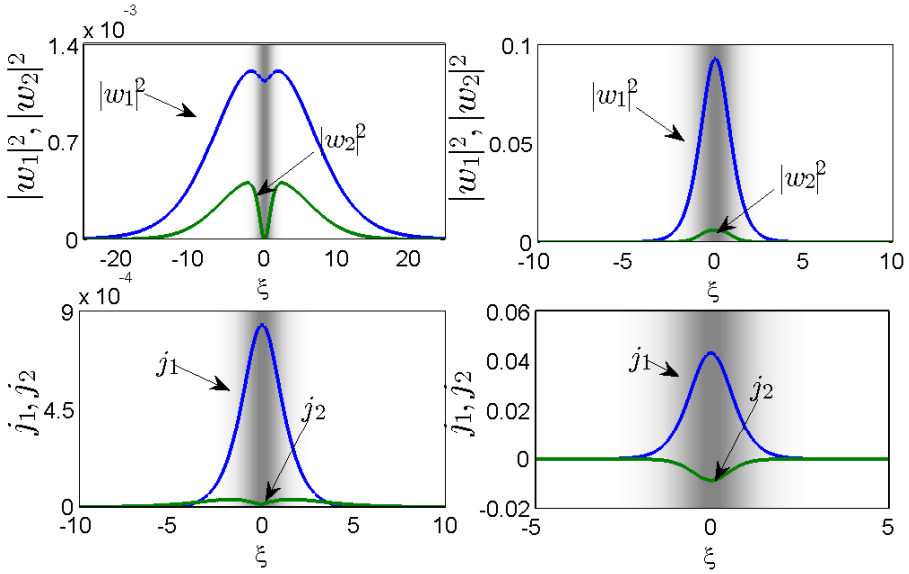

Figure 6.3: Spatial distributions of the intensities $|w_\beta|^2$ (upper panels) and the currents j_β (lower panels). The left panels corresponds to a stable solution with $b = 0.024$, as marked by a black circle in Fig. 6.1, pertaining to the fundamental branch that bifurcates from $b_{1,0} = 0.034$, where $V = 1/2$, $q = 0$ and $\alpha = 1.452$. The right panels corresponds to a stable solution with $b = 0.82$, pertaining to the fundamental branch that bifurcates from $b_{1,0} = 0.92$, where $V = 2$, $q = 0$ and $\alpha = 0.5$. Shadowed domains show the localized impurity (darker areas represent higher values of its real part, $V\mathrm{sech}^2\xi$.

There is no low amplitude linear limit for w_1 in this case.

In Fig. 6.3 we show the typical distributions of the fields w_β and the real-valued currents j_β as defined in (4.11) By construction $|w_\beta|^2$ and j_β are even functions. The effective width of the intensities of modes may significantly exceed the size of the impurity, particularly in the modes closer to the edge of the continuous spectrum (the left panels of Fig. 6.3).

We note that in the left panels of Fig. 6.3 the solution has a relatively small amplitude. This is a peculiarity of the chosen strength of the potential (it was $V = 1/2$, solitons with larger amplitudes were found to be unstable). While this potential (ensuring the existence of only one linear defect level in the localized potential) is used below along the text, in the right panels of Fig. 6.3 we show a higher amplitude soliton for the potential well having the width $V = 2$ (and the

parameters $\alpha = 0.5$ and $q = 0$).

6.4 Nonlinear modes without linear limit

In this section we investigate the case when the second harmonic remains finite at $w_1 \to 0$, i.e., case (4.5). Then one can neglect the nonlinear term w_1^2 in (6.4b) reducing it to the well known linear eigenvalue problem (5.6) with (see e.g. [40])

$$\mathcal{L}_2 = \frac{1}{2}\frac{d^2}{d\xi^2} + 2\left(V\frac{1}{\cosh^2\xi} + q\right), \tag{6.11}$$

whose eigenvalues are

$$b_{2,n} = \frac{(n-\eta_2)^2}{4} + q, \quad n < 0, 1, ..., \eta_2 = \sqrt{\frac{1}{4} + 4V} - \frac{1}{2} \tag{6.12}$$

Here we again consider the case when there is only one localized mode. This leads to the requirement that $\eta_2 \leq 1$ and consequently $V \leq 1/2$. The corresponding eigenfunction of $b_{2,0}$ reads

$$w_{2,0}(\xi) = W_2 \mathrm{sech}^{\eta_2}\xi. \tag{6.13}$$

where W_2 is some constant which must be determined. This can be done from the condition that the propagation constants in the equations (6.11) and (6.4a) are the same. In the vicinity of the bifurcation point one can approximate $w_2 \approx w_{2l}$, i.e., Eq. (6.4a) can be approximated by the following linear system

$$\mathcal{L}\begin{pmatrix} \bar{w}_1 \\ w_1 \end{pmatrix} = W_2 \begin{pmatrix} \bar{w}_1 \\ w_1 \end{pmatrix}, \quad \mathcal{L} = -\frac{1}{2}\cosh^{\eta_2}(\xi)\begin{pmatrix} 0 & \mathcal{L}_1 - b_{2,0} \\ \bar{\mathcal{L}}_1 - b_{2,0} & 0 \end{pmatrix}. \tag{6.14}$$

Let us note that (6.14) is an eigenvalue equation and so the allowed values of W_2 are simply the eigenvalues. Next we define a bra– and ket– vectors: $\langle\psi| \equiv (\psi(\xi), \bar{\psi}(\xi))$ and $|\psi\rangle \equiv (\bar{\psi}(\xi), \psi(\xi))^T$ (T stays for the transpose matrix), where $\psi(\xi) \to 0$ at $\xi \to \pm\infty$, and verify that the operator $\mathcal{L}$ is Hermitian with respect

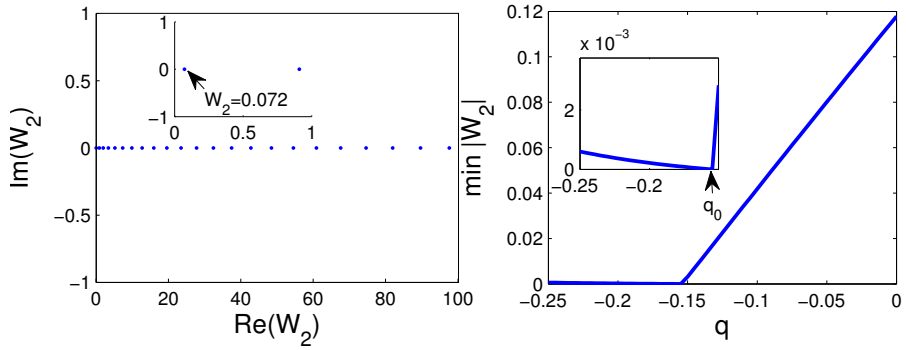

Figure 6.4: Left panel: The eigenvalues W_2 of (6.14). The parameters of the structure are $V = 1/2$, $\alpha = 1.4$ and $q = 0$. Insertion shows the first few eigenvalues in detail. Right panel: The lowest $|W_2|$ of (6.14) as a function of the mismatch q of the lowest P branch. The insertion shows how the minimum value of W_2 reaches zero at $q = q_0$.

to the weighted inner product:

$$\langle \psi_1 | \psi_2 \rangle = \int_{-\infty}^{\infty} \operatorname{sech}^{\eta_2}(\xi) \left[\psi_1(\xi) \bar{\psi}_2(\xi) + \bar{\psi}_1(\xi) \psi_2(\xi) \right] d\xi. \tag{6.15}$$

The Hermiticity of $\mathcal{L}$ ensures the reality of the admissible W_2. We also note that if $(\bar{w}_1(\xi), w_1(\xi))^T$ is a solution of (6.14) with eigenvalue W_2, then $-W_2$ is also an eigenvalue with eigenfunction $(-i\bar{w}_1(\xi), iw_1(\xi))^T$. This allows us to restrict the consideration to $W_2 > 0$.

We investigated the system (6.14) numerically and found that there is an infinite number of discrete eigenvalues W_2. The ones having the smalest absolute values are shown in Fig. 6.4. The amplitude of the second harmonic W_2 depends on $b = b_{2,0}$ (See Eq.(6.14)). In Fig. 6.4, we show the dependence of W_2 on q corresponding to the lowest $|W_2|$ branch. The special case, when for a certain value of q the amplitude of the second harmonic $W_2 \to 0$, happens when $b_{1,0} = b_{2,0}$. This leads to

$$q = q_0, \qquad q_0 = \eta_1^2 - \frac{1}{4}\eta_2^2, \tag{6.16}$$

which is precisely the case (4.4), however we consider it in the next section.

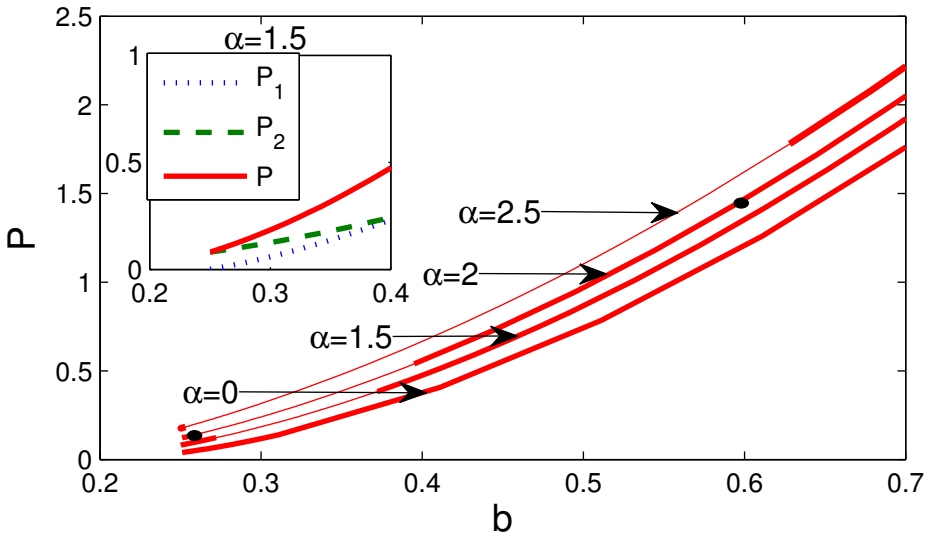

Figure 6.5: The power diagrams of the fundamental branches bifurcating from the linear mode $b_{2,0} = 0.25$ for several values of α. Thick (thin) lines represent stable (unstable) solutions. Insertion shows in detail that P_1 goes to zero in the vicinity of $b_{2,0}$ while P_2 remains finite. Filled circles represents two stable solutions shown below in Fig. 6.6. The parameters of the structure are $V = 1/2$ and $q = 0$.

We numerically studied the existence of bifurcations satisfying (4.5) in Fig. 6.5. It is possible to see in the insertion of Fig. 6.5 that at the bifurcation point the branches satisfy $P_1(b_{2,0}) = 0$ and consequently $P(b_{2,0}) = P_2(b_{2,0})$. A simple integration in (4.10) after the substitution $w_2 = w_{2l}$, reveals that for each α when $V = 1/2$ and $\eta_2 = 1$ (the case of Fig. 6.5) one has $P(b_{2,0}) = 4W_2^2$.

It can be seen in Fig. 6.5 for the power diagrams of the fundamental branches, where stable solutions exist above the $\mathcal{PT}$- symmetry breaking point. The existence of stable nonlinear modes even when the spectrum of the linear system is not purely real has been earlier reported in [28] (see also recent work [105].)

In Fig. 6.6 there is an example of a mode in the case (4.5).

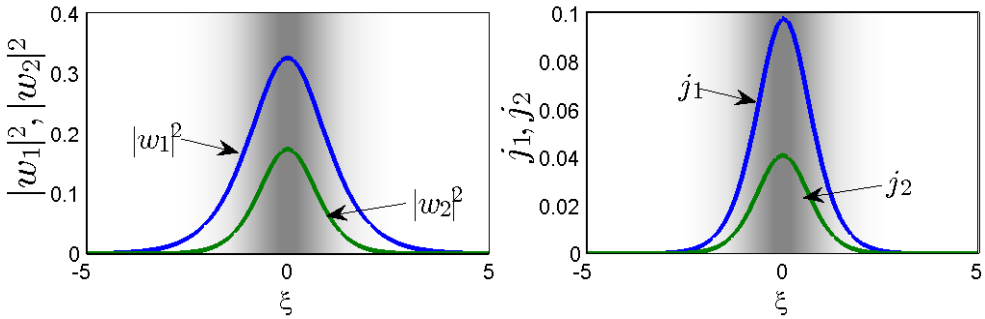

Figure 6.6: An example of a stable solution of case (4.4) with $b = 0.6$ and $\alpha = 2 > \alpha_{cr}$, marked with the filled circle in Fig. 6.5. Shadowed domains show the localized impurity (darker areas representing higher values of the real part of the localized potential). The parameters of the structure are $V = 1/2$ and $q = 0$.

6.5 Bifurcation of the nonlinear modes from the linear spectrum

Now we consider the case which the relation (4.4) holds. Previously we have shown that if the bifurcation point is at the same time an eigenvalue of (6.5) and (6.11), i.e., $b_{1,0} = b_{2,0}$, then the mismatch must have the special value $q = q_0$. We also have seen that in this case $W_2 = 0$. As a direct consequence, (6.14) reduces to (6.5) and not only $w_2 \to w_{2l}$ but also the FF satisfy $w_1 \to w_{1l}$ at the bifurcation point.

The Fig. 6.7 shows power diagrams of solutions satisfying (4.4) for several values of α.

It is possible to see that two bifurcations occur at $b = b_{1,0} = b_{2,0}$ (See the dashed line in the insertion of Fig. 6.7). The branch that goes to the right is a bifurcation of $b_{2,0}$ and the branch that goes to the left is a bifurcation of $b_{1,0}$. Both branches have a behaviour very similar to branches of case (i) and (ii). We observed in the numerical simulations, that there may be a collision of the fundamental branch with a non-fundamental branch with two-peaked solutions. The Fig. 6.8 shows the corresponding bifurcation diagrams, whereas Fig. 6.9 illustrates the distribution of the intensities and the currents in a two-hump soliton solution. The intensities and the current j_2 are largely distributed far from the

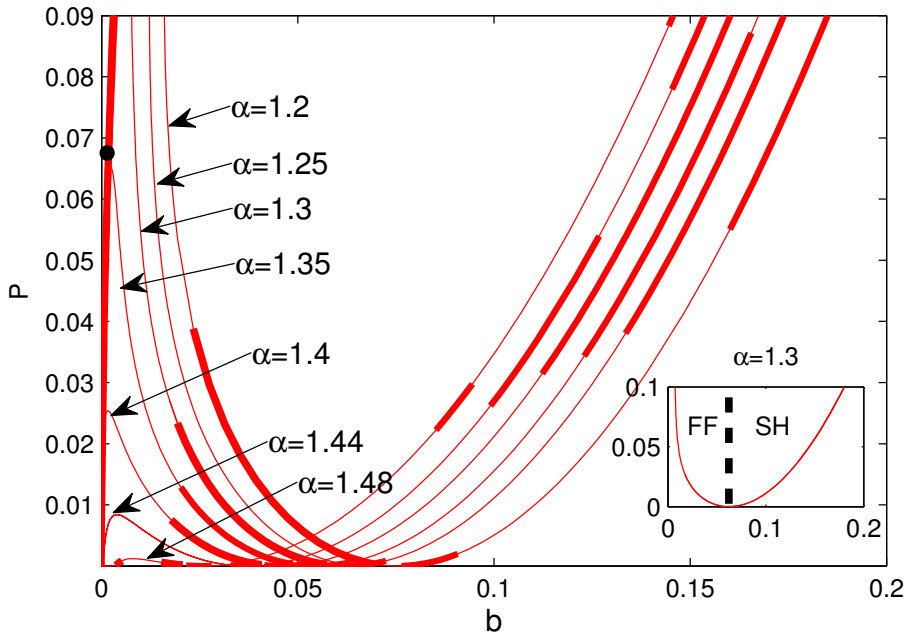

Figure 6.7: Several fundamental branches for the case (4.4) with different values of α. Note that the branch disappear when $\alpha \to \alpha_{cr} = 3/2$. Stable (unstable) solutions are represented by thick(thin) lines. Insertion shows the regions of bifurcations from $b_{1,0}$ (FF) and $b_{2,0}$ separated by a vertical dashed line. The parameters of the structure are $V = 1/2$ and $q = q_0(\alpha_{cr} = 1.5)$.

center of the potential, while the current j_1 is localized at the defect.

One can see in Fig. 6.10 that as b decreases, $|w_1(0)|^2$ decreases at the same time that two emergent peaks become increasingly separated. The intensity $|w_2(0)|^2$ (not shown) decreases as well.

In respect to phase, we found all stable solutions that bifurcate from $b_{1,0}$ to satisfy $w_\beta(\xi) = \overline{w_\beta}\,(-\xi)$. This means that the peaks of the two-hump solution shown in Fig. 6.10 are out of phase.

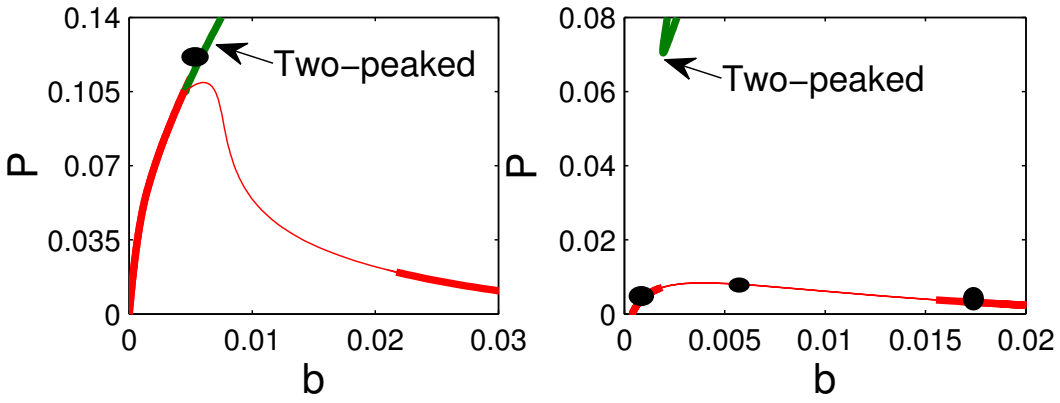

Figure 6.8: Left panel: Shows the fundamental branch (line) of case (4.4) with $\alpha = 1.3$ near $b = 0$ and the merged two-peaked branch. Thick lines (lines) are stable (unstable) solutions. Right panel: Shows a fundamental branch and a two-peaked branch with $\alpha = 1.44$ near $b = 0$. Black circles are solutions represented in Fig. 6.9 and in Fig.6.14. The parameters of the structure are $V = 1/2$ and $q = q_0$.

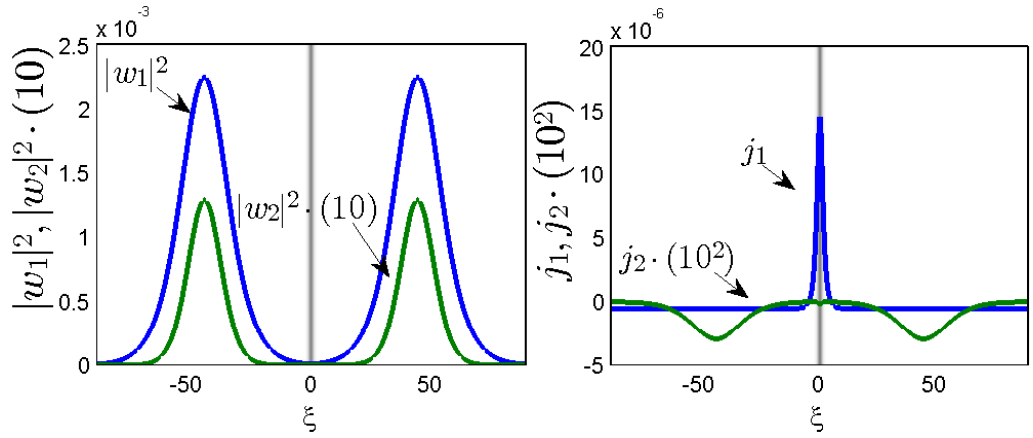

Figure 6.9: Stable double peaked solution with $b = 0.0057$ corresponding to the black circle in left panel of Fig. 6.8. Left panel shows the intensities $|w_\beta|^2$, right panel shows the currents j_β. Shadowed domain show the localized impurity $V\text{sech}^2(\xi)$ (darker areas represent higher values of the real part of the localized potential). The parameters of the structure are $V = 1/2$, $\alpha = 1.3$ and $q = q_0$.

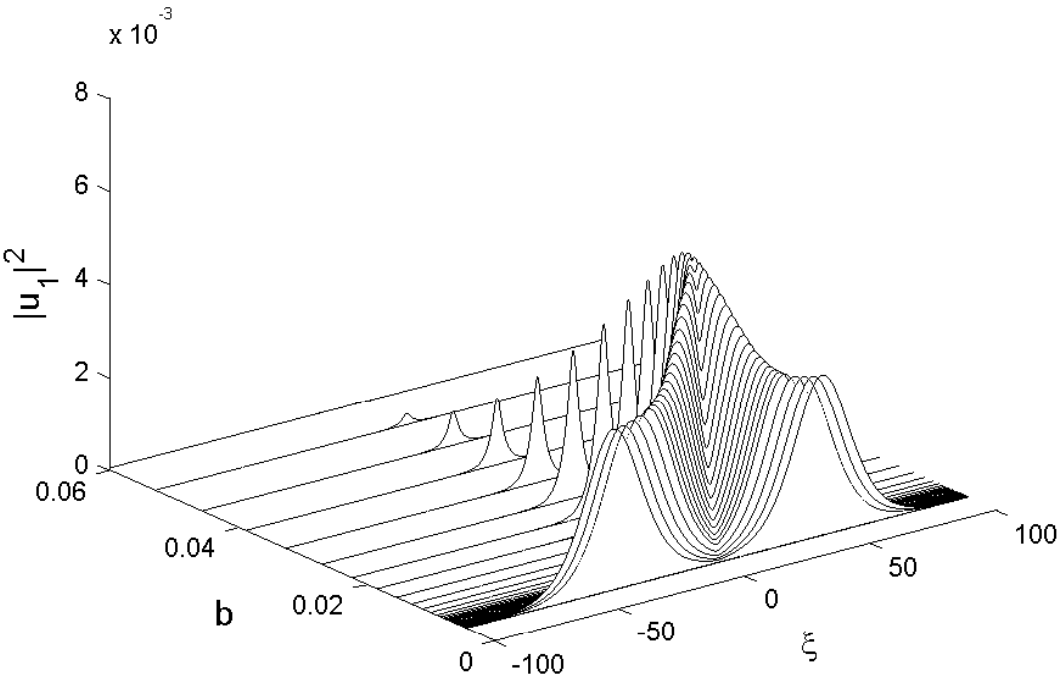

Figure 6.10: The intensity profiles $|w_1|^2$ of solutions, pertaining to the fundamental branch of case (4.4) bifurcating from $b_{1,0} = 0.063$, at different b illustrating the transition of a single-peaked profile into a double-peaked one. The local minimum occurs exactly at $\xi = 0$. The parameters of the structure are $V = 1/2$, $\alpha = 1.3$ and $q = q_0$.

6.6 Stability and dynamics of localized solutions

The stability was studied by direct numerical simulations of the system (6.1), using the split-step method described in Section 3.3, and within the framework of eigenvalue evaluation of the eigenvalue problem (See The Appendix B. Let us start the stability analysis with case (4.6). Then the branches have two stable regions, one close to $b_{1,0}$ and the other close to $b = 0$ as is shown in Fig. 6.1. It was found numerically that only low amplitude solutions are stable. The instability is produced by pairs of purely imaginary eigenvalues λ , see Fig. 6.11 showing the eigenvalues and the typical evolution of the soliton resulting in its rapid

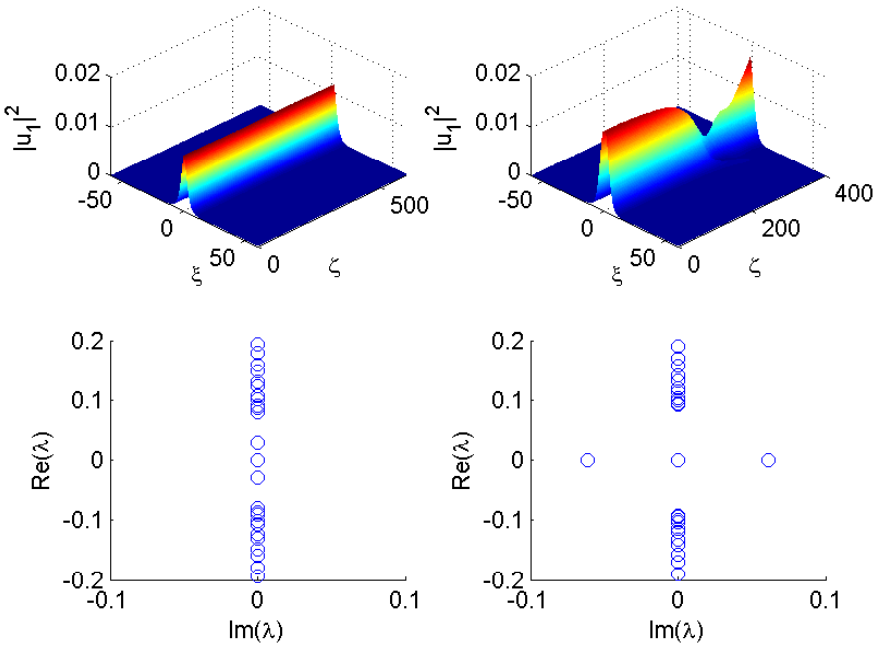

Figure 6.11: The evolution of a stable solution with $b = 0.076$ (left upper panel) and an unstable solution with $b = 0.09$ (right upper panel) of the fundamental branch of case (4.5). The corresponding eigenvalues of the linear stability analysis are given in the lower panels. The parameters of the structure are $V = 1/2$, $q = 0$ and $\alpha = 0.9$.

decay. For case (4.5), we investigate the stability and found that all the solutions are stable if $\alpha \lessapprox 0.9$, for $\alpha \gtrapprox 0.9$ some parts of the bifurcation curve become unstable, see Fig. 6.12. Also inn Fig. 6.12 one can see that the unstable part of the bifurcation curve becomes larger when α increases, but the stable solutions survive even for $\alpha \gg \alpha_{cr}$. The linear stability analysis shows that the instability arises from quartets of complex eigenvalues (See Fig. 6.13).

Finally we discuss the case (4.4). We found that in respect to stability, the behaviour is similar to case (4.6) and (4.5). For values $b > b_{1,0}$, i.e., bifurcations of $b_{2,0}$, the stability behaves like in case (ii), with the appearance of instability intervals that increase in length as α increases. The region $b < b_{1,0}$ has solutions that bifurcates from $b_{1,0}$. There is always a stable region adjacent to $b_{1,0}$ and also another stable region close to $b = 0$. The instability, when observed, was due to

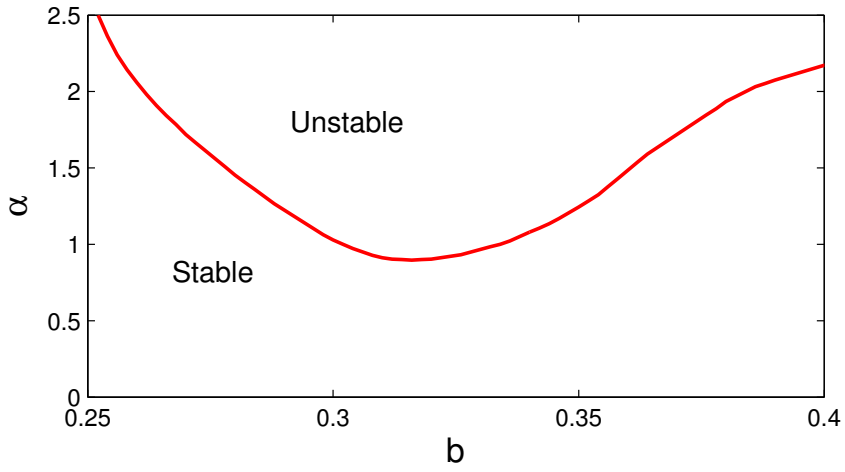

Figure 6.12: Panel shows the maximal value of α for which a fundamental branch solution is stable as a function of b. The branch bifurcates from $b_{2,0}$. The parameters of the structure are $V = 1/2$ and $q = 0$.

a quartet of complex eigenvalues of the stability matrix contained in the region $b > b_{1,0}$ and two purely imaginary eigenvalues in the region contained in $b < b_{1,0}$ (See the middle panel of the Fig. 6.14).

We observed that there are stable solutions in the region where the fundamental branch bifurcating from $b_{1,0}$ merges with a two-peaked branch (See Fig. 6.8).

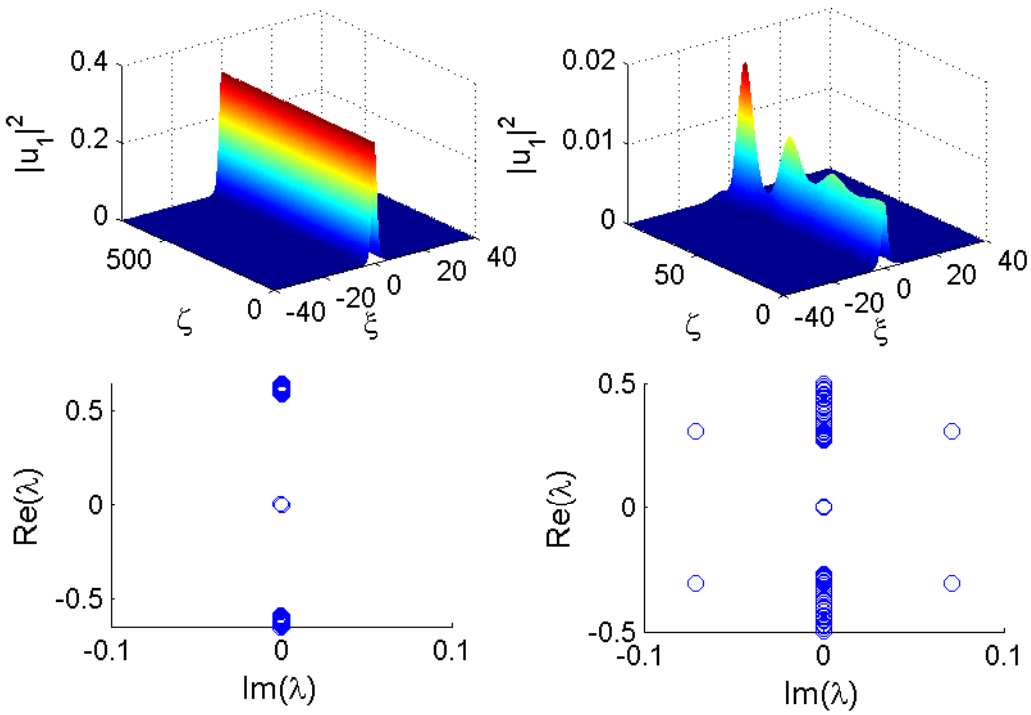

Figure 6.13: The evolution of a stable solution with $b = 0.6$ (left upper panel) and an unstable solution with $b = 0.27$ (right upper panel) of the fundamental branch of case (4.5) that bifurcates from $b_{2,0}$. Both solutions were perturbed by 10% of amplitude random noise. The corresponding eigenvalues of the linear stability matrix are given in the lower panels. Both solutions are marked by black circles in Fig. 6.5. The parameters of the structure are $V = 1/2$, $q = 0$ and $\alpha = 2$.

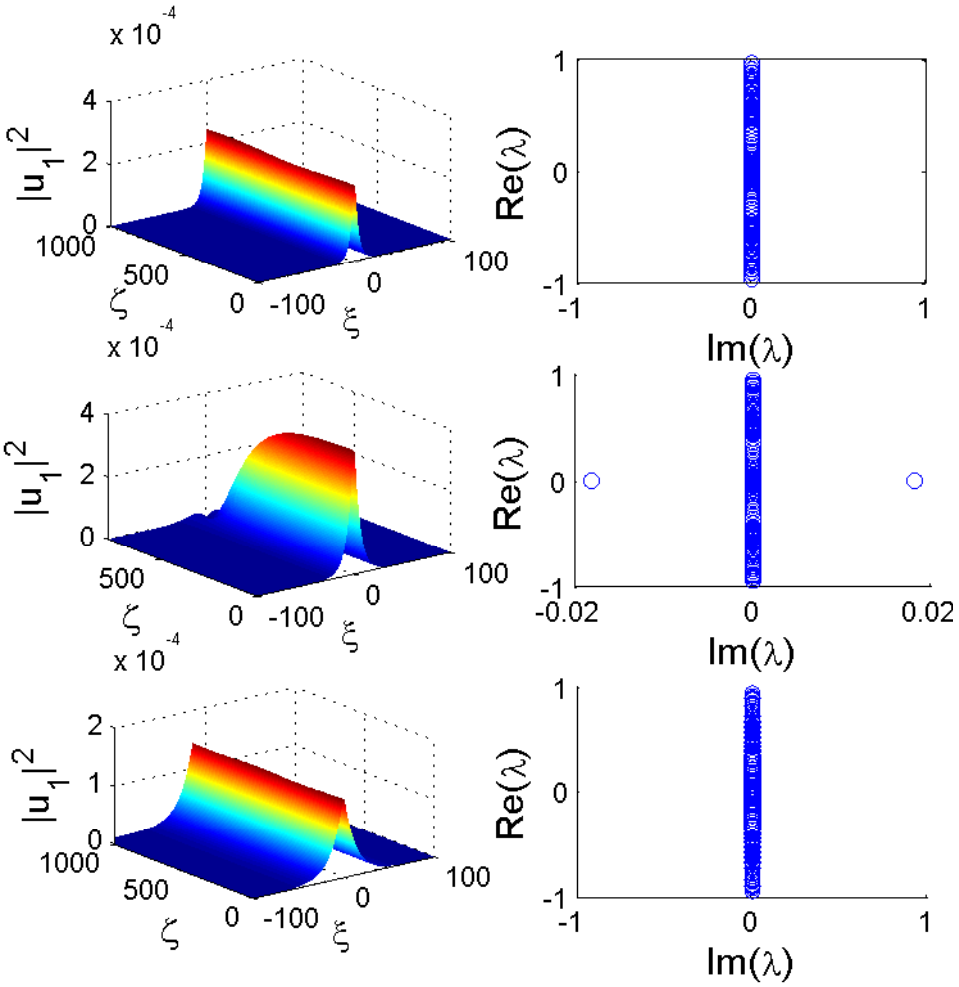

Figure 6.14: Left panels: Propagation of 10% of amplitude perturbations of solutions marked by black circles in lower panel of Fig. 6.8 corresponding to case (4.4). The upper left panel has $b = 0.0172$, the midle left panel has $b = 0.0072$ and lower left panel has $b = 0.0017$. Right panels are the respective eigenvalues of the linear problem. Parameters of the structure are $V = 1/2$, $\alpha = 1.45$ and $q = q_0$.

6.7 Conclusions

In this chapter we studied solitons in a nonlinear quadratic medium with a localized $\mathcal{PT}$-symmetric modulation of dielectric permittivity. Branches with a small amplitude limit were studied in detail. It was found that a soliton with a SH component with finite amplitude exists when the amplitude of the FF goes to zero. It was found that numerous branches, possibly an infinite number, exist with this conditions, with different amplitudes of the SH. Only the branch with smaller SH amplitude in the limit of vanishing FF amplitude was found to have stable solutions. Also in the case of bifurcations from the linear localized mode of the SH, we found stable solutions well above the $\mathcal{PT}$-symmetry breaking threshold. No such stable solutions were found when the bifurcation is from a linear localized mode of the FF.

Chapter 7

Conclusions

This thesis had as a primary objective the investigation of the dynamics of solitons in three different types of media with quadratic nonlinearity. Through the thesis one-dimensional modulations were used and envelope equations with one transverse spatial dimension and a propagation dimension were considered. Families of the solitons have been constructed, and their stability was investigated by means of the linearization and direct simulations alike.

In the first problem considered in this thesis we have introduced the model combining the linear parity-time symmetric part and the $\chi^{(2)}$ nonlinearity. The parity-time symmetric terms are represented by the complex potential acting on the fundamental field component, whose imaginary part, accounting for the spatially separated and mutually balanced gain and loss, is, as usual, the odd function of the coordinate. The potential acting on the second-harmonic wave is assumed to be purely real. The complex linear potential gives rise to the corresponding band-gap spectrum. Solitons were found semi-infinite and finite gaps, starting from the bifurcation which gives rise to such solitons at edges of the respective gap. We found that by properly adjusting the gain and loss parameter or the mismatch between harmonics it is possible to merge the bifurcations from edges of the fundamental field with edges of the second-harmonic. Solitons were found to become delocalized in the second-harmonic component as propagation constant approaches that of the second-harmonic gap edge. The amplitude of these solutions were found to depend on the gain and loss parameter and mismatch. Bifurcations from a second-harmonic gap edge were found to have a small

amplitude limit only when the edges of the second-harmonic and the fundamental field have the same value of propagation constant.

While the system contains several parameters, we have primarily focused on effects produced by the variation of the amplitude of the imaginary part of the potential, which is specific to the parity-time symmetric system. A noteworthy result is that the present system may support of continuous family of solitons embedded into the continuous spectrum of the SH component, and a part of the family of such embedded solitons is stable. The analysis has been reported, chiefly, for the most physically relevant case of equal effective amplitudes of the real potentials acting on the fundamental field and second harmonic waves. In addition, the *virtual grating* case, where the real potential acting solely on the FF component was investigated. It was found that the solutions have stable solutions in the semi-infinite gap with higher values of gain and loss coefficient than the ones when the modulation is present in both harmonics.

A natural extension of this analysis may be performed for the two-dimensional version of the $\chi^{(2)}$ system with the parity-timesymmetric periodic potential. In that case, it may be also interesting to construct vortex solitons, in addition to the fundamental ones, and investigate their stability.

We have investigated, in the second problem considered in this thesis, the existence, spatial properties, and stability of localized modes in lossless nonlinear quadratic materials with periodically modulated linear refractive index and quadratic nonlinearity. An important assumption about the structure was that its quadratic nonlinearity averaged over the transverse direction is zero. We considered in details asymptotic properties of the solutions which revealed two different types of the behavior, corresponding to dominating asymptotic of either fundamental field or of the second harmonic. These asymptotics were used for the shooting method, used for computing computed the branches of the stationary solutions existing in the semi-infinite and three higher gaps. We have shown that solitons may possess different symmetries (i.e. have profiles described either by even or by odd functions) of the fundamental field, but the symmetry of the second-harmonic is directly related to the symmetry of the nonlinear modulation, being even in the case of even nonlinear modulation.

The modes may have the field energy to be concentrated either in slabs with

higher of with lower dielectric permittivity. However only the former ones turn out to be stable. Moreover, we found that only small amplitude gap solitons are stable in the cases of finite total gaps. Such modes can bifurcate only from the edge of the total gap (i.e. the domain of the propagation constant which in the linear limit is forbidden for both fundamental and second harmonics) when it coincides with the band-edge of the first harmonic. We derived an effective cubic equation that was used to predict when a band-edge of the first harmonic supports a branch with small amplitude limit. We found that the nonlinear modulation is fundamental in wether such a bifurcation occurs, as opposed to the case with a linear modulation only. Moreover, in the case of solitons in finite gaps, a stable mode and can be excited with their centers belonging either to a slab with higher refractive index or in a slab with the lower one. This simultaneous existence of different stable localized can be viewed as a bistability of gap solitons. Solitons in the semi-infinite total gap where found to have an opposite behavior, having a minimal amplitude for unstable solitons, all solutions with higher amplitudes being stable.

We mention quite different physical system where similar kind of gap solitons may be observable. It is an atomic-molecular Bose-Einstein condensate loaded in an optical lattices [106], where the modulation of the "quadratic nonlinearity" is performed by manipulating the atomic-molecule scattering length in space using the Feshbach resonance technique [107].

In the last problem investigated in this thesis we have show the existence of solitons in quadratic nonlinear media with localized parity-time symmetric modulations of linear refractive index. Families of stable one and two-hump solitons were found. We found that it is possible that the two families to merge. The region were the branches merge was found to have stable solutions.

The properties of nonlinear modes bifurcating from a linear limit of small fundamental harmonic field were investigated. The bifurcations were found start from linear modes of the fundamental field or the second-harmonic. In the case of bifurcations from a linear mode of the fundamental field we found that the fundamental branch have a maximum in power. This maximum is decreasing with the strength of of imaginary part of the dielectric permittivity. This maximum approaches zero when the gain and loss coefficient approaches the parity-time

breaking threshold.

We found, for nonlinear modes no having linear limit, i.e., approaching a finite amplitude of the second-harmonic field when the amplitude of the fundamental field becomes negligible, that this limit depends on the gain and loss parameter and mismatch. The amplitude of the second-harmonic becomes negligible as a given choice of these parameters make the propagation constant of the linear modes of the second-harmonic and the fundamental field coincide. The difference between the localized modulation and the periodic modulation systems in this case is that the second-harmonic field is always localized, even at the limit of negligible fundamental field. We found that unstable regions occur, their range in propagation constant was found to increase as the gain and loss parameter increases. However we found that even for values of gain and loss coefficients much higher than the parity-time-symmetry breaking threshold, two stable regions still exists, one close to the linear mode of the second-harmonic and other for high values of amplitude.

As a final conclusion, the work we developed really helped to expand the frontiers of nonlinear optics, specially the new topic of parity-time symmetric systems in an optics context. There are natural further developments which can be made, such as, extension to two-dimensional models, the study of the effects of the inclusion of parity-time symmetric defects in periodic structures and the addition of other types of nonlinearity to the models presented in this thesis.

Appendix A

Derivation of Eq. (5.19)

Let us notice that the wave-vector can be at the center ($k_0 = 0$) or at the edge ($k_0 = 1/2$) of the first Brillouin zone and use $\phi^{(m)}_{\beta,k}(\xi_0)$ and $b^{(m)}_{\beta,k}$ for the orthonormal Bloch states and the respective eigenvalues of the operator $\mathcal{L}_\beta$. It follows from the Floquet theorem that $\phi^{(m)}_{1,k} = \varphi^{(m)}_{1,k}(\xi_0)\, e^{ik\xi}$ and $\varphi^{(m)}_{1,k}(\xi + 2\pi) = \varphi^{(m)}_{1,k}(\xi_0)$.

For the sake of simplicity and approaching the statement of the problem closer to the reality we consider a finite structure, having a large length $L = 2N\pi$ ($N \gg 1$ is an integer) and impose the cyclic boundary conditions in the interval $0 \le \xi_0 \le L$, where $L = 2N\pi$ and N is a large integer.

Substituting (5.17) and the scaled variables (2.7) in (2.9) we obtain in the first order of η, $i\frac{\partial u_1^{(1)}}{\partial \zeta_0} - \mathcal{L}_1 u_1^{(1)} = 0$. This equation is solved by the ansatz (5.18)

In the second order of η we have

$$i\frac{\partial u_1^{(2)}}{\partial \zeta_0} - \mathcal{L}_1 u_1^{(2)} = -2\frac{\partial \phi^{(m_0)}_{1,k_0}}{\partial \xi_0}\frac{\partial U_1}{\partial \xi_1} - i\phi^{(m_0)}_{1,k_0}\frac{\partial U_1}{\partial \zeta_1}. \tag{A.1}$$

The solution $u_1^{(2)}$ is searched in the form

$$u_1^{(2)} = \sum_{m \neq m_0} g_m \phi_1^{(m)} e^{ib_1^{(m_0)}\zeta_0} + c.c. \tag{A.2}$$

In above $\phi_1^{(m)} = \phi_{1,k_0}^{(m)}$. Substituting (A.2) in (A.1) and projecting in all Bloch functions is possible to obtain

$$g_m = 2\frac{\Gamma_1^{(m)}}{b_1^{(m_0)} - b_1^{(m)}}\frac{\partial U_1}{\partial \xi_1}, \quad \Gamma_1^{(m)} = \int_0^{2\pi} \varphi_1^{(m)} \frac{\partial \varphi_1^{(m_0)}}{\partial \xi_0} d\xi_0. \tag{A.3}$$

Now the investigate the η^2 order equation of the SH

$$\frac{1}{2} i \frac{\partial u_2^{(2)}}{\partial \zeta_0} - \mathcal{L}_2 u_2^{(2)} = -\frac{1}{2} f(\xi_0) \left(\phi_1^{(m_0)}\right)^2 U_1^2. \tag{A.4}$$

We look for solutions in the form

$$u_2^{(2)} = \sum_{(m,k)} c_{m,k}(\xi_1, \zeta_2)\, \phi_{2,k}^{(m)} e^{2ib_1^{(m_0)}\zeta_0} + c.c. \tag{A.5}$$

The expansion (A.5) is valid since we excluded a possibility for $b_{2,k}^{(m)}$ to approach $b_1^{(m_0)}$ (see Fig.5.1). Next we substitute (A.5) in (A.4) and project on $\phi_{2,k}^{(m)}$ obtain

$$c_m = \frac{\Gamma_2^{(m)} U_1^2}{2\left(b_1^{(m_0)} - b_2^{(m)}\right)}, \quad \Gamma_2^{(m)} = \int_0^{2\pi} \varphi_m^{(2)} f(\xi_0) \left(\varphi_{m_0}^{(1)}\right)^2 d\xi_0$$

Here we took into account that only wave vectors $k = 2k_0$ give nonzero terms in the expansion. Since $2k_0$ is either 0 or a vector of the reciprocal lattice, only the functions $\phi_2^{(m_0)}$ enter in (A.6).

Notice that $f(\xi_0)\left(\varphi_{m_0}^{(1)}\right)^2$ is always even. This means that $c_m = 0$ if $\varphi_m^{(2)}$ is odd. Finally we write the equation of order η^3

$$\begin{aligned} i\frac{\partial u_1^{(3)}}{\partial \zeta_0} - \mathcal{L}_1 u_1^{(3)} = -i\frac{\partial u_1^{(1)}}{\partial \zeta_2} - i\frac{\partial u_1^{(2)}}{\partial \zeta_1} - \frac{\partial^2 u_1^{(1)}}{\partial \xi_1^2} \\ -2\frac{\partial}{\partial \xi_0}\frac{\partial}{\partial \xi_1} u_1^{(2)} - 2f(\xi)\,\overline{u_1^{(1)}} u_2^{(2)}. \end{aligned}$$

Projecting this equation on $\phi^{(1)}_{m_0}$ and rescaling $U = \sqrt{|G/D|}U_1$ where

$$D = 1 + 2\sum_{m\neq m_0} \frac{\left|\Gamma_1^{(m)}\right|^2}{b_1^{(m_0)} - b_1^{(m)}}, \quad G = \sum_m \frac{\left|\Gamma_2^{(m)}\right|^2}{b_2^{(m)} - b_1^{(m_0)}}, \tag{A.6}$$

$Z = D\zeta_2$ and $X = \xi_1$ we arrive at Eq. (5.19) where

$$S = \mathsf{sign}(GD) \tag{A.7}$$

Notice that the function $f(\xi)$ plays a fundamental role in definition of the sign of F while D is fixed by linear potential $\mathcal{V}_1(\xi)$.

Appendix B

Linear stability analysis

In this appendix I consider the effect of small amplitude perturbations on localized solutions in the framework of linear stability analysis. A detailed explanation of the procedure can be found in [108].

The perturbed solution has the following form

$$u_\beta(\xi,\zeta) = \left[w_\beta(\xi) + p_{\beta+}(\xi,\zeta) + \overline{p}_{\beta-}(\xi,\zeta)\right] e^{i\beta b\zeta}. \tag{B.1}$$

The functions $p_{\beta+}(\xi,\zeta)$ and $p_{\beta-}(\xi,\zeta)$ represent small perturbations and w_β being the localized stationary solutions which are subjected to stability analysis.

The interest here is to see if the small perturbations $p_{\beta\pm}(\xi,\zeta)$ grows along the propagation distance. Substitution of (B.1) in (2.9) results in a nonlinear partial differential equation, but the assumption that the perturbation are small compared to the amplitude of the localized solution, i.e. $|p_{\beta\pm}| \ll w_\beta$ allows the nonlinear terms to be neglected. At first order is is possible to write four different linear evolution equations

$$M \begin{pmatrix} p_{2+} \\ p_{1+} \\ p_{2-} \\ p_{1-} \end{pmatrix} = -i\frac{\partial}{\partial\zeta} \begin{pmatrix} p_{2+} \\ p_{1+} \\ p_{2-} \\ p_{1-} \end{pmatrix}, \tag{B.2a}$$

$$M = \begin{pmatrix} \mathcal{L}_2 + 2(q-b) & 2f_2(\xi)w_1 & 0 & 0 \\ 2f_1(\xi)\bar{w}_1 & \mathcal{L}_1 - b & 0 & 2f_1(\xi)w_2 \\ 0 & 0 & -\bar{\mathcal{L}}_2 - 2(q-b) & -2\bar{f}_2(\xi)\bar{w}_1 \\ 0 & -2\bar{f}_1(\xi)\bar{w}_2 & -2\bar{f}_1(\xi)w_1 & -\bar{\mathcal{L}}_1 + b \end{pmatrix}. \tag{B.2b}$$

Where M is called the stability operator.

Next we note that (B.2b) does not depend on ζ. We separate variables in the perturbation components as $p_{\beta,+}(\xi,\zeta) \equiv p_{\beta,+}(\xi)\exp(-i\lambda\zeta)$ and $p_{\beta,-}(\xi,\zeta) \equiv p_{\beta,-}(\xi)\exp(i\bar{\lambda}\zeta)$ to obtain

$$M \begin{pmatrix} p_{2+} \\ p_{1+} \\ p_{2-} \\ p_{1-} \end{pmatrix} = \lambda \begin{pmatrix} p_{2+} \\ p_{1+} \\ p_{2-} \\ p_{1-} \end{pmatrix}. \tag{B.3}$$

In all numerical calculations we approximate the second order differential operator $d^2/d\xi^2$ by finite differences in a equally spaced finite grid with N points and all continuous functions are represented by their values at the grid points as in Sec. 3.2. Then M becomes a $4N$ x $4N$ matrix. The eigenvalues are obtained numerically using the **eig** routine of MATLAB. The routine itself can use multiple LAPACK [81] routines depending on the specific type of M, e.g., if it is symmetric, hermitian or real valued.

A solution is said to be unstable if at least one eigenvalue $\mathrm{Im}(\lambda_{n'}) > 0$, where $n' = 1, 2, ..., 4N$.

References

[1] P. A. Franken, A. E. Hill, C. W. Peters, and G. Weinreich, "Generation of optical harmonics," *Phys. Rev. Lett.*, vol. 7, pp. 118–119, Aug 1961. 1

[2] J. A. Armstrong, N. Bloembergen, J. Ducuing, and P. S. Pershan, "Interactions between light waves in a nonlinear dielectric," *Phys. Rev.*, vol. 127, p. 1918, 1962. 1

[3] M. V. I. N. R. Belashenkov, S. V. Gagarskii, "On the nonlinear light refraction under the 2nd-harmonic generation," *Opt. Spectrosc.*, vol. 66, p. 809, 1989. 1

[4] R. DeSalvo, D. J. Hagan, M. Sheik-Bahae, G. Stegeman, E. W. V. Stryland, and H. Vanherzeele, "Self-focusing and self-defocusing by cascaded second-order effects in ktp," *Opt. Lett.*, vol. 17, pp. 28–30, Jan 1992. 1

[5] V. E. Zakharov, "Instability of self-focusing of light," *Sov. Phys. JETP*, vol. 26, no. 5, p. 994, 1968. 1

[6] A. Hasegawa and F. Tappert, "Transmission of stationary nonlinear optical pulses in dispersive dielectric fibers. i. anomalous dispersion," *Applied Physics Letters*, vol. 23, pp. 142 –144, aug 1973. 1

[7] A. P. S. Yu. N. Karamzin, "Nonlinear interaction of diffracted light beams in a medium with quadratic nonlinearity: mutual focusing of beams and limitation on the efficiency of optical frequency converters," *JETP Lett.*, vol. 20, no. 11, p. 339, 1974. 2

[8] W. E. Torruellas, Z. Wang, D. J. Hagan, E. W. VanStryland, G. I. Stegeman, L. Torner, and C. R. Menyuk, "Observation of two-dimensional spatial solitary waves in a quadratic medium," *Phys. Rev. Lett.*, vol. 74, pp. 5036–5039, Jun 1995. 2

[9] R. Schiek, Y. Baek, and G. I. Stegeman, "One-dimensional spatial solitary waves due to cascaded second-order nonlinearities in planar waveguides," *Phys. Rev. E*, vol. 53, pp. 1138–1141, Jan 1996. 2

[10] D. Bliss, C. Lynch, D. Weyburne, K. O'Hearn, and J. Bailey, "Epitaxial growth of thick gaas on orientation-patterned wafers for nonlinear optical applications," *Journal of Crystal Growth*, vol. 287, no. 2, pp. 673 – 678, 2006. 2, 60

[11] W. T. Tsang and M. Ilegems, "Selective area growth of gaas/al[sub x]ga[sub 1 - x]as multilayer structures with molecular beam epitaxy using si shadow masks," *Applied Physics Letters*, vol. 31, no. 4, pp. 301–304, 1977. 2, 60

[12] E. Ozbay, E. Michel, G. Tuttle, R. Biswas, M. Sigalas, and K.-M. Ho, "Micromachined millimeter-wave photonic band-gap crystals," *Applied Physics Letters*, vol. 64, no. 16, pp. 2059–2061, 1994. 2

[13] S. Yang, M. Megens, J. Aizenberg, P. Wiltzius, P. M. Chaikin, and W. B. Russel, "Creating periodic three-dimensional structures by multibeam interference of visible laser," *Chemistry of Materials*, vol. 14, no. 7, pp. 2831–2833, 2002. 2

[14] X. Wang, J. F. Xu, H. M. Su, Z. H. Zeng, Y. L. Chen, H. Z. Wang, Y. K. Pang, and W. Y. Tam, "Three-dimensional photonic crystals fabricated by visible light holographic lithography," *Applied Physics Letters*, vol. 82, no. 14, pp. 2212–2214, 2003. 2

[15] J. H. Moon, A. Small, G.-R. Yi, S.-K. Lee, W.-S. Chang, D. J. Pine, and S.-M. Yang, "Patterned polymer photonic crystals using soft lithography and holographic lithography," *Synthetic Metals*, vol. 148, no. 1, pp. 99 – 102, 2005. 2

[16] C. M. Bender and S. Boettcher, "Real spectra in non-hermitian hamiltonians having $\mathcal{PT}$ symmetry," *Phys. Rev. Lett.*, vol. 80, pp. 5243–5246, Jun 1998. 2, 10

[17] C. M. Bender, "Making sense of non-hermitian hamiltonians," *Reports on Progress in Physics*, vol. 70, no. 6, p. 947, 2007. 2, 10, 31

[18] A. Mostafazadeh, "Exact $\mathcal{PT}$-symmetry is equivalent to hermiticity," *Journal of Physics A: Mathematical and General*, vol. 36, no. 25, p. 7081, 2003. 2

[19] A. Ruschhaupt, F. Delgado, and J. G. Muga, "Physical realization of $\mathcal{PT}$-symmetric potential scattering in a planar slab waveguide," *Journal of Physics A: Mathematical and General*, vol. 38, no. 9, p. L171, 2005. 2

[20] C. E. Ruter, K. G. Makris, R. El-Ganainy, D. N. Christodoulides, M. Segev, and D. Kip, "Observation of parity-time symmetry in optics," *Nat Phys*, vol. 6, pp. 192–195, 03 2010. 2, 28

[21] H. Geyer, D. Heiss, and M. Znojil, "The physics of non-hermitian operators," *Journal of Physics A: Mathematical and General*, vol. 39, no. 32, 2006. 2

[22] K. G. Makris, R. El-Ganainy, D. N. Christodoulides, and Z. H. Musslimani, "Beam dynamics in $\mathcal{PT}$ symmetric optical lattices," *Phys. Rev. Lett.*, vol. 100, p. 103904, Mar 2008. 2, 31

[23] K. Makris, R. El-Ganainy, D. Christodoulides, and Z. Musslimani, "$\mathcal{PT}$-symmetric periodic optical potentials," *International Journal of Theoretical Physics*, vol. 50, pp. 1019–1041, 2011. 2

[24] B. A. Malomed, "Evolution of nonsoliton and "quasi-classical" wavetrains in nonlinear schrödinger and korteweg-de vries equations with dissipative perturbations," *Physica D: Nonlinear Phenomena*, vol. 29, no. 1â"2, pp. 155 – 172, 1987. 3

[25] S. Fauve and O. Thual, "Solitary waves generated by subcritical instabilities in dissipative systems," *Phys. Rev. Lett.*, vol. 64, pp. 282–284, Jan 1990. 3

[26] F. K. Abdullaev, V. V. Konotop, M. Salerno, and A. V. Yulin, "Dissipative periodic waves, solitons, and breathers of the nonlinear schrödinger equation with complex potentials," *Phys. Rev. E*, vol. 82, p. 056606, Nov 2010. 3

[27] H. Sakaguchi and B. A. Malomed, "Two-dimensional dissipative gap solitons," *Phys. Rev. E*, vol. 80, p. 026606, Aug 2009. 3

[28] D. A. Zezyulin and V. V. Konotop, "Nonlinear modes in finite-dimensional $\mathcal{PT}$-symmetric systems," *Phys. Rev. Lett.*, vol. 108, p. 213906, May 2012. 3, 78

[29] Z. H. Musslimani, K. G. Makris, R. El-Ganainy, and D. N. Christodoulides, "Optical solitons in $\mathcal{PT}$ periodic potentials," *Phys. Rev. Lett.*, vol. 100, p. 030402, Jan 2008. 3, 12, 30, 49, 70, 71

[30] Z. Shi, X. Jiang, X. Zhu, and H. Li, "Bright spatial solitons in defocusing kerr media with $\mathcal{PT}$-symmetric potentials," *Phys. Rev. A*, vol. 84, p. 053855, Nov 2011. 3, 12

[31] X. Zhu, H. Wang, L.-X. Zheng, H. Li, and Y.-J. He, "Gap solitons in parity-time complex periodic optical lattices with the real part of superlattices," *Opt. Lett.*, vol. 36, pp. 2680–2682, Jul 2011. 3, 12

[32] C. Li, H. Liu, and L. Dong, "Multi-stable solitons in $\mathcal{PT}$-symmetric optical lattices," *Opt. Express*, vol. 20, pp. 16823–16831, Jul 2012. 3, 12

[33] F. C. Moreira, V. V. Konotop, and B. A. Malomed, "Solitons in $\mathcal{PT}$-symmetric periodic systems with the quadratic nonlinearity," *Phys. Rev. A*, vol. 87, p. 013832, Jan 2013. 4, 13

[34] F. C. Moreira, F. K. Abdullaev, and V. V. Konotop, "Gap solitons in nonlinear periodic $\chi^{(2)}$ media," *Phys. Rev. A*, vol. 85, p. 023843, Feb 2012. 4, 11, 15, 29, 40, 46

[35] F. C. Moreira, F. K. Abdullaev, V. V. Konotop, and A. V. Yulin, "Localized modes in $\chi^{(2)}$ media with $\mathcal{PT}$-symmetric localized potential," *Phys. Rev. A*, vol. 86, p. 053815, Nov 2012. 4, 13, 28, 30, 31, 40

[36] Y. R. Shen, *The Principles of Nonlinear Optics*. Wiley Classics Library, 1984. 8, 56

[37] Y. S. Kivshar, "Gap solitons due to cascading," *Phys. Rev. E*, vol. 51, pp. 1613–1615, Feb 1995. 8

[38] A. V. Buryak, P. D. Trapani, D. V. Skryabin, and S. Trillo, "Optical solitons due to quadratic nonlinearities: from basic physics to futuristic applications," *Physics Reports*, vol. 370, no. 2, pp. 63 – 235, 2002. 8, 10, 11

[39] W. Magnus and W. Winkler, *Hill's Equation*. Dover Phoenix Editions Series, Dover Publications, 2004. 10, 16, 17, 57

[40] L. Landau and E. Lifshitz, *Quantum Mechanics: Non-Relativistic Theory*. Teoreticheskaia fizika (Izd. 3-e) (Landau, L. D, 1908-1968), Butterworth-Heinemann, 1977. 10, 76

[41] Y. V. Kartashov, V. A. Vysloukh, and L. Torner, "Soliton shape and mobility control in optical lattices," in *Progress in Optics* (E. Wolf, ed.), vol. 52 of *Progress in Optics*, pp. 63 – 148, Elsevier, 2009. 10, 30

[42] Y. V. Kartashov, B. A. Malomed, and L. Torner, "Solitons in nonlinear lattices," *Rev. Mod. Phys.*, vol. 83, pp. 247–305, Apr 2011. 10

[43] S. Trillo, C. Conti, G. Assanto, and A. Buryak, "From parametric gap solitons to chaos by means of second-harmonic generation in Bragg gratings," *CHAOS*, vol. 10, pp. 590–599, SEP 2000. 10

[44] A. B. Aceves, "Optical gap solitons: Past, present, and future; theory and experiments," *Chaos: An Interdisciplinary Journal of Nonlinear Science*, vol. 10, no. 3, pp. 584–589, 2000. 10

[45] F. Lederer, G. I. Stegeman, D. N. Christodoulides, G. Assanto, M. Segev, and Y. Silberberg, "Discrete solitons in optics," *Physics Reports*, vol. 463, no. 1â"3, pp. 1 – 126, 2008. 10

[46] H. He and P. D. Drummond, "Ideal soliton environment using parametric band gaps," *Phys. Rev. Lett.*, vol. 78, pp. 4311–4315, Jun 1997. 11

[47] T. Peschel, U. Peschel, F. Lederer, and B. A. Malomed, "Solitary waves in bragg gratings with a quadratic nonlinearity," *Phys. Rev. E*, vol. 55, pp. 4730–4739, Apr 1997. 11

[48] A. Arraf and C. Martijn de Sterke, "Coupled-mode equations for quadratically nonlinear deep gratings," *Phys. Rev. E*, vol. 58, pp. 7951–7958, Dec 1998. 11

[49] Z. Xu, Y. V. Kartashov, L.-C. Crasovan, D. Mihalache, and L. Torner, "Multicolor vortex solitons in two-dimensional photonic lattices," *Phys. Rev. E*, vol. 71, p. 016616, Jan 2005. 11, 30

[50] Y. V. Kartashov, L. Torner, and V. A. Vysloukh, "Multicolor lattice solitons," *Opt. Lett.*, vol. 29, pp. 1117–1119, May 2004. 11, 29, 30, 40, 46, 56

[51] Y. V. Kartashov, V. A. Vysloukh, and L. Torner, "Packing, unpacking, and steering of multicolor solitons in opticallattices," *Opt. Lett.*, vol. 29, pp. 1399–1401, Jun 2004. 11

[52] V. A. Brazhnyi, V. V. Konotop, S. Coulibaly, and M. Taki, "Field patterns in periodically modulated optical parametric amplifiers and oscillators," *Chaos: An Interdisciplinary Journal of Nonlinear Science*, vol. 17, no. 3, p. 037111, 2007. 11, 15, 56, 57

[53] M. Scalora, J. P. Dowling, C. M. Bowden, and M. J. Bloemer, "Optical limiting and switching of ultrashort pulses in nonlinear photonic band gap materials," *Phys. Rev. Lett.*, vol. 73, pp. 1368–1371, Sep 1994. 11

[54] A. Pasquazi and G. Assanto, "Quadratic solitons in degenerate quasi-phase-matched noncollinear geometry," *Phys. Rev. A*, vol. 80, p. 021801, Aug 2009. 11, 56

[55] V. Berger, "Nonlinear photonic crystals," *Phys. Rev. Lett.*, vol. 81, pp. 4136–4139, Nov 1998. 11

[56] K. Gallo, A. Pasquazi, S. Stivala, and G. Assanto, "Parametric solitons in two-dimensional lattices of purely nonlinear origin," *Phys. Rev. Lett.*, vol. 100, p. 053901, Feb 2008. 11

[57] A. A. Sukhorukov, Y. S. Kivshar, O. Bang, and C. M. Soukoulis, "Parametric localized modes in quadratic nonlinear photonic structures," *Phys. Rev. E*, vol. 63, p. 016615, Dec 2000. 11

[58] O. Bang, P. L. Christiansen, and C. B. Clausen, "Stationary solutions and self-trapping in discrete quadratic nonlinear systems," *Phys. Rev. E*, vol. 56, pp. 7257–7266, Dec 1997. 11

[59] A. Arraf, C. Martijn de Sterke, and H. He, "Bright stationary solitary waves in deep gratings with a quadratic nonlinearity," *Phys. Rev. E*, vol. 63, p. 026611, Jan 2001. 11

[60] F. C. Moreira and S. B. Cavalcanti, "Dynamical manipulation of quadratic non-linearity photonic crystal gap solitons through thermooptic induced index modulations," in *Proc. SPIE 8001, International Conference on Applications of Optics and Photonics*, pp. 800107–800107–8, 2011. 11

[61] Z. Lin, H. Ramezani, T. Eichelkraut, T. Kottos, H. Cao, and D. N. Christodoulides, "Unidirectional invisibility induced by $\mathcal{PT}$-symmetric periodic structures," *Phys. Rev. Lett.*, vol. 106, p. 213901, May 2011. 12

[62] S. Nixon, L. Ge, and J. Yang, "Stability analysis for solitons in $\mathcal{PT}$-symmetric optical lattices," *Phys. Rev. A*, vol. 85, p. 023822, Feb 2012. 12, 30

[63] R. Driben and B. A. Malomed, "Dynamics of higher-order solitons in regular and $\mathcal{PT}$-symmetric nonlinear couplers," *EPL (Europhysics Letters)*, vol. 99, no. 5, p. 54001, 2012. 12, 49

[64] S. V. Suchkov, B. A. Malomed, S. V. Dmitriev, and Y. S. Kivshar, "Solitons in a chain of parity-time-invariant dimers," *Phys. Rev. E*, vol. 84, p. 046609, Oct 2011. 12

[65] V. V. Konotop, D. E. Pelinovsky, and D. A. Zezyulin, "Discrete solitons in PT-symmetric lattices," *ArXiv e-prints*, Oct. 2012. 12

[66] D. A. Zezyulin, Y. V. Kartashov, and V. V. Konotop, "Stability of solitons in $\mathcal{PT}$-symmetric nonlinear potentials," *EPL (Europhysics Letters)*, vol. 96, no. 6, p. 64003, 2011. 12

[67] D. A. Zezyulin and V. V. Konotop, "Nonlinear modes in the harmonic $\mathcal{PT}$-symmetric potential," *Phys. Rev. A*, vol. 85, p. 043840, Apr 2012. 12

[68] Y. He, X. Zhu, D. Mihalache, J. Liu, and Z. Chen, "Lattice solitons in $\mathcal{PT}$-symmetric mixed linear-nonlinear optical lattices," *Phys. Rev. A*, vol. 85, p. 013831, Jan 2012. 12

[69] Y. He, X. Zhu, D. Mihalache, J. Liu, and Z. Chen, "Solitons in pt symmetric optical lattices with spatially periodic modulation of nonlinearity," *Optics Communications*, vol. 285, no. 15, pp. 3320 – 3324, 2012. 12

[70] M. Znojil, "Shape invariant potentials with $\mathcal{PT}$ symmetry," *Journal of Physics A: Mathematical and General*, vol. 33, no. 7, p. L61, 2000. 12, 70, 71, 72, 73

[71] Z. Ahmed, "Real and complex discrete eigenvalues in an exactly solvable one-dimensional complex $\mathcal{PT}$-invariant potential," *Physics Letters A*, vol. 282, no. 6, pp. 343 – 348, 2001. 12, 70, 71, 72, 73

[72] A. Mostafazadeh, "Resonance phenomenon related to spectral singularities, complex barrier potential, and resonating waveguides," *Phys. Rev. A*, vol. 80, p. 032711, Sep 2009. 12

[73] O. Bendix, R. Fleischmann, T. Kottos, and B. Shapiro, "Exponentially fragile $\mathcal{PT}$ symmetry in lattices with localized eigenmodes," *Phys. Rev. Lett.*, vol. 103, p. 030402, Jul 2009. 12

[74] S. Hu, X. Ma, D. Lu, Z. Yang, Y. Zheng, and W. Hu, "Solitons supported by complex $\mathcal{PT}$-symmetric gaussian potentials," *Phys. Rev. A*, vol. 84, p. 043818, Oct 2011. 12

[75] F. K. Abdullaev, V. V. Konotop, M. Ögren, and M. P. Sørensen, "Zeno effect and switching of solitons in nonlinear couplers," *Opt. Lett.*, vol. 36, pp. 4566–4568, Dec 2011. 12

[76] H. Cartarius and G. Wunner, "Model of a $\mathcal{PT}$-symmetric bose-einstein condensate in a δ-function double-well potential," *Phys. Rev. A*, vol. 86, p. 013612, Jul 2012. 13

[77] C. B. Clausen, J. P. Torres, and L. Torner, "Impurity solitons with quadratic nonlinearities," *Physics Letters A*, vol. 249, no. 5, pp. 455 – 458, 1998. 13

[78] C. Balslev Clausen and L. Torner, "Self-bouncing of quadratic solitons," *Phys. Rev. Lett.*, vol. 81, pp. 790–793, Jul 1998. 13

[79] L. Shampine and M. Reichelt, "The matlab ode suite," *SIAM Journal on Scientific Computing*, vol. 18, no. 1, pp. 1–22, 1997. 20

[80] J. Dormand and P. Prince, "A family of embedded runge-kutta formulae," *Journal of Computational and Applied Mathematics*, vol. 6, no. 1, pp. 19 – 26, 1980. 20

[81] E. Anderson, Z. Bai, C. Bischof, S. Blackford, J. Demmel, J. Dongarra, J. Du Croz, A. Greenbaum, S. Hammarling, A. McKenney, *et al.*, *LAPACK Users' Guide*. Software, Environments and Tools, Society for Industrial and Applied Mathematics, 1987. 23, 97

[82] G. Strang, "On the construction and comparison of difference schemes," *SIAM Journal on Numerical Analysis*, vol. 5, no. 3, pp. 506–517, 1968. 24

[83] N. N. Yanenko, *The method of fractional steps*. Springer-Verlag, 1971. 24

[84] J. Boyd, *Chebyshev and Fourier Spectral Methods: Second Revised Edition*. Dover Books on Mathematics Series, Dover Publ., 2001. 24, 26

[85] G. Agrawal, *Nonlinear Fiber Optics*. Academic Press, 2012. 24

[86] W. Press, S. Teukolsky, W. Vetterling, and B. Flannery, *Numerical Recipes 3rd Edition: The Art of Scientific Computing*. Cambridge University Press, 2007. 24, 26

[87] J. Yang, *Nonlinear Waves in Integrable and Non-integrable Systems*. Mathematical Modeling and Computation, Society for Industrial and Applied Mathematics, 2011. 24, 28

[88] C. Shannon, "Communication in the presence of noise," *Proceedings of the IRE*, vol. 37, pp. 10 – 21, jan. 1949. 25

[89] R. Voigt, D. Gottlieb, and Y. Hussaini, *Spectral methods for partial differential equations*. Proceedings in Applied Mathematics Series, SIAM, 1984. 26

[90] G. I. Stegeman, D. J. Hagan, and L. Torner, "Cascading phenomena and their applications to all-optical signal processing, mode-locking, pulse compression and solitons," *Optical and Quantum Electronics*, vol. 28, pp. 1691–1740, 1996. 10.1007/BF00698538. 28, 30

[91] C. Hang and V. V. Konotop, "All-optical steering of light via spatial bloch oscillations in a gas of three-level atoms," *Phys. Rev. A*, vol. 81, p. 053849, May 2010. 29

[92] Y. Li, B. A. Malomed, M. Feng, and J. Zhou, "Double symmetry breaking of solitons in one-dimensional virtual photonic crystals," *Phys. Rev. A*, vol. 83, p. 053832, May 2011. 29

[93] A. V. Buryak, Y. S. Kivshar, and S. Trillo, "Optical solitons supported by competing nonlinearities," *Opt. Lett.*, vol. 20, pp. 1961–1963, Oct 1995. 30

[94] H. Sakaguchi and B. A. Malomed, "Stabilizing single- and two-color vortex beams in quadratic media by a trapping potential," *J. Opt. Soc. Am. B*, vol. 29, pp. 2741–2748, Oct 2012. 30

[95] E.-M. Graefe and H. F. Jones, "$\mathcal{PT}$-symmetric sinusoidal optical lattices at the symmetry-breaking threshold," *Phys. Rev. A*, vol. 84, p. 013818, Jul 2011. 31

[96] J. Yang, B. A. Malomed, and D. J. Kaup, "Embedded solitons in second-harmonic-generating systems," *Phys. Rev. Lett.*, vol. 83, pp. 1958–1961, Sep 1999. 46

[97] J. Yang, B. Malomed, D. Kaup, and A. Champneys, "Embedded solitons: a new type of solitary wave," *Mathematics and Computers in Simulation*, vol. 56, no. 6, pp. 585 – 600, 2001. 46

[98] B. A. Malomed, D. J. Kaup, and R. A. Van Gorder, "Unstaggered-staggered solitons in two-component discrete nonlinear schrödinger lattices," *Phys. Rev. E*, vol. 85, p. 026604, Feb 2012. 46

[99] J. Yang and T. R. Akylas, "Continuous families of embedded solitons in the third-order nonlinear schrödinger equation," *Studies in Applied Mathematics*, vol. 111, no. 3, pp. 359–375, 2003. 47

[100] W. C. K. Mak, B. A. Malomed, and P. L. Chu, "Three-wave gap solitons in waveguides with quadratic nonlinearity," *Phys. Rev. E*, vol. 58, pp. 6708–6722, Nov 1998. 59

[101] S. Adachi, *GaAs and related materials: bulk semiconducting and superlattice properties*. World Scientific, 1994. 60

[102] T. Skauli, K. L. Vodopyanov, T. J. Pinguet, A. Schober, O. Levi, L. A. Eyres, M. M. Fejer, J. S. Harris, B. Gerard, L. Becouarn, E. Lallier, and G. Arisholm, "Measurement of the nonlinear coefficient of orientation-patterned gaas and demonstration of highly efficient second-harmonic generation," *Opt. Lett.*, vol. 27, pp. 628–630, Apr 2002. 61

[103] C. M. de Sterke and J. E. Sipe, "Envelope-function approach for the electrodynamics of nonlinear periodic structures," *Phys. Rev. A*, vol. 38, pp. 5149–5165, Nov 1988. 63

[104] B. Midya, B. Roy, and R. Roychoudhury, "A note on the invariant periodic potential," *Physics Letters A*, vol. 374, no. 26, pp. 2605 – 2607, 2010. 72

[105] E. N. Tsoy, S. S. Tadjimuratov, and F. K. Abdullaev, "Beam propagation in gain-loss balanced waveguides," *Optics Communications*, vol. 285, no. 16, pp. 3441 – 3444, 2012. 78

[106] F. K. Abdullaev and V. V. Konotop, "Intrinsic localized modes in arrays of atomic-molecular bose-einstein condensates," *Phys. Rev. A*, vol. 68, p. 013605, Jul 2003. 91

[107] R. Yamazaki, S. Taie, S. Sugawa, and Y. Takahashi, "Submicron spatial modulation of an interatomic interaction in a bose-einstein condensate," *Phys. Rev. Lett.*, vol. 105, p. 050405, Jul 2010. 91

[108] M. Tabor, *Chaos and integrability in nonlinear dynamics: an introduction*. Wiley-Interscience publication, Wiley, 1989. 96